

New distance estimates to Pulsating RR Lyrae Star *DM And*.

ADANNA FRAZIER^{1,*} AND THOMAS O'KUMA¹

¹Lee College, Baytown, Texas, United States. afraier@lee.edu

* afraier@lee.edu

This is a study of the photometric data of the RR Lyrae star, DM And, in the B, V, sdss-i, and sdss-z filters. The light curve shapes and estimated period 0.631 ± 0.011 d in the B-filter, 0.631 ± 0.012 d in the V-filter, 0.631 ± 0.011 d in the sdss-i filter, 0.631 ± 0.011 d in the sdss-z filter, and an average period of 0.6301 ± 0.011 d represent that of a typical R Rab type RR Lyrae star. DM And's magnitude is 12.175 ± 0.010 in B, 11.70 ± 0.010 in V, 11.60 ± 0.03 in sdss-i and 11.475 ± 0.046 in sdss-z, with an average magnitude of 11.738 ± 0.024 . DM And has a measured distance averaged over all filters of 1647 ± 42 pc, 1558 ± 46 pc in V, 1728 ± 77 pc in sdss-i, and 1653 ± 95 pc in sdss-z. These results are comparable to GAIA's measured distance of 1572 ± 157 pc.

© 2021 Astronomy Theory, Observations and Methods Journal

Keywords: Stars: variables: RR Lyrae – stars: variables: Cepheids – stars: distances

<https://doi.org/10.32374/atom.2021.2.1>

INTRODUCTION

RR Lyrae pulsating stars are important for the measurement of distance within space (Catelan & Smith, 2014). The star of interest in this study is DM And which has had a right ascension of 23:32:00.71 and a declination of +35:11:48.90, according to prior observations (Maintz, 2005). It has a radial velocity of 265 m/s (Beers et al., 2000). DM And has a documented period of 0.630387 days (Bramich et al., 2014), which is typical for R Rab type stars and a V apparent magnitude of 12.40 (Maintz, 2005).

It is interesting to note that previous investigations have resulted in the discovery of a Blazhko effect displayed by DM And (Skarka, 2014). The Blazhko Effect is “a modulation of the light curve of an RR Lyrae star that has a period much longer than that of the primary pulsation cycle.” (Catelan & Smith,

2014). This type of modulation explained by the Blazhko Effect is not uncommon in RR Lyrae type pulsating stars (Catelan & Smith, 2014). DM And has a documented metallicity [Fe/H] of -2.32 (Bramich et al., 2014). This means the DM And is a metal poor star with very few elements heavier than helium and hydrogen within it.

RR Lyrae type stars (DM And, in this study) have a better period-luminosity-metallicity relationship in the sdss filters, particularly i and z, in comparison to other optical filters (Cáceres & Catelan, 2008). Since this has not been studied extensively, the data measured in this study is useful and relevant to the period-luminosity-metallicity relationship. Using this, DM And was compared to previously recorded distance measurements by GAIA.

OBSERVATIONS AND METHODS

Table 1-4 lists the telescopes and their associated observatories, each of them 0.4m telescopes of Las Cumbres Observatory (Brown et al., 2013), used to capture the images used in this study and the number of images captured by each telescope per filter.

Table 1. Telescopes Used B-Filter

Telescope	Images Captured
Haleakala Observatory	15
Tiede Observatory	29
McDonald Observatory	9

Table 2. Telescopes Used V-Filter

Telescope	Images Captured
Haleakala Observatory	15
Tiede Observatory	31
McDonald Observatory	9

Table 3. Telescopes Used sdss-i Filter

Telescope	Images Captured
Haleakala Observatory	15
Tiede Observatory	31
McDonald Observatory	9

The observation period lasted for 12 days from October 6, 2019 to October 18, 2019. Each picture was scheduled to be taken every 4.5 hours through four filters: blue filter (B), visual filter (V), infrared filter (sdss-i) and a deep infrared filter (sdss-z), with different exposure times for each filter. The B filter had an exposure time of 120 seconds, the sdss-z filter had an exposure time of 60 seconds, and the sdss-i and v filters had an exposure time of 45 seconds.

The Our Solar Siblings (OSS) Pipeline (Fitzgerald, 2018) was used to gather images and prepare them for the user. The OSS Pipeline works with various observatories and automatically processes a full night's worth of images. The OSS Pipeline consists of four parts: The image processing and cleaning

Table 4. Telescopes Used sdss-z Filter

Telescope	Images Captured
Haleakala Observatory	15
Tiede Observatory	31
McDonald Observatory	9

pipeline, the photometry pipeline, the all-sky calibration pipeline, and the catalogue construction pipeline. The image processing and cleaning pipeline makes adjustments to the image so that it is user friendly. The photometry pipeline takes place after the image processing and cleaning pipeline and uses automated photometry routines on the images captured and sorted into photometry catalogues.

The type of photometry used in this study was the Point Spread Function Extractor, PSFEX (Bertin, 2011). This type of photometry assigns a function to the pixels that make up a star and calculates the total light under the function. The photometry catalogues produced by the OSS Pipeline cleans are ready to be used with Astrosource (Fitzgerald, Gomez, Salimpour, Singleton, & Wibowo, 2021). Astrosource was used along with Spyder (via Python Anaconda) to analyze the data on DM And's period as well as plotting the graphs and light curves using the images captured by the telescope, which are provided in the results section.

The first step was to identify all the stars (including DM And) in every image that is being studied. Once all the stars common to the imageset were identified, the least variable stars were selected to be compared to the target star, DM And. In order to assure the accuracy of the magnitude measurements for the sdss-z and sdss-i filter's there were adjustments made to the number of comparison stars used. This will be described in more detail in the discussion section of the paper. From there, the light curves for DM And were constructed and the period was determined.

The following equations listed below were used to find the absolute magnitude from the period-luminosity-metallicity relationships, which were then used to undertake distance measurements. Then the distance and distance error measured by GAIA DR2 (Prusti et al., 2016) was found as well as a reddening or E(B-V) value of 0.08, which was estimated using the NASA/IPAC Infrared Science Archives dust maps (Schlafly & Finkbeiner, 2011; Schlegel, Finkbeiner, &

Davis, 1998).

$$M_v = 2.288 + 0.882 \log Z + 0.108 (\log Z)^2 \quad (1)$$

(Catelan, Pritzl, & Smith, 2004)

$$M_z = 0.839 - 1.295 \log P + 0.211 \log Z \quad (2)$$

(Cáceres & Catelan, 2008)

$$M_i = 0.908 - 1.035 \log P + 0.220 \log Z \quad (3)$$

(Cáceres & Catelan, 2008)

$$\log Z = [M/H] - 1.765 \quad (4)$$

(Cáceres & Catelan, 2008)

$$[M/H] = [Fe/H] + \log(0.638f + 0.362) \quad (5)$$

(Cáceres & Catelan, 2008)

While measuring DM And's period, two period estimation algorithms were used, the minimum distance method and the minimum standard deviation method (presented in Table's 5-8) (Altunin, Caputo, & Tock, 2020). The minimum distance method and minimum standard deviation method use trialled periods. The distance method uses a repeated process in which distances between two adjacent points on flux versus phase plot of DM And are calculated and summed for each trial period. The standard deviation method sorts fluxes based on their phase into binned intervals of .1 from 0 to 1 and the standard deviation of each interval is taken and summed. Both of these methods were used in Astrosource to calculate the period of DM And.

RESULTS

DM And has an measured period of 0.631 ± 0.011 days along with lightcurve that has a very steep incline and a steady decline, which strongly correlates to RRab type RR Lyrae stars.

Tables 5-8 display the middle magnitude, period measurements (through the distance method and PDM method), amplitude and the errors associated with each of these values for the B, V, sdss-i, and sdss-z filters.

Table 9 displays the distance measurements and measurement errors for GAIA, the V filter, sdss-i filter, sdss-z filter, and the average of all three filters (Viz).

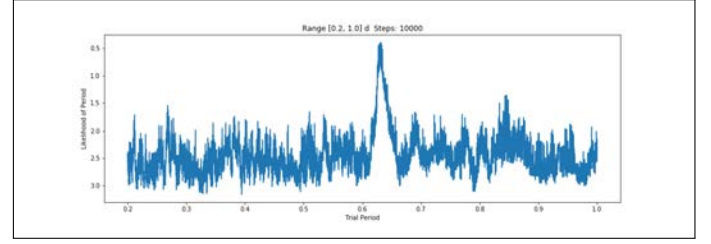


Fig. 1. B-Filter: A likelihood of period versus trial period

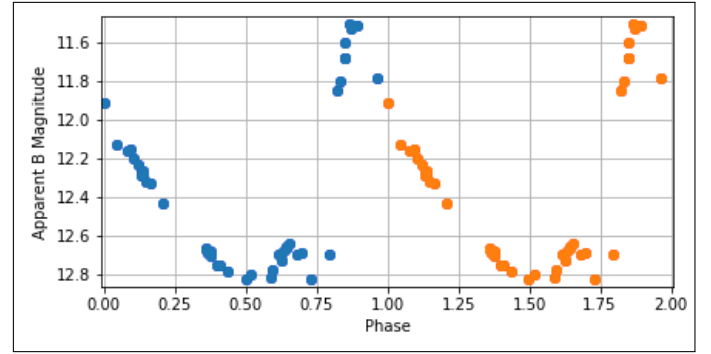


Fig. 2. B-filter: Apparent Magnitude versus Phase

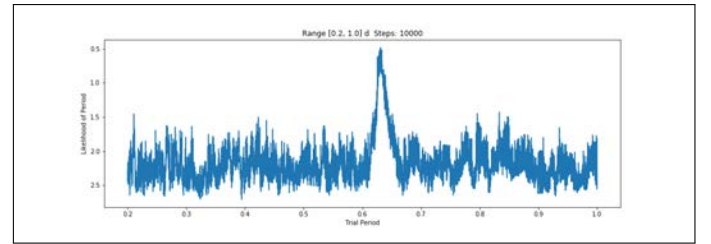


Fig. 3. ip-Filter: A likelihood of period versus trial period

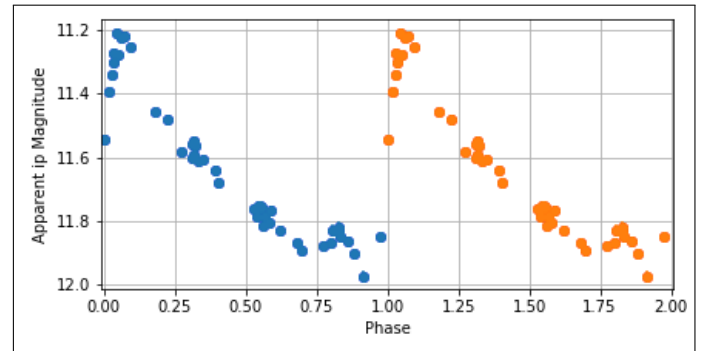


Fig. 4. ip-Filter: Apparent Magnitude versus Phase

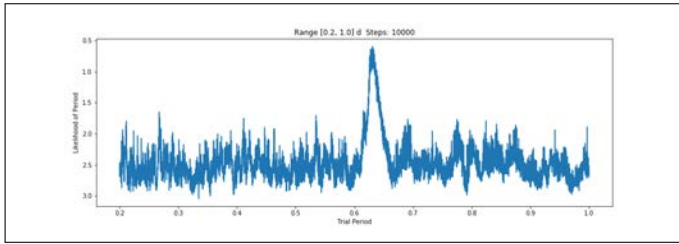


Fig. 5. V-Filter: A likelihood of period versus trial period

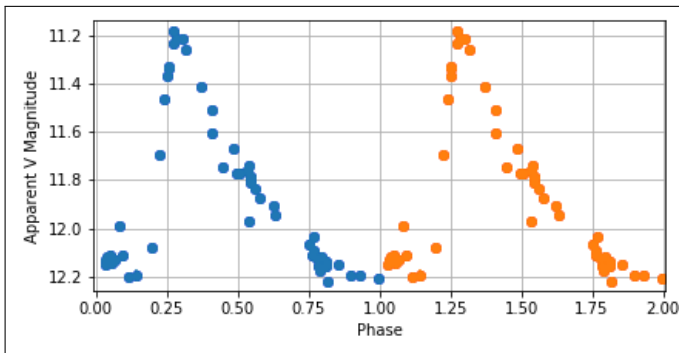


Fig. 6. V-Filter: Apparent Magnitude versus Phase

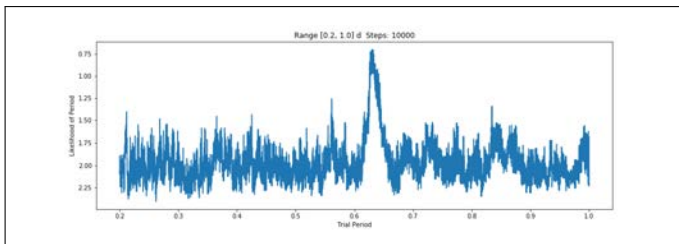


Fig. 7. Zs-Filter: A likelihood of period versus trial period

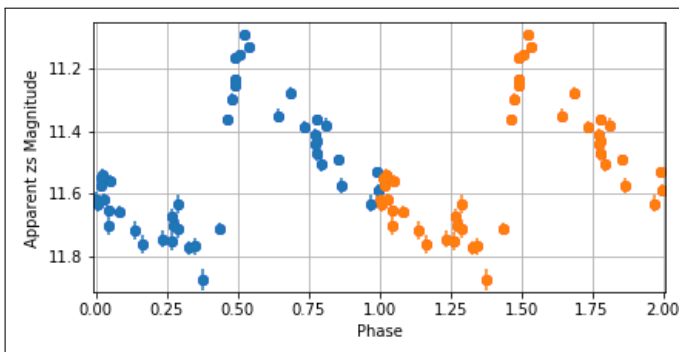


Fig. 8. Zs-Filter: Apparent Magnitude versus Phase

Table 5. Measurements in the B-Filter

	B	error
middle mag	12.175	0.010
distance method (days)	0.6309	0.012
PDM Method(days)	0.6311	0.01
amplitude(magnitude)	0.625	

Table 6. Measurements in the V-Filter

	V	error
middle mag	11.70	0.01
distance method(days)	0.6304	0.012
PDM Method(days)	0.6306	0.011
amplitude(magnitude)	0.5	

Table 7. Measurements in the i-Filter

	i	error
middle mag	11.60	0.030
distance method(days)	0.63088	0.012
PDM Method(days)	0.63088	0.01
amplitude(magnitude)	0.4	

Table 8. Measurements in the zs-Filter

	zs	error
middle mag	11.475	0.046
distance method(days)	0.63088	0.011
PDM Method(days)	0.6303	0.01
amplitude (magnitude)	0.375	

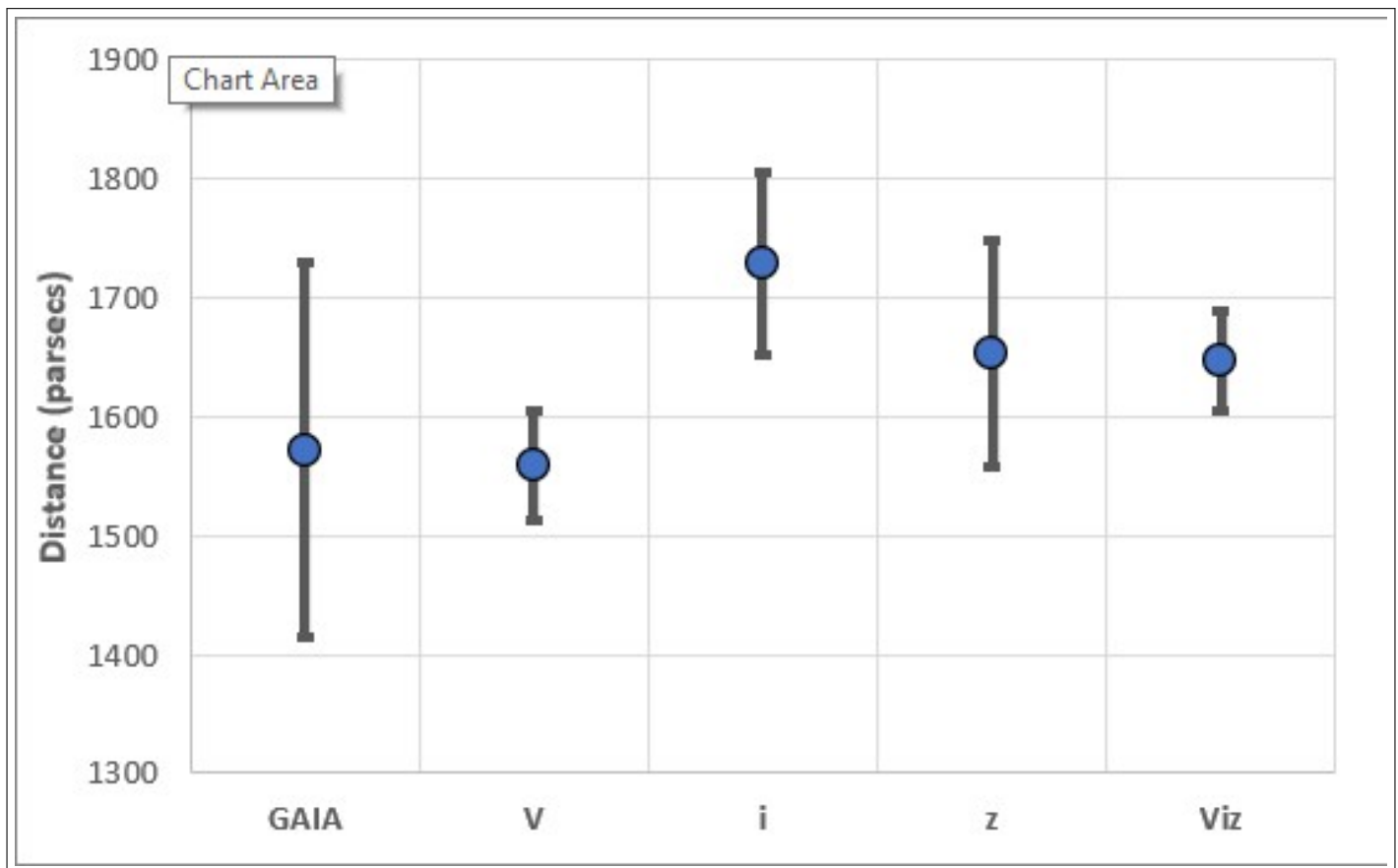


Fig. 9. Distance and Distance Errors

Table 9. Measured Distance Variations for DM And

	Distance (parsec)	Distance Error (parsec)
GAIA	1572	157
V	1558	46
i	1728	77
zs	1653	95
Viz	1647	42

Figure 9 visually represents the distance measurements and distance errors. Figures 10 displays a comparison in magnitudes between DM And and another RR Lyrae star, AF Vel. The magnitude measurement for AF Vel strongly correlates with previously recorded GAIA data, so AF Vel was an ideal candidate when comparing DM And's magnitude to other RR Lyrae type stars. While DM And follows an expected path in the B and V filter there is a noticeable dimming of DM And's magnitude in the sdss-i and sdss-z filters compared to AF Vel before corrections noted in the discussion.

DISCUSSION

The twelve day observation period was not sufficient to witness a Blazhko Effect, as previous research has described. This lack of data does not discredit the possibility of a Blazhko Effect but could be explored in the future with longer-duration observations.

Initially, there was an unusually dim magnitude measured in the sdss-z filter of 12.4, 0.74 magnitudes dimmer than expected compared to AF Vel, and a smaller, but existing, deficiency of 0.1 in the sdss-i filter, with a magnitude of 11.8, compared to the data from other filters. Astrosource was used to investigate the inconsistency. In Astrosource, the number of comparison stars used was changed to test whether there was a problem with the comparison stars and/or calibration or an actual effect from the star. In the first test, the first five comparison stars out of ten were used which resulted in a magnitude of 12.35 and after that the last five comparison stars were used which resulted in a magnitude 12.35 as well. To further investigate this, Astrosource was run ten times, using one of each of the ten comparison stars individually. The magnitudes of these ten tests were consistent with the results before varying in magni-

tude from 12.35-12.45, which is not a substantial variation compared to the deficiency. This indicated the abnormality in the sdss-z filter was not caused by an outlier single comparison star or the calibration.

Further issues included that there was also a significant distance measurement variation between the measured distances of this study and previously measured distance done by GAIA. The range of the distance difference was 959 parsec between the lowest distance measurement done by GAIA at 1572 ± 157 parsec and the largest distance measurement in the sdss-z filter at 2531 ± 160 parsec.

However, it was discovered that the dimming in magnitude of the sdss-i and sdss-z filters and the variation in the distant measurements compared to GAIA was not an effect of DM And. In the PANSTARRS survey (Chambers et al., 2016) - used to calibrate the photometry for DM And, accessed via Aladin, there appears to be a spot in the center of some brighter stars, shown in Figure 12, where the pixels are black. When comparing the amount of light per pixel, to determine a stars magnitude and comparing it to DM And, they appear much dimmer than what they really are. Adjustments were made to the Astrosource program to avoid those stars contributing to the photometry. Once these issues were corrected for, the magnitude and distance values represented expected values for an RR Lyrae at the distance of DM And.

CONCLUSION

RR Lyrae stars are used to determine distance. The data collected in this study for DM And shows a typical trend for most RRab type RR Lyrae Pulsating stars, as shown above, with an average measured distance of 1647 ± 42 parsecs and an average period of 0.631 ± 0.011 days. This is comparable to GAIA's measured distance of 1572 ± 157 pc. The V filter derived distance, 1558 ± 46 pc, individually agrees very well with the GAIA distance.

ACKNOWLEDGMENTS

This research has made use of the SIMBAD database, operated at CDS, Strasbourg, France 2000,A&AS,143,9 , "The SIMBAD astronomical database", Wenger et al.

This research has made use of "Aladin sky atlas" developed at CDS, Strasbourg Observatory, France 2000A&AS..143...33B and 2014ASPC..485..277B.

This work makes use of observations from the LCOGT network.

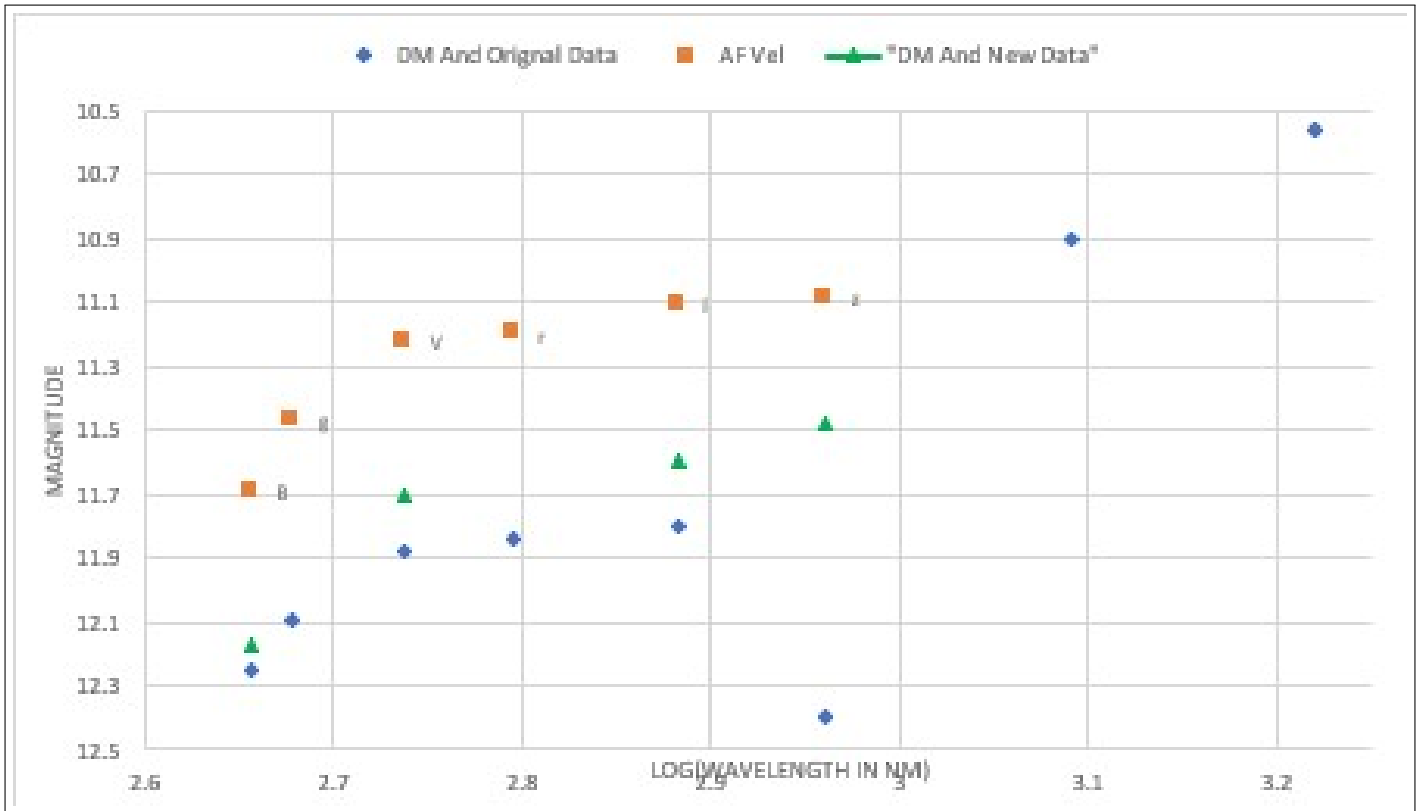


Fig. 10. Original magnitudes of DM And (both original magnitude measurements and current magnitude measurements) and AF Vel before any adjustments to m-M.

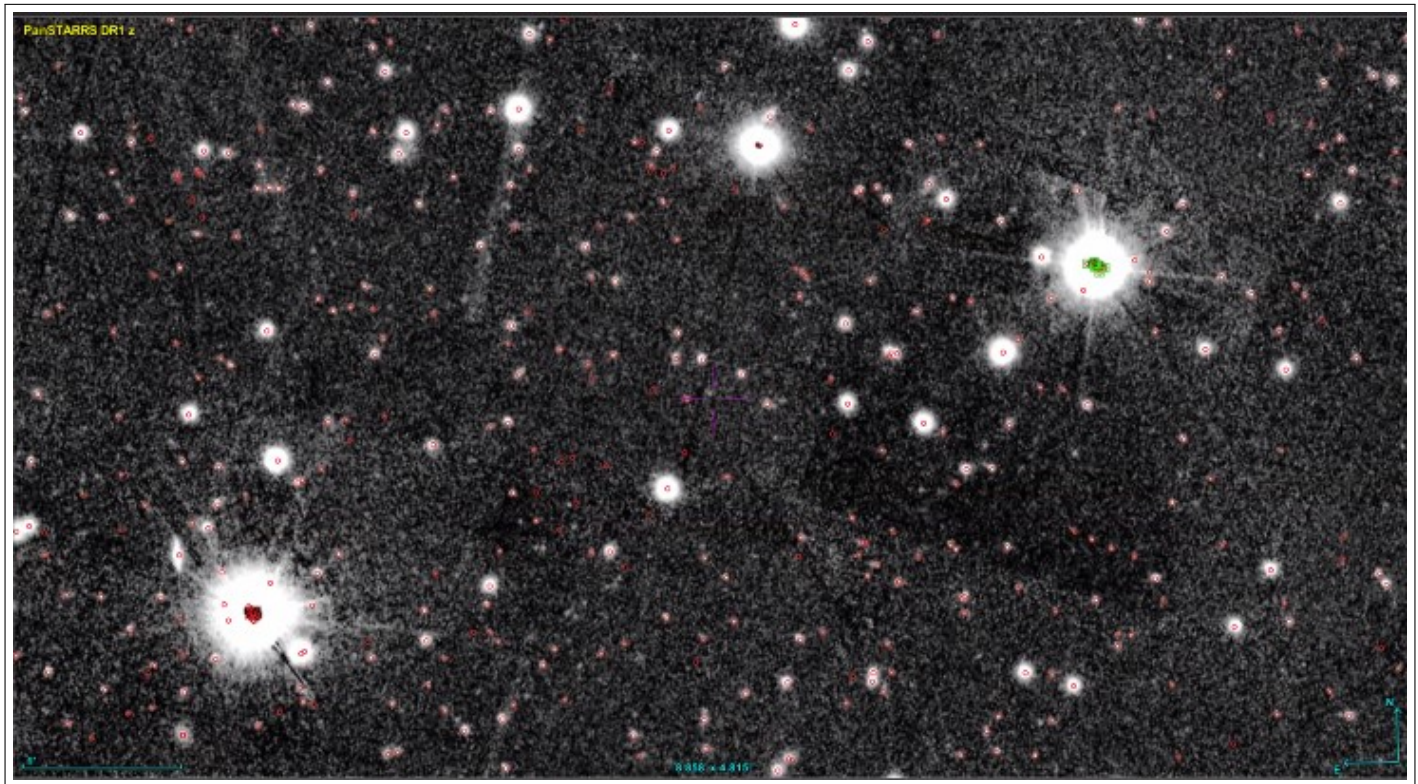


Fig. 11. The following is an image captured of the PANSTAARS survey in Aladin, showing the black spots in the center of the star, as well as multiple stars being counted in the black spot of a single star.

This research has made use of the NASA/IPAC Infrared Science Archive, which is funded by the National Aeronautics and Space Administration and operated by the California Institute of Technology.

Special thanks to Michael Fitzgerald of Our Solar Siblings for his inspiration and generous and frequent support throughout this project.

REFERENCES

- Altunin, I., Caputo, R., & Tock, K. (2020). Period of eclipsing binary epic 201458798.
- Beers, T. C., Chiba, M., Yoshii, Y., Platais, I., Hanson, R. B., Fuchs, B., & Rossi, S. (2000). Kinematics of metal-poor stars in the galaxy. ii. proper motions for a large nonkinematically selected sample. *The Astronomical Journal*, 119(6), 2866.
- Bertin, E. (2011). Automated morphometry with sextractor and psfex. In *Astronomical data analysis software and systems xx* (Vol. 442, p. 435).
- Bramich, D. M., Alsubai, K., Ferro, A. A., Parley, N., Cameron, A. C., Horne, K., ... West, R. (2014). Rr lyrae stars in the gcvs observed by the qatar exoplanet survey. *arXiv preprint arXiv:1405.3417*.
- Brown, T., Baliber, N., Bianco, F., Bowman, M., Burleson, B., Conway, P., ... others (2013). Las cumbres observatory global telescope network. *Publications of the Astronomical Society of the Pacific*, 125(931), 1031.
- Cáceres, C., & Catelan, M. (2008). The period-luminosity relation of rr lyrae stars in the sdss photometric system. *The Astrophysical Journal Supplement Series*, 179(1), 242.
- Catelan, M., Pritzl, B. J., & Smith, H. A. (2004). The rr lyrae period-luminosity relation. i. theoretical calibration. *The Astrophysical Journal Supplement Series*, 154(2), 633.
- Catelan, M., & Smith, H. A. (2014). *Pulsating stars*. John Wiley & Sons.
- Chambers, K. C., Magnier, E., Metcalfe, N., Flewelling, H., Huber, M., Waters, C., ... others (2016). The pan-starrs1 surveys. *arXiv preprint arXiv:1612.05560*.
- Fitzgerald, M. T. (2018). The our solar siblings pipeline: Tackling the data issues of the scaling problem for robotic telescope based astronomy education projects.
- Fitzgerald, M. T., Gomez, E., Salimpour, S., Singleton, J., & Wibowo, R. W. (2021). "astrosources": automating optical astronomy measurement, calibration and analysis for variable stellar sources from provided photometry. *Journal of Open Source Software*, 6(58), 2641.
- Maintz, G. (2005). Proper identification of rr lyrae stars brighter than 12.5 mag. *Astronomy & Astrophysics*, 442(1), 381–384.
- Prusti, T., De Bruijne, J., Brown, A. G., Vallenari, A., Babusiaux, C., Bailer-Jones, C., ... others (2016). The gaia mission. *Astronomy & astrophysics*, 595, A1.
- Schlafly, E. F., & Finkbeiner, D. P. (2011). Measuring reddening with sloan digital sky survey stellar spectra and recalibrating sfid. *The Astrophysical Journal*, 737(2), 103.
- Schlegel, D. J., Finkbeiner, D. P., & Davis, M. (1998). Maps of dust infrared emission for use in estimation of reddening and cosmic microwave background radiation foregrounds. *The Astrophysical Journal*, 500(2), 525.
- Skarka, M. (2014). Bright blazhko rrab lyrae stars observed by asas and the superwasp surveys. *Astronomy & Astrophysics*, 562, A90.

AW Mic: The RR Lyrae That Wasn't

GERRI BERNARD^{1,*}

¹Brisbane Girls Grammar School, Brisbane, QLD, Australia

*Corresponding author: gbernard@bggs.qld.edu.au

AW Mic is a neglected star that has previously been categorised as an ‘unusual’ RRc variable. This paper makes use of new and archival observations of AW Mic to establish that this star is no longer varying in magnitude and should no longer be classified as an RR Lyrae variable. Mid magnitudes of 9.171 ± 0.026 and 9.001 ± 0.014 are reported for this star in the *B*- and *V*-bands, respectively.

© 2021 Astronomy Theory, Observations and Methods Journal

Keywords: RR Lyrae, Variable stars

<https://doi.org/10.32374/atom.2020.2.2>

INTRODUCTION

RR Lyrae are low mass, evolved stars that have moved off the main sequence and initiated core helium burning. These stars can radially pulsate in various modes (fundamental, first overtone, or both) and generally exhibit periods of 0.2 – 1 days. They are found at the intersection of the horizontal branch and the classical instability strip (Catelan & Smith, 2015).

Stars on the horizontal branch may cross the instability strip in either direction, resulting in an increase in observed period for those stars evolving from blue to red, or a decrease in period for those stars evolving from red to blue. RR Lyrae that have moved out of the instability strip in either direction would cease pulsation and become either blue HB stars or red AGB stars (Le Borgne et al., 2007).

First classified as a horizontal branch star by MacConnell, Frye, Bidelman and Bond (1971), AW Mic (HD 202759) was later found by Przybylski and Bessell (1974) to be an unusual RRc with a ‘complex and irregular light curve’. In their paper, Przybylski and Bessell present a reasonable, low amplitude light curve ($\Delta\text{magnitude} < 0.1$) based on 164 observations and generate a period estimate of 11.5 hours

for this star, but note that more observations would be required to deduce a full description of the star’s behaviour. They cite the relatively high effective temperature of the star (7 400 K) as evidence that this star may lie close to the blue edge of the instability strip.

Some authors have concurred with Przybylski and Bessel’s assessment that this is an RR Lyrae star based on their own measurements of T_{eff} (Kodaira & Philip, 1984), however, more recent sources find that the star is more similar to a non-varying blue horizontal branch star (Kinman et al., 2000). A summary of some of the reported properties of AW Mic is presented in Table 1. Overall, the period appears not to be well-established and the amplitude of the magnitude in the *V*-band is underreported. The effective temperature and metallicity of AW Mic seem to be corroborated across various sources.

METHODS

Observations

The data for this project was gathered using the The Dorothy Hill Observatory (DHO), located at the Mar-

Table 1. Reported properties of AW Mic

Property	Value	Source
ICRSd Right Ascension	319.775	(Gaia et al., 2018)
ICRSd Declination	-33.919	
Period	0.478d (11.5hrs)	(Przybylski & Bessell, 1974)
	0.478d (11.5hrs)	(Samus', Kazarovets, Durlevich, Kireeva, & Pastukhova, 2017)
	0.305684d (7.3664hrs)	(Kafka, 2016)
V_{mag}	8.86 ^a	(Jayasinghe et al., 2019; Shappee et al., 2014)
	8.97 ^b	(Przybylski & Bessell, 1974)
	9.015	(Henden et al., 2016)
	9.09 ^c	(Kinman et al., 2000)
	9.04-9.13	(Kafka, 2016)
Max V_{mag} -Min V_{mag}	0.08	(Przybylski & Bessell, 1974)
	0.09	(Kafka, 2016)
T_{eff}	7 400 K	(Kodaira & Philip, 1984)
	7 431 K	(Wilhelm, Beers, & Gray, 1999)
	7 465 K	(Kinman et al., 2000)
	7 500 K	(Gaia et al., 2018)
$[Fe/H]$	-2.35	(Cortés et al., 2009)
	-2.37	(Wilhelm et al., 1999)
	-2.40	(Kinman et al., 2000)

^aMean ^bReported as V_0 ^creported as 9.09v

rapatta Memorial Outdoor Education Centre, near Imbil, QLD, Australia. *B*- and *V*-band observations of AW Mic were taken between 3 August 2020–7 August 2020 with an FLI CCD attached to a robotically-controlled 356mm Planewave reflecting telescope. The pixel scale of the camera was $0.72''/\text{pixel}$ in 1×1 binning mode with a $50' \times 50'$ field of view. Exposure time was ten seconds for all of the 328 observations, which resulted in an approximate integrated ADU count value of 250,000 from the target star, and a cadence of five minutes was used.

Photometry

The images and photometry were processed using SEK (Source Extractor Kron) (Bertin & Arnouts, 1996) and PSX (PSFEx) (Bertin, 2011) files from the Our SolarSiblings Pipeline (M. Fitzgerald, 2018). Data analysis was carried out using astrosource (M. T. Fitzgerald, Gomez, Salimpour, Singleton, & Wibowo, 2021), a python script that carries out differential photometry based on optimal comparison stars in each filter. Astrosource identified the comparison stars shown in Figure 1 as being the least variable in the field (having the smallest standard deviation of differential magnitude across all images used), with variabilities between 0.004 and 0.03 for all comparison stars in both filters. Due to a lack of stars in the field with sufficient brightness in the *B*-band, only one suitable comparison star was identified by astrosource for comparison in this band. Differential photometry was then performed using known comparison star magnitudes from APASS (Henden et al., 2016) and calibrated magnitudes for AW Mic for each observation were generated in *B*- and *V*-bands.

Spectroscopy

Spectroscopy was carried out using the FLOYDS spectrograph on the Las Cumbres Observatory 2.0m telescope at Siding Springs, Australia (Brown et al., 2013). FLOYDS is a cross-dispersed, low resolution ($R \sim 550$) spectrograph with wavelength coverage of 3200\AA – 10000\AA . Two highly similar spectra were measured on HJD 2459108.85924 and HJD 2459108.85925.

RESULTS AND DISCUSSION

Photometry

Table 2 shows photometric results for DHO observations of AW Mic, including calibrated magnitudes in

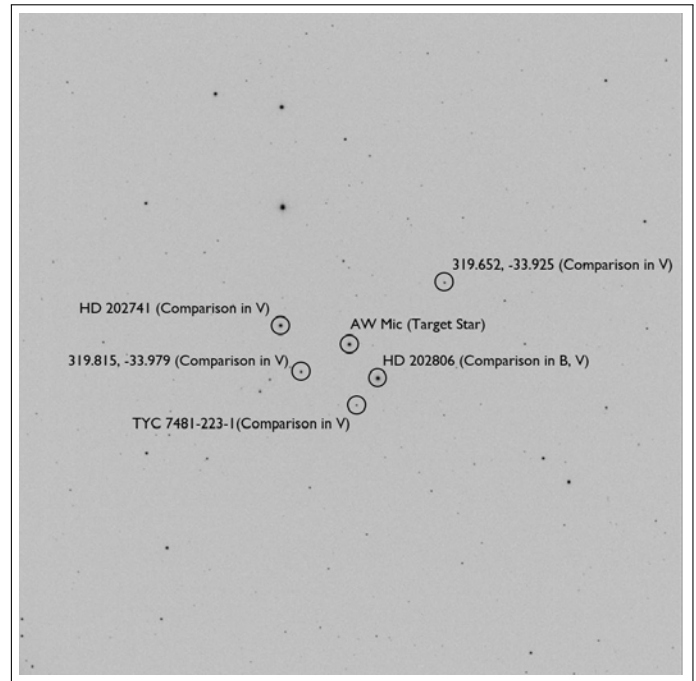


Fig. 1. Inverted image of field analysed in DHO observations. Field of view is $50' \times 50'$.

B- and *V*-bands. *V*-band magnitudes match well with those previously reported in the literature.

Figure 2 shows a plot of period likelihood vs tested periods, as generated by the astrosource analysis. The possible expected periods of AW Mic from Table 1 are shown to have no more likelihood than any other period in the expected range of an RR Lyrae variable.

Figures 3 and 4 show calibrated magnitudes of AW Mic in *B*- and *V*-bands, generated from photometry derived from 328 DHO observations (see Table 2). There is quite a bit of scatter and attempts to fold the lightcurve around previously reported periods for AW Mic resulted in plots that showed no evidence of pulsation.

Photometry results from observations at the DHO were compared to photometry data from the All Sky Automated Survey (Pojmanski & Maciejewski, 2005) and the Wide Angle Search for Planets (Butters et al., 2010). The ASAS data is based on observations made between HJD 2451872.53857–2455166.56762 and the SuperWASP data is from observations made between HJD 2453862.551–2454614.69.

Figures 5 and 6 show calibrated, phased light curves from SuperWASP and ASAS, respectively, for comparison to those generated from DHO observations. Both comparison light curves were generated assuming the AAVSO reported period of 0.3056840d

Table 2. Observation results from DHO.

B-Band	
First Observation BJD	2459072.108
Last Observation BJD	2459078.271
Minimum Magnitude	9.218 ± 0.026
Mid Magnitude	9.171 ± 0.026
Maximum Magnitude	9.124 ± 0.026
V-Band	
First Observation BJD	2459072.086
Last Observation BJD	2459078.275
Minimum Magnitude	8.900 ± 0.014
Mid Magnitude	9.001 ± 0.014
Maximum Magnitude	9.101 ± 0.014

for AW Mic. As with the results from DHO observations, no periodicity is evident for the expected period.

As an additional test, phased SuperWASP and ASAS light curves were generated using Przybylski and Bessel's (1974) reported period of 0.478d. These are shown in Figures 7 and 8 and, again, no periodicity is evident.

This leads to the conclusion that AW Mic, which may have been variable in the past, is not currently changing magnitude in a periodic way and certainly not in a manner consistent with the behaviour of an RRc. Therefore, this star should no longer be classified as an RRc variable.

Spectroscopy

Figure 9 shows a spectrum of AW Mic between 3300Å–10500Å. Visual inspection indicates that the metallicities reported in the literature for AW Mic seem reasonable (see Table 1).

CONCLUSION

This research demonstrated that AW Mic, previously assumed to be an RRc variable star, appears to be non-variable. Recent observations from the DHO that demonstrate non-variability are confirmed by archival observations made by the All Sky Automated Survey and by the Wide Angle Search for Planets, indicating

that AW Mic has been non-variable for at least twenty years. Therefore, it is likely that AW Mic will need to be removed from common databases and catalogues for variable stars.

FUNDING

Observations in this paper made use of telescopes at the Dorothy Hill Observatory (DHO) in Queensland, Australia. The DHO is a facility established and funded by Brisbane Girls Grammar School.

ACKNOWLEDGMENTS

The author would like to acknowledge Dr Michael Fitzgerald, Dr David Trappett, and Anthony Lumsden for their major contributions to the data collection for this project. This paper makes use of data from the DR1 of the WASP data (Butters et al. 2010) as provided by the WASP consortium, and the computing and storage facilities at the CERIT Scientific Cloud, reg. no. CZ.1.05/3.2.00/08.0144 which is operated by Masaryk University, Czech Republic. This research has made use of the International Variable Star Index (VSX) database, operated at AAVSO, Cambridge, Massachusetts, USA. This research has made use of the SIMBAD database, operated at CDS, Strasbourg, France.

SUPPLEMENTAL DOCUMENTS

REFERENCES

- Bertin, E. (2011). Automated morphometry with sextractor and psfex. In *Astronomical data analysis software and systems xx* (Vol. 442, p. 435).
- Bertin, E., & Arnouts, S. (1996). SExtractor: Software for source extraction. *Astronomy and Astrophysics Supplement Series*, 117(2), 393–404.
- Brown, T., Baliber, N., Bianco, F., Bowman, M., Burleson, B., Conway, P., ... et al. (2013). Las cumbres observatory global telescope network. *Publications of the Astronomical Society of the Pacific*, 125(931), 1031.
- Butters, O., West, R., Anderson, D., Cameron, A., Clarkson, W., Enoch, B., ... Todd, I. (2010, 09). The first wasp public data release. <http://dx.doi.org/10.1051/0004-6361/201015655>, 520. doi:
- Catelan, M., & Smith, H. A. (2015). *Pulsating stars* (1st ed.). Weinheim: Wiley-VCH Verlag GmbH Co. KGaA.

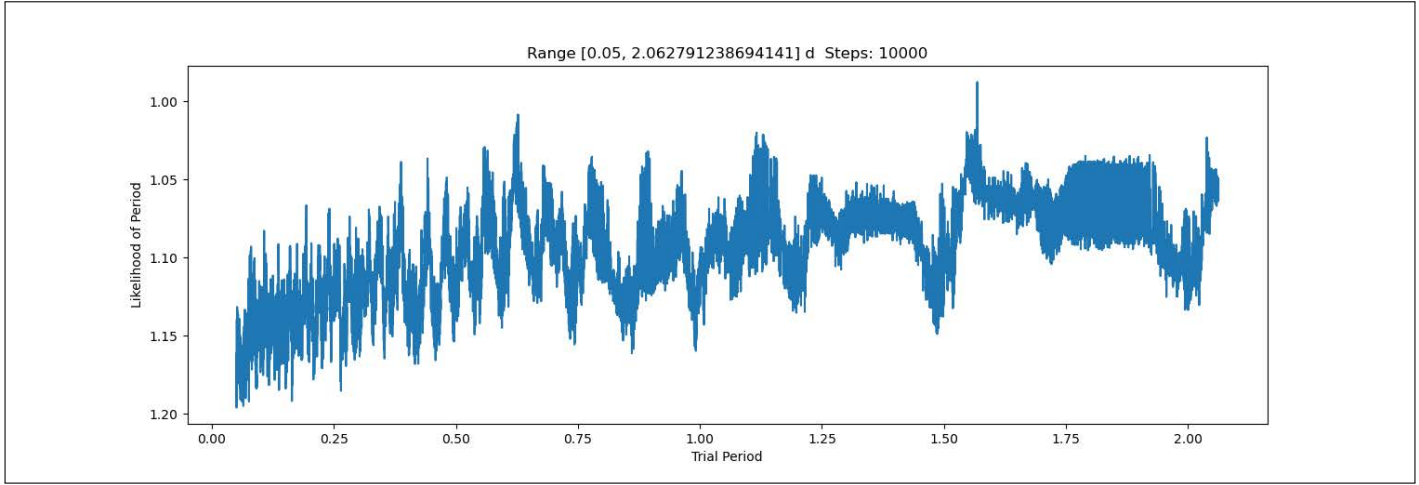


Fig. 2. Phase dispersion minimization (PDM) likelihood plot in V-band from DHO observations. Note that the y-axis (unitless) is inverted, with larger numbers indicating higher likelihood of particular periods (in days), as determined by PDM analysis.

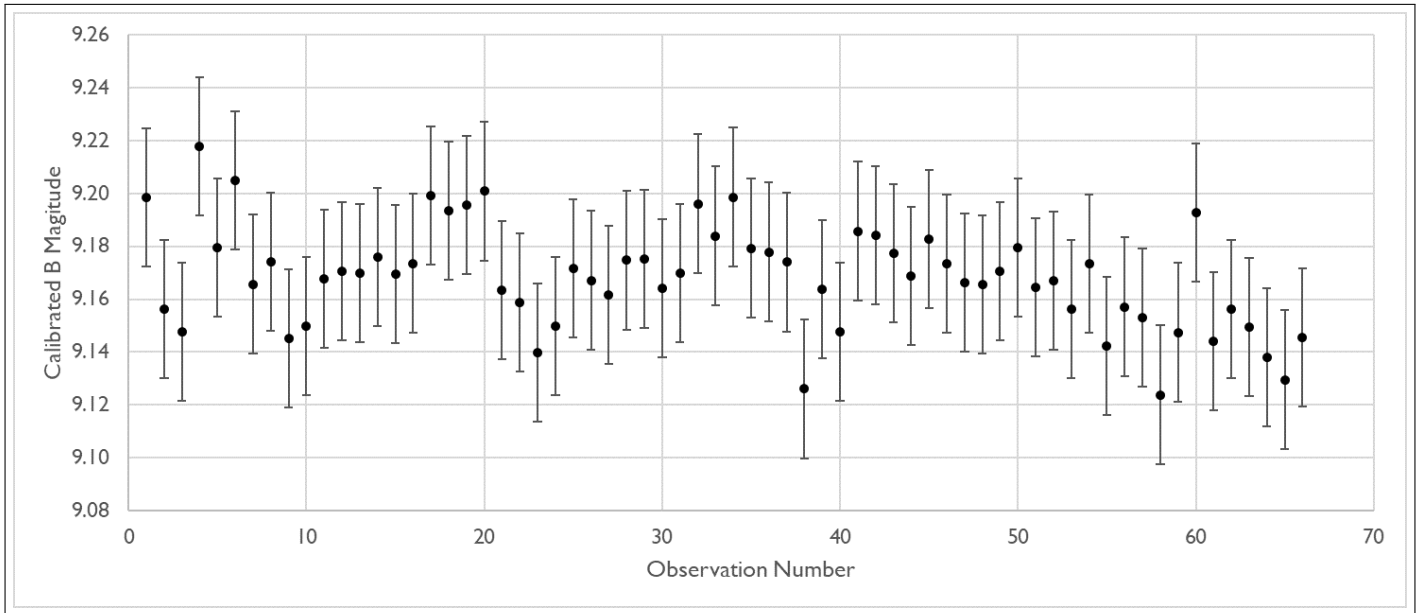


Fig. 3. Calibrated *B*-band magnitude for AW Mic from 66 DHO observations. The BJDs of the first and last observation shown are 2459072.10775511 and 2459078.27149761, respectively.

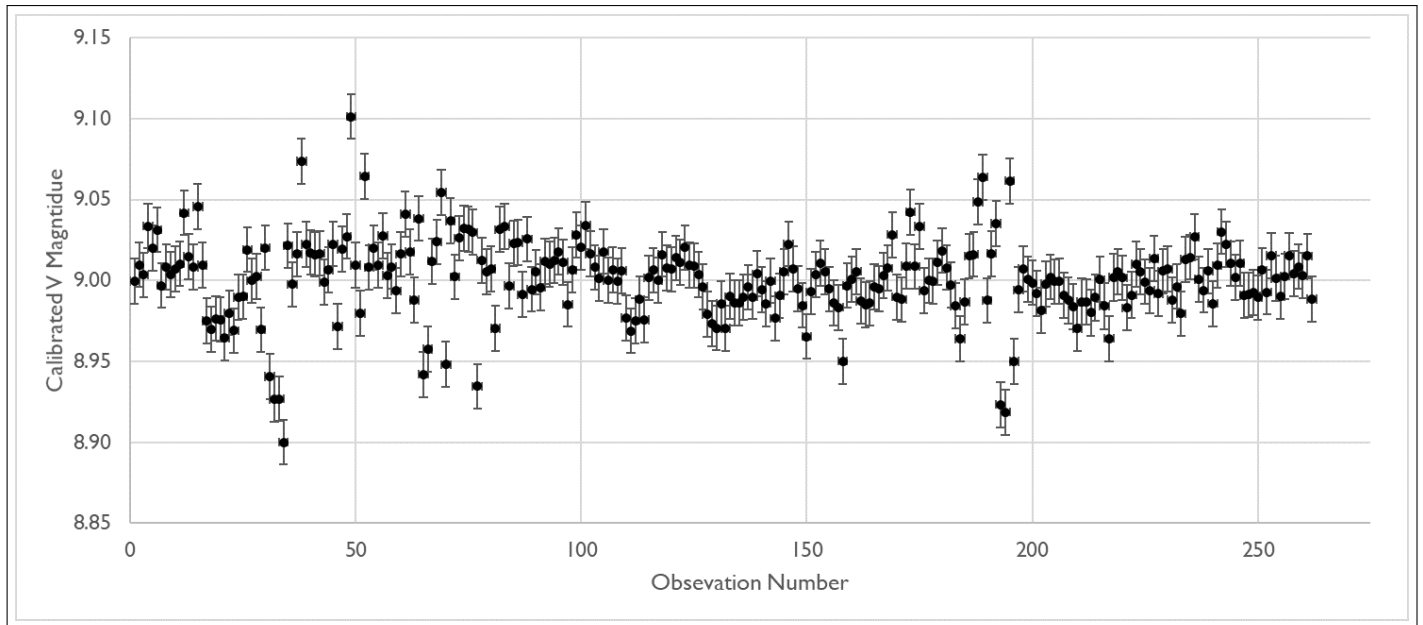


Fig. 4. Calibrated V-band magnitude for AW Mic from 262 DHO observations. The BJDs of the first and last observation shown are 2459072.08644584 and 2459078.27481956, respectively.

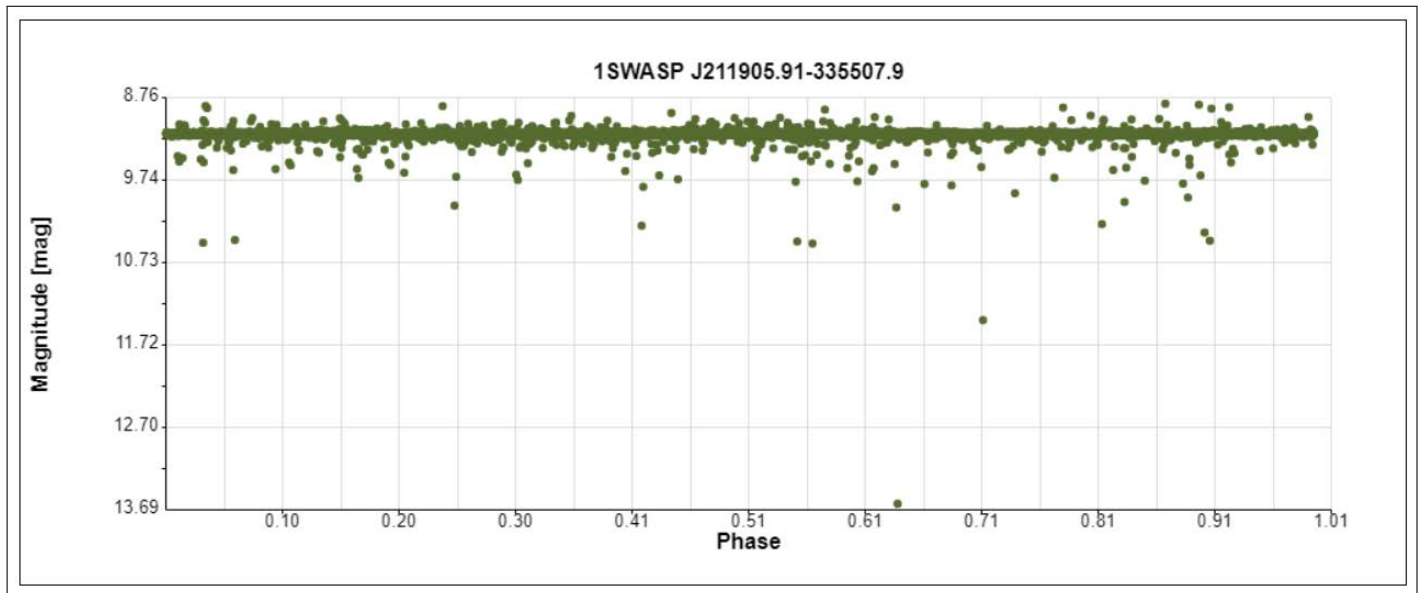


Fig. 5. Calibrated, phased light curve from SUPERWasp observations of RA: 319.77465/DEC: -33.918869, using AAVSO reported period of 0.3056840d (Butters et al., 2010), accessed on 12 October 2020.

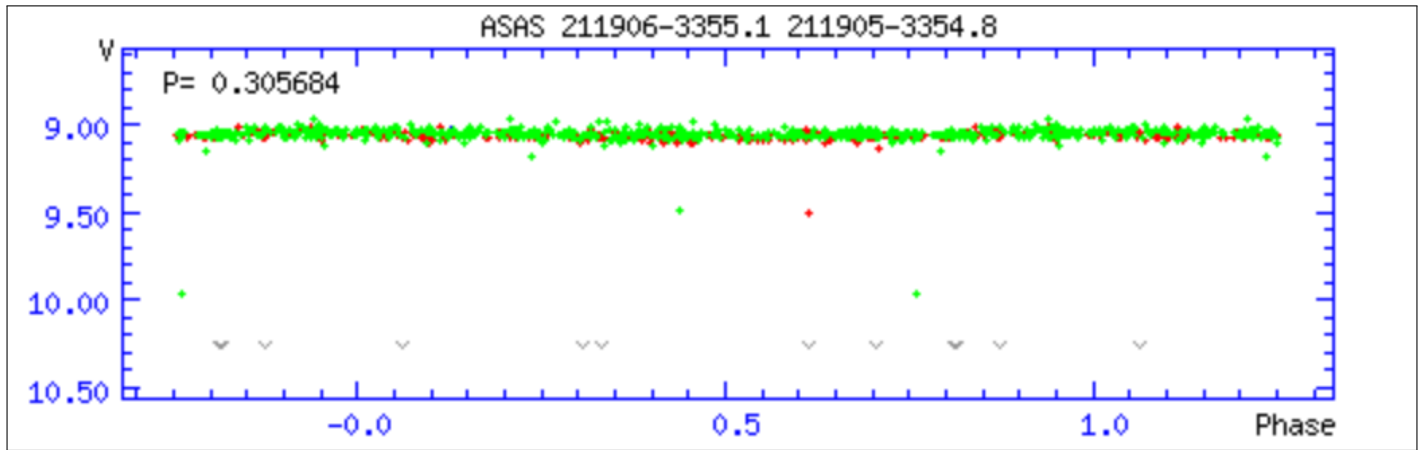


Fig. 6. Calibrated, phased light curve in V-band from ASAS observations, using AAVSO reported period of 0.305684d (Pojmanski & Maciejewski, 2005), accessed on 12 October 2020. Y-axis is calibrated magnitude.

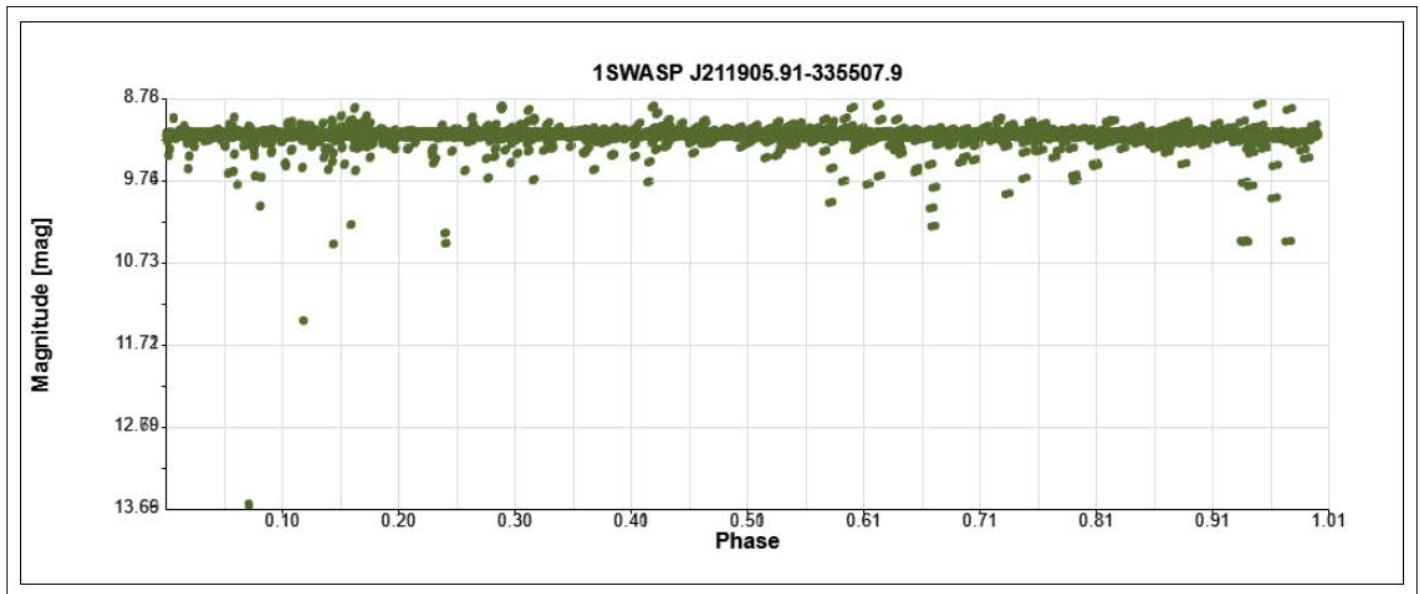


Fig. 7. Calibrated, phased light curve from SUPERWasp observations of RA: 319.77465/DEC: -33.918869 (Butters et al., 2010), using Przybylski and Bessel's (1974) reported period of 0.478d, accessed on 12 October 2020.

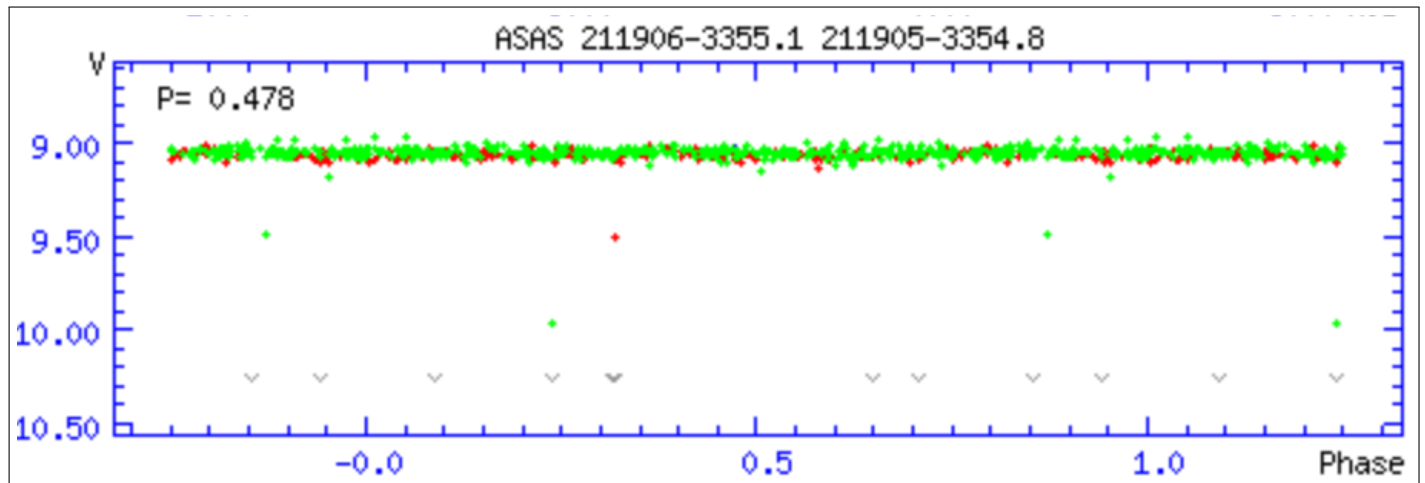


Fig. 8. Calibrated, phased light curve in V-band from ASAS observations (Pojmanski & Maciejewski, 2005), using Przybylski and Bessel's (1974) reported period of 0.478d, accessed on 12 October 2020. Y-axis is calibrated magnitude.

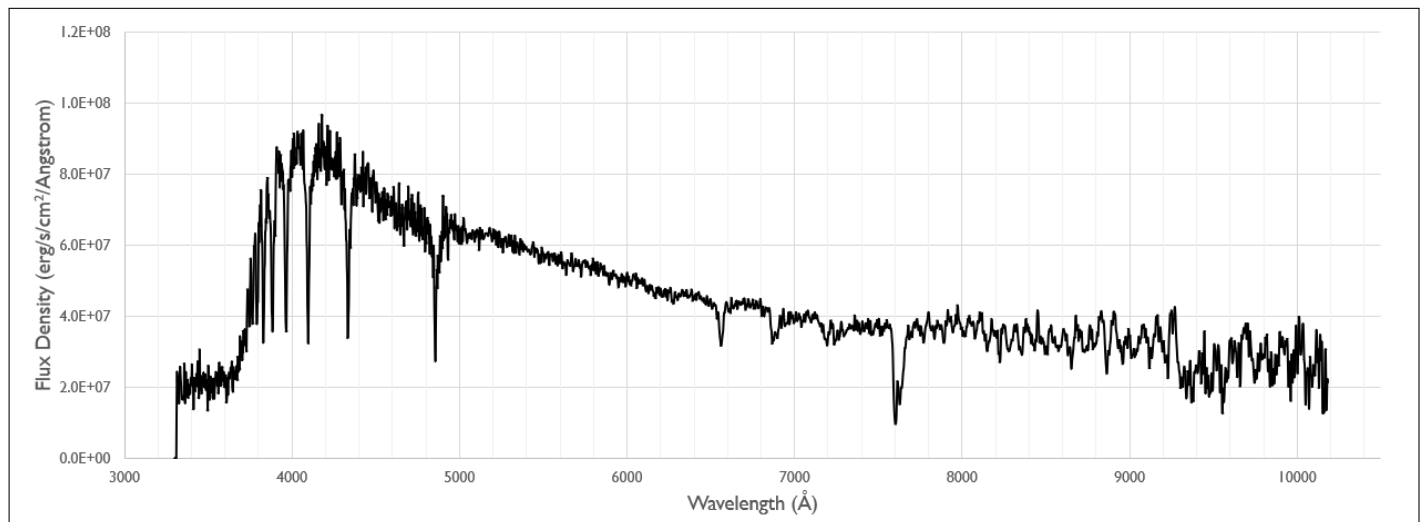


Fig. 9. FLOYDS spectrum of AW Mic from 3300Å to 10100Å.

- Cortés, C., Silva, J., Recio-Blanco, A., Catelan, M., Do Nascimento Jr, J., & De Medeiros, J. (2009). An overview of the rotational behavior of metal-poor stars. *The Astrophysical Journal*, 704(1), 750.
- Fitzgerald, M. (2018). The our solar siblings pipeline: Tackling the data issues of the scaling problem for robotic telescope based astronomy education projects.
- Fitzgerald, M. T., Gomez, E., Salimpour, S., Singleton, J., & Wibowo, R. W. (2021). “astrosources”: automating optical astronomy measurement, calibration and analysis for variable stellar sources from provided photometry. *Journal of Open Source Software*, 6(58), 2641.
- Gaia, C., Brown, A., Vallenari, A., Prusti, T., de Bruijne, J., Babusiaux, C., ... others (2018). Gaia data release 2 summary of the contents and survey properties. *Astronomy & Astrophysics*, 616(1).
- Henden, A. A., Templeton, M., Terrell, D., Smith, T. C., Levine, S., & Welch, D. (2016, January). VizieR Online Data Catalog: AAVSO Photometric All Sky Survey (APASS) DR9 (Henden+, 2016). *VizieR Online Data Catalog*, II/336.
- Jayasinghe, T., Stanek, K., Kochanek, C., Shappee, B., Holoién, T. W., Thompson, T. A., ... others (2019). The asas-sn catalogue of variable stars—ii. uniform classification of 412 000 known variables. *Monthly Notices of the Royal Astronomical Society*, 486(2), 1907–1943.
- Kafka, S. (2016). *Observations from the aavso international database*.
- Kinman, T., Castelli, F., Cacciari, C., Bragaglia, A., Harmer, D., & Valdes, F. (2000). A spectroscopic study of field bhb star candidates. *arXiv preprint astro-ph/0006179*.
- Kodaira, K., & Philip, A. (1984). High-dispersion spectroscopic investigation of field horizontal-branch, high-luminosity, and main-sequence stars. *The Astrophysical Journal*, 278, 208–214.
- Le Borgne, J., Paschke, A., Vandenbroere, J., Poretti, E., Klotz, A., Boër, M., ... Acerbi, F. (2007). Stellar evolution through the ages: period variations in galactic rrab stars as derived from the geos database and tarot telescopes. *Astronomy & Astrophysics*, 476(1), 307–316.
- MacConnell, D., Frye, R., Bidelman, W., & Bond, H. E. (1971). Discoveries on southern objective-prism plates. ii. new probable field horizontal-branch stars. *Publications of the Astronomical Society of the Pacific*, 83(491), 98.
- Pojmanski, G., & Maciejewski, G. (2005). The all sky automated survey. catalog of variable stars. iv. 18° h-24° h quarter of the southern hemisphere. *Acta Astronomica*, 55, 97–122.
- Przybylski, A., & Bessell, M. (1974). An unusual rrl yrae-type variable. *Publications of the Astronomical Society of the Pacific*, 86(512), 403.
- Samus', N., Kazarovets, E., Durlevich, O., Kireeva, N., & Pastukhova, E. (2017, 01). General catalogue of variable stars: Version gcvs 5.1. *Astronomy Reports*, 61, 80-88. doi:
- Shappee, B. J., Prieto, J., Grupe, D., Kochanek, C., Stanek, K., De Rosa, G., ... others (2014). The man behind the curtain: X-rays drive the uv through nrr variability in the 2013 active galactic nucleus outburst in ngc 2617. *The Astrophysical Journal*, 788(1), 48.
- The Dorothy Hill Observatory. (n.d.). Retrieved from <https://www.bggs.qld.edu.au/about-brisbane-girls-grammar/facilities/dorothy-hill-observatory/>
- Wilhelm, R., Beers, T. C., & Gray, R. O. (1999). Spectroscopy of hot stars in the galactic halo. ii. the identification and classification of horizontal-branch and other a-type stars. *The Astronomical Journal*, 117(5), 2308.

Observations of U Leporis

LARSON S. PAVEY, TYLER Z. SMITH, SAMUEL G. WYSS, AND MATTHEW P. PERKINS COPPOLA

Corresponding author: perkinsm@pfw.edu

U Leporis (U Lep) is a pulsating variable that demonstrates periodic variation in apparent magnitude consistent with RR Lyrae variable stars. Images were acquired by the 0.4 meter telescopes of the Las Cumbres Observatory Global Telescope network in the visible (B, V) and near infrared (i and z) over a two week period in October 2019 and analyzed using Astrosource. Light curves were constructed for each of the four bandpasses, yielding a mean period of 0.581 ± 0.011 days. The middle apparent magnitudes determined for the B, V, i, and z filters were 10.75, 10.55, 10.30, and 10.35 respectively. Color excess $E(B-V)$ was determined by two methods (1) minimizing variance in the calculated distances for the V, i, and z bands (0.065) and (2) galactic dust (0.029), with the second method preferred. Distances in parsecs to U Lep were determined for the V (968 ± 38), i (932 ± 33), and z (951 ± 38) filters. The average distance of 950 ± 21 compares favorably to that obtained by Klein (977 ± 8 pc) and less so to Gaia DR2 (1076 ± 36 pc).

© 2021 Astronomy Theory, Observations and Methods Journal

Keywords: Variables, RR Lyrae, notices — miscellaneous — catalogs — surveys

<https://doi.org/10.32374/atom.2020.2.3>

INTRODUCTION

U Leporis (U Lep) is a variable star which lies within the Milky Way Galaxy. U Leporis has a right ascension of 04h 56m 17.96 and Declination of $-21^{\circ} 13' 01.5$. This star is in the constellation of Lepus located just south of the celestial equator. Another name for U Lep is HIP22952 from the Hipparcos Star Catalogue.

RR Lyrae stars (RRL) are understood to be low-mass (0.6 to $0.8 M_{\odot}$) stars found at the intersection of the horizontal branch (HB) and the instability strip of the Hertzsprung-Russell diagram (Catelan & Smith, 2015). These older Population II (> 10 Gyr) giant ($4-6 R_{\odot}$) stars, post-helium flash, are able to fuse

helium in their cores as hydrogen fusion occurs in a shell surrounding the core. RR Lyrae stars were first used to determine the distance to globular clusters, though today more RR Lyrae stars are known in other parts of the Milky Way galaxy and are used to study the structure of the Galactic halo (Keller, Murphy, Prior, DaCosta, & Schmidt, 2008; Hernitschek et al., 2018; Iorio & Belokurov, 2018; Wegg, Gerhard, & Bieth, 2019), bulge (Du, Mao, Athanassoula, Shen, & Pietrukowicz, 2020; Soszyński et al., 2019), and the thick disk (Mateu & Vivas, 2018). Others are using RRL to study metallicity and other details within nearby galaxies (Clementini et al., 2001; Sarajedini, Barker, Geisler, Harding, & Schommer, 2006).

RRL pulsate radially with periods between 1.5 to 24 hours and are divided into two classes. RRab stars pulsate in the fundamental radial mode with a light curve resembling an inverted sawtooth wave, rising rapidly then gradually fading to minimum. RRC stars pulsate in the first-overtone radial mode, producing a light curve resembling a sinusoidal pattern. The pulsation in both types is the result of layers of stellar material falling inward, compressing layers of gases found deeper within the star. At some depth a layer of hydrogen gas partially ionizes rather than increasing in temperature. Deeper still inside the star, compression forms a layer of partially ionized helium II. The opacity κ of these layers is directly proportional to the density ρ and inversely proportional to the temperature T raised to the 3.5 power, a relationship known as Kramer's Law.

$$\kappa \propto \frac{\rho}{T^{3.5}}$$

The steady temperature and increasing density of these partially ionized layers increases the opacity, allowing them to act as a blanket over the layers of gas beneath. Contraction continues until a build up of heat under the blanketed areas forces an expansion. During this outward movement the blanket expands, cools, and becomes less opaque, allowing the trapped heat to escape outward. This mechanism causes the radius of the star to vary, thus varying the surface area and luminosity of the star.

When the effective surface temperature of the star is between 5500K and 7500K, referred to as the "instability strip," the location of these partially ionized layers of hydrogen and helium II is just right to drive stable periodic oscillations. Hotter stars form partially ionized layers too close to the surface, while cooler stars form partial ionization zones deeper in the star, where convection prevents heat from building up to cause expansion.

RRL stars are useful standard candles for determining distances but, unlike Cepheid variables, the period-luminosity relation they display is not so straightforward (Catelan, Pritzl, & Smith, 2004). It appears the metallicity [Fe/H] of the star must be factored into the determination of distance. Until the recent Gaia mission, distances to most known RRL were too far to be determined accurately by spectroscopic parallax (Catelan & Smith, 2015). Previous calibrations derived from the Sloan Digital Sky Survey (C  ceres & Catelan, 2008) for the near infrared i and z bandpasses suggest a reliable period-luminosity-

metallicity relationship exists. This research project observes a single RRL at B, V, i, z bandpasses to compare the calibrations to parallax measures determined by Gaia and previous observations.

U Lep is a class RRab variable. Previous light curve measurements using Hipparcos data determined a period for U Lep of 0.581236 days (Wu, Qiu, Deng, Hu, & Zhao, 2006) to 0.581479 days (Feast, Laney, Kinman, Van Leeuwen, & Whitelock, 2008). Klein et al. (2011) used this period and the preliminary data release of the Wide-field Infrared Survey Explorer (WISE) to determine a distance of 976.8 pc to U Lep. Gaia DR2 (A. Brown et al., 2018) as accessed through Simbad (Wenger et al., 2000) yielded a corrected parallax of 0.9298 ± 0.0276 mas, for a distance of 1076 ± 36 pc.

OBSERVATIONS

The Las Cumbres Observatory Global Telescope Network (LCOGT) was used to observe the target variable star, U Lep, in the B, V, i, and z bandpasses. The 0.4-meter SBIG telescopes at multiple LCOGT nodes provided images with a field of view of 19'x29' (T. Brown et al., 2013) (<https://lco.global/observatory/telescopes/0-4m/>). Figure 1 is a representative sample from the data set.



Fig. 1. A picture of U Leporis (center) taken with the 0.4-meter SBIG

First, a set of test images was obtained to determine the optimal exposure time to view U Lep for each of the four bandpasses. Each test image was examined in AstroImageJ, using the aperture tool to measure the number of counts for the target star. The number of counts for each pixel is proportional to

the number of photons received during the exposure. Incoming photons strike the CCD, liberating electrons (e-) via the photoelectric effect, which are then collected by a capacitor. The voltage of the capacitor is converted by an Analog-To-Digital unit. The SBIG STL-6303 at the LCOGT were set for a gain (e-/ADU) of 1.6. Remembering that U Lep varies in magnitude, an acceptable range of counts was established to be between 25,000 and 250,000 and the value of 200,000 was chosen for determining the optimal exposure time. For each bandpass, the ratio of the optimal and test image exposure times was set equal to the ratio of the desired counts (200,000) and those measured for the test image. The exposure times used for each band are summarized in Table 1.

Table 1. Exposure times for different color bands.

Band	Wavelength Center (Å)	Exposure (s)
B	4361	28.4
V	5448	12
i	7545	16.2
z	8700	62

Data was collected over the course of twelve days from October 02 to October 14, 2019. The LCOGT was used to request 75 observations of our target star. The goal was to have at least 50 points of data to evaluate for each bandpass. Requesting more observations than the goal was necessary for two reasons. First, there were windows of time during which an observation might not be able to be scheduled. Despite the availability of multiple telescopes across the globe, the target star might be too low on the horizon to be viewed by any telescope in the network. Of the 75 requested observations, only 59 were able to be scheduled within the range of dates. Second, more are requested to minimize the impact of expired observation windows, or failed observations. Windows of observation expire due to weather events or equipment failures at a particular site. At the end of the observation window, 50 observations were completed with only 9 failures.

METHODS

The photometric data produced by the Our Solar Siblings pipeline (M. Fitzgerald, 2018) was processed using Astrosource (M. T. Fitzgerald, Gomez, Salimpour,

Singleton, & Wibowo, 2021). The first step in this process was to identify the exact galactic coordinates for the target star. This was accomplished by loading the .fits files for each respective filter into Aladin. Changing the frame to ICRSd for decimal coordinates gave us the required position to enter into Astrosource. This information must be entered with each filter to ensure the location of the star is correct for the rest of the program.

The images were then run through a filter to locate stars that could be seen in each picture with an acceptable brightness. The accepted range in counts by Astrosource was 2000-1000000. This was done to ensure there were brightness comparisons to use for the observed variable star (U Lep). The variability of the remaining stars was then measured. The goal was to identify the least variable of the remaining candidate stars to use as comparisons for U Lep. The location data for the least variable comparison stars was then used to identify known stars within the set. Depending on the bandpass, locations were cross-referenced with Skymapper (Wolf et al., 2018) or APASS (Henden et al., 2016) and the magnitude of the comparison stars was determined.

In order to obtain the light curve from the data set, the variability in magnitude was found. This was done by using the comparison stars to measure the difference in magnitude compared to the target star. The last part of the program calculates the period. This was done by testing several values for the period and looking for the most likely candidate. The data taken over the course of 12 days was tested for varying periods until a light curve could be found.

RESULTS

After taking data over the course of two weeks from October 02, 2019 to October 14, 2019, we confirmed the period of U Lep to be 0.581 days with an error of 0.011 days. This value was calculated by taking the mean of our period and error measurements for each band. The resulting period was consistent with those reported in the literature, including Hipparcos 0.581474 (Agency, 1997), 0.581479 (Feast et al., 2008), and 0.5814762 days (Kazarovets, Durlevich, Kireeva, Pastukhova, et al., 2017). The final periods, as calculated for each bandpass, was noted in Table 2.

U Leporis completed 20.6 cycles of variation during the 12 day observation window. Astrosource generated four phased light curves from the data collected,

Table 2. Period from each filter used.

Band	Period (d)	Error (d)
B	0.58276	0.01050
V	0.58006	0.01208
i	0.58106	0.01053
z	0.58101	0.01225

as seen in Figure 2. The shape of each light curve (a sharp peak followed by a gradual decline) was consistent with those of other RRab-type RRL variables, which pulsate in the fundamental radial mode (Catelan & Smith, 2015).

The resulting data lists several apparent magnitudes for each filter taken over the course of 12 days of observation. Table 3 shows the range and amplitude of apparent magnitudes for each band.

Table 3. Variation in apparent magnitude.

Band	Min	Mid	Max	Amp
B	11.53	10.75	9.96	1.57
V	11.08	10.55	10.01	1.06
i	10.82	10.30	9.77	1.04
z	10.76	10.35	9.93	0.83

Table 3 and Figure 2 reveal two trends in the light curves related to bandpass. First, the minimum apparent magnitude brightens as the peak wavelength of the bandpass increases. This trend is consistent with the idea that galactic reddening and metallicity increase apparent magnitudes of visible bandpasses more than near infrared. Second, the amplitude of the variation decreases as the peak wavelength of the bandpass increases. Both trends are consistent with observations of other RRL (Catelan & Smith, 2015).

Calibrations for V, i, and z (Catelan et al., 2004; Cáceres & Catelan, 2008) and established metallicity ($[\text{Fe}/\text{H}] = -1.93$) (Dambis et al., 2013) were used to determine the distance to U Lep. Two methods were attempted and compared in order to account for reddening. The first of these, minimized variance, was based on the fact that the distance to U Lep should be the same regardless of filter. The value for color excess was adjusted until the standard deviation of

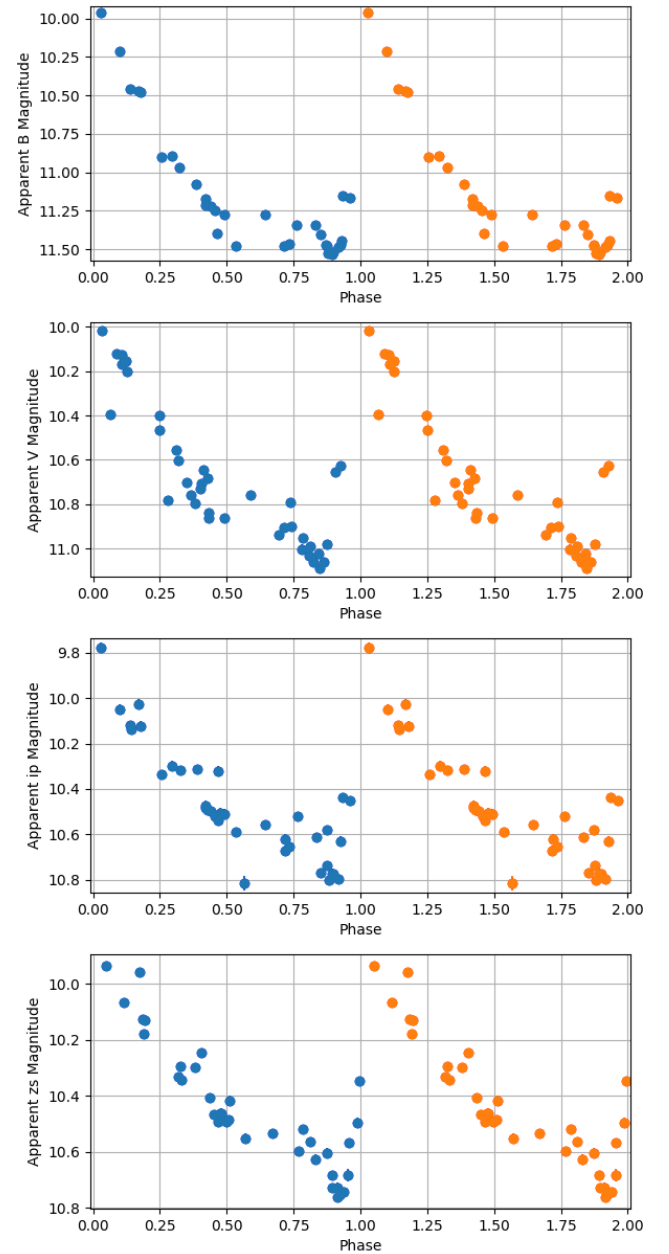


Fig. 2. Light curves taken from the four different bands that were observed. One 'phase' on the x axis is equivalent to the calculated period for each band respectively.

the distances predicted by calibrations of the V, i, z filters was minimized. Trial and error yielded a value of $E(B-V)=0.065$. The second method employed estimates of Galactic dust extinction of the Sloan Digital Sky Survey (Schlafly & Finkbeiner, 2011). The mean color excess was determined to be $E(B-V) = 0.0290 \pm 0.0015$. This value was less than half the value suggested by the first method.

The distances determined for each bandpass and

by each method are reported in Table 4 and shown visually in Figure 3. The average distances based on minimized variance and by mean galactic dust were determined to be 903 ± 20 pc and 938 ± 21 pc respectively.

Table 4. Distance to U Lep for each bandpass.

Band	variance		SDSS	
	Dist (pc)	Error (pc)	Dist (pc)	Error (pc)
V	926	37	968	38
i	904	33	932	33
z	930	37	951	38
AVG	920	20	950	21

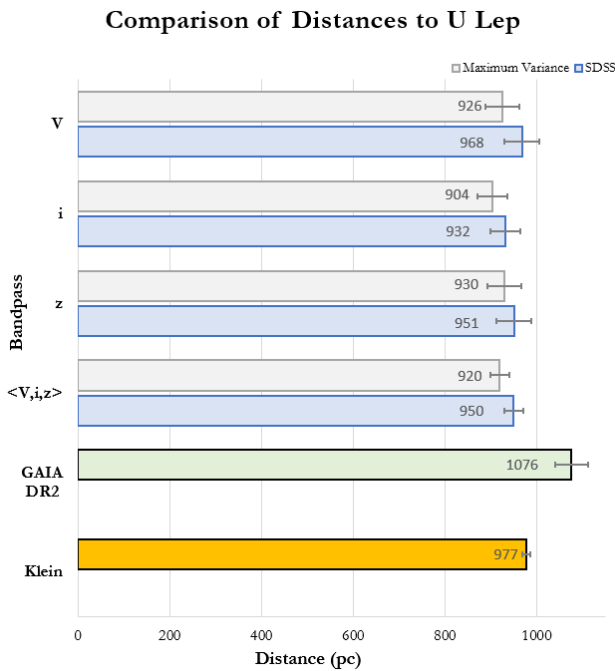


Fig. 3. Distances to U Lep for each bandpass using two different models for extinction.

DISCUSSION

The determined periods from light curves taken through four filters are consistent with one another and previously established values. The three calibration models for V, i, and z provided distances to U Lep that were inconsistent with one another and with Gaia and Klein.

Adjusting the color excess to minimize the variance reduced the inconsistencies within the filters but led to a reddening factor that exceeds estimates based on previous measurements of galactic dust by a factor of two. This method also widened the gap between the mean of the three distances and Gaia to 156 pc or 16 % closer to Earth.

Using the mean galactic reddening yielded an average distance only about 12% less than that determined by parallax using the Gaia DR2 data (1076 ± 36 pc). The mean distance of 950 ± 21 pc was closer to the distance of 977 ± 8.3 pc determined by Klein (2011) using data from WISE. The distances for V and z are within one standard deviation of this mark.

The calibrations used in this study were based on the realization that the Horizontal Band is not horizontal toward the near-infrared i and z (Catelan et al., 2004; Catelan & Smith, 2015) and thus a period-luminosity (PL) relationship could be determined:

$$M_V = 2.288 - 0.882 \log Z + 0.108(\log Z)^2$$

$$M_i = 0.908 - 1.035 \log P + 0.220 \log Z$$

$$M_z = 0.839 - 1.295 \log P + 0.211 \log Z$$

where

$$\log Z = [Fe/H] + \log(0.638f + 0.362)$$

and

$$f = 10^3$$

The calibrations for i and z were determined through an extensive analysis of the Sloan Digital Sky Survey, with strong correlation coefficients for each ($r_i=0.95$, $r_z=0.97$). For U Lep the calculated period and calibrated magnitudes determined for i and z yielded distances well within the estimated error range, each of which are less than 4% of the determined distances.

One curiosity was that the observed apparent magnitudes did not follow the anticipated trend of increase as wavelength decreased. The middle magnitude of the i bandpass (10.30) is slightly less than that measured for z (10.35). This quirk led the distance estimated based on the i bandpass (904 pc) to be the shortest of the three (926 pc and 930 pc for V and z, respectively). The minimized variance method brought the V and z estimates to within 4 pc of one another but failed to close the much larger gap between i and V (22 pc). The trend in decreased amplitude of apparent magnitude with increasing wavelength was not disrupted, however the amplitude variations for V (1.06) and i (1.04) were almost identical.

CONCLUSION

The four light curves generated for U Lep were consistent with those expected for class RRab stars and with previously reported observations of U Lep. The mean period of 0.581 ± 0.011 days was consistent with previously reported measurements. Distances to U Lep were calculated for each bandpass using calibrations for V (Catelan et al., 2004) and i and z (Cáceres & Catelan, 2008). Magnitudes were adjusted for color excess using two methods: (1) minimizing variance and (2) mean galactic reddening based on the Sloan Digital Sky Survey. The first method yielded distances in parsecs for V, i, z of 926 ± 37 , 904 ± 33 , and 930 ± 37 , for an average of 920 ± 20 . The second method yielded distances in parsecs for V, i, z of 968 ± 38 , 932 ± 33 , and 951 ± 38 , for an average of 950 ± 21 . These distances to U Lep were closer to those determined using Hipparcos data adjusted for galactic reddening (Klein et al., 2011) than to the more precise parallax measures determined by Gaia (A. Brown et al., 2018).

The lack of agreement in the distances suggests errors either in the Gaia DR2 measures or in the empirically determined period-luminosity relationships for near infrared i and z. The difference of 12% between the SDSS and Gaia DR2 measurements is greater than the error estimates would bridge but is not an obscene difference. Application of the two methods to a larger set of RRL variables is necessary to better understand the significance in the difference in estimated distances.

ACKNOWLEDGMENTS

This work makes use of observations from the LCOGT network. This research has made use of "Aladin sky atlas" (Bonnarel et al., 2000; Boch & Fernique, 2014) and the SIMBAD database (Wenger et al., 2000) developed at CDS, Strasbourg Observatory, France. This research used Astrosource 1.1.1, developed by Michael Fitzgerald and Edward Gomez, to identify comparison stars in the images <https://pypi.org/project/astrosource>.

REFERENCES

- Agency, E. S. (1997). *The hipparcos and tycho catalogues: astrometric and photometric star catalogues derived from the esa hipparcos space astrometry mission. 11. hipparcos variability annex: periodic and unsolved variables and spectral types*. ESA Publ. Division.
- Boch, T., & Fernique, P. (2014). Aladin lite: Embed your sky in the browser. In *Astronomical data analysis software and systems xxiii* (Vol. 485, p. 277).
- Bonnarel, F., Fernique, P., Bienaymé, O., Egret, D., Genova, F., Louys, M., ... Bartlett, J. G. (2000). The aladin interactive sky atlas-a reference tool for identification of astronomical sources. *Astronomy and Astrophysics Supplement Series*, 143(1), 33–40.
- Brown, A., Vallenari, A., Prusti, T., De Bruijne, J., Babusiaux, C., Bailer-Jones, C., ... others (2018). Gaia data release 2-summary of the contents and survey properties. *Astronomy & astrophysics*, 616, A1.
- Brown, T., Baliber, N., Bianco, F., Bowman, B. B., M., Conway, P., Crellin, M., ... et al. (2013). Las cumbres observatory global telescope network. *Publications of the Astronomical Society of the Pacific*, 125, 1031-1055.
- Catelan, M., Pritzl, B. J., & Smith, H. A. (2004). The RR Lyrae period-luminosity relation. i. theoretical calibration..
- Catelan, M., & Smith, H. A. (2015). *Pulsating stars*. Wiley-VCH.
- Clementini, G., Federici, L., Corsi, C., Cacciari, C., Bellazzini, M., & Smith, H. A. (2001). Rr lyrae variables in the globular clusters of m31: a first detection of likely candidates. *The Astrophysical Journal Letters*, 559(2), L109.
- Cáceres, C., & Catelan, M. (2008, Nov). The period-luminosity relation of RR Lyrae stars in the SDSS photometric system. *The Astrophysical Journal Supplement Series*, 179(1), 242–248. Retrieved from <http://dx.doi.org/10.1086/591231>
- Dambis, A. K., Berdnikov, L. N., Kniazev, A. Y., Kravtsov, V. V., Rastorguev, A. S., Sefako, R., & Vozyakova, O. V. (2013, 09). RR Lyrae variables: visual and infrared luminosities, intrinsic colours and kinematics. *Monthly Notices of the Royal Astronomical Society*, 435(4), 3206-3220. Retrieved from <https://doi.org/10.1093/mnras/stt1514>
- Du, H., Mao, S., Athanassoula, E., Shen, J., & Pietrukowicz, P. (2020). Kinematics of rr lyrae stars in the galactic bulge with ogle-iv and gaia dr2. *Monthly Notices of the Royal Astronomical*

- Society*, 498(4), 5629–5642.
- Feast, M. W., Laney, C. D., Kinman, T. D., Van Leeuwen, F., & Whitelock, P. A. (2008). The luminosities and distance scales of type II Cepheid and RR Lyrae variables. *Monthly Notices of the Royal Astronomical Society*, 386(4), 2115–2134.
- Fitzgerald, M. (2018). The our solar siblings pipeline: Tackling the data issues of the scaling problem for robotic telescope based astronomy education projects.
- Fitzgerald, M. T., Gomez, E., Salimpour, S., Singleton, J., & Wibowo, R. W. (2021). “astrosource”: automating optical astronomy measurement, calibration and analysis for variable stellar sources from provided photometry. *Journal of Open Source Software*, 6(58), 2641.
- Henden, A. A., Templeton, M., Terrell, D., Smith, T. C., Levine, S., & Welch, D. (2016, January). VizieR Online Data Catalog: AAVSO Photometric All Sky Survey (APASS) DR9 (Henden+, 2016). *VizieR Online Data Catalog*, II/336.
- Hernitschek, N., Cohen, J. G., Rix, H.-W., Sesar, B., Martin, N. F., Magnier, E., ... others (2018). The profile of the galactic halo from pan-starrs1 3π rr lyrae. *The Astrophysical Journal*, 859(1), 31.
- Iorio, G., & Belokurov, V. (2018, 10). The shape of the Galactic halo with Gaia DR2 RR Lyrae. Anatomy of an ancient major merger. *Monthly Notices of the Royal Astronomical Society*, 482(3), 3868–3879. Retrieved from <https://doi.org/10.1093/mnras/sty2806> doi:
- Kazarovets, E., Durlevich, O., Kireeva, N., Pastukhova, E., et al. (2017). General catalogue of variable stars: Version gcvs 5.1. *Astronomy Reports*, 61(1), 80–88.
- Keller, S. C., Murphy, S., Prior, S., DaCosta, G., & Schmidt, B. (2008). Revealing substructure in the galactic halo: the sekbo rr lyrae survey. *The Astrophysical Journal*, 678(2), 851.
- Klein, C. R., Richards, J. W., Butler, N. R., & Bloom, J. S. (2011). Mid-infrared period-luminosity relations of RR Lyrae stars derived from the WISE preliminary data release. *The Astrophysical Journal*, 738(2), 185.
- Mateu, C., & Vivas, A. K. (2018). The galactic thick disc density profile traced with rr lyrae stars. *Monthly Notices of the Royal Astronomical Society*, 479(1), 211–227.
- Sarajedini, A., Barker, M., Geisler, D., Harding, P., & Schommer, R. (2006). Rr lyrae variables in m33. i. evidence for a field halo population. *The Astronomical Journal*, 132(3), 1361.
- Schlafly, E. F., & Finkbeiner, D. P. (2011). Measuring reddening with sloan digital sky survey stellar spectra and recalibrating sfid. *The Astrophysical Journal*, 737(2), 103.
- Soszyński, I., Udalski, A., Wrona, M., Szymański, M., Pietrukowicz, P., Skowron, J., ... others (2019). Over 78 000 rr lyrae stars in the galactic bulge and disk from the ogle survey. *arXiv preprint arXiv:2001.00025*.
- Wegg, C., Gerhard, O., & Bieth, M. (2019, 02). The gravitational force field of the Galaxy measured from the kinematics of RR Lyrae in Gaia. *Monthly Notices of the Royal Astronomical Society*, 485(3), 3296–3316. Retrieved from <https://doi.org/10.1093/mnras/stz572> doi:
- Wenger, M., Ochsenbein, F., Egret, D., Dubois, P., Bonnarel, F., Borde, S., ... Monier, R. (2000, Apr). The SIMBAD astronomical database. The CDS reference database for astronomical objects. *aaps*, 143, 9–22. doi:
- Wolf, C., Onken, C. A., Luvaul, L. C., Schmidt, B. P., Bessell, M. S., Chang, S.-W., ... others (2018). Skymapper southern survey: first data release (dr1). *Publications of the Astronomical Society of Australia*, 35.
- Wu, C., Qiu, Y., Deng, J., Hu, J., & Zhao, Y. (2006). [Fe/H] derived from the light curves of RR Lyrae stars in the Galactic halo. *Astronomy & Astrophysics*, 453(3), 895–902.

Original Research By Young Twinkle Students (ORBYTS): Ephemeris Refinement of Transiting Exoplanets III

**BILLY EDWARDS^{1,2,†,*}, CYNTHIA S. K. HO^{3,*}, HANNAH L. M. OSBORNE^{3,*},
NABEEHA DEEN^{4,*}, ELLIE HATHORN^{4,*}, SOLOMON JOHNSON^{4,*}, JIYA
PATEL^{4,*}, VARUN VOGIREDDY^{4,*}, ANSH WADDON^{4,*}, AYUUB AHMED^{5,*},
MUHAMMAD BHAM^{5,*}, NATHAN CAMPBELL^{5,*}, ZAHRA CHUMMUN^{5,*},
NICHOLAS CROSSLEY^{5,*}, REGGIE DUNSDON^{5,*}, ROBERT HAYES^{5,*}, HAROON
MALIK^{5,*}, FRANK MARSDEN^{5,*}, LOIS MAYFIELD^{5,*}, LISTON MITCHELL^{5,*},
AGNES PROSSER^{5,*}, VALENTINA RABRENOVIC^{5,*}, EMMA SMITH^{5,*}, RICO
THOMAS^{5,*}, ANASTASIA KOKORI¹, ANGELOS TSIARAS¹, MARCELL
TESSENYI^{2,1}, GIOVANNA TINETTI^{1,2}, AND JONATHAN TENNYSON^{1,2}**

¹Department of Physics and Astronomy, University College London, Gower Street, London, WC1E 6BT, United Kingdom

²Blue Skies Space Ltd., 69 Wilson Street, London, EC2A 2BB, United Kingdom

³Mullard Space Science Laboratory, University College London, Holmbury St. Mary, Dorking, RH5 6NT, United Kingdom

⁴London Academy of Excellence, 322 High Street, London, E15 1AJ, United Kingdom

⁵Highams Park School, Handsworth Avenue, London, E4 9PJ, United Kingdom

[†]Corresponding author: billy.edwards.16@ucl.ac.uk

*These authors contributed equally to this work.

Received November 1, 2021

We report photometric follow-up observations of thirteen exoplanets (HATS-1 b, HATS-2 b, HATS-3 b, HAT-P-18 b, HAT-P-27 b, HAT-P-30 b, HAT-P-55 b, KELT-4A b, WASP-25 b, WASP-42 b, WASP-57 b, WASP-61 b and WASP-123 b), as part of the Original Research By Young Twinkle Students (ORBYTS) programme. All these planets are potentially viable targets for atmospheric characterisation and our data, which were taken using the LCOGT network of ground-based telescopes, will be combined with observations from other users of ExoClock to ensure that the transit times of these planets continue to be well-known, far into the future.

© 2021 Astronomy Theory, Observations and Methods Journal

Keywords: exoplanets, transit photometry, ground-based telescopes, HATS-1 b, HATS-2 b, HATS-3 b, HAT-P-18 b, HAT-P-27 b, HAT-P-30 b, HAT-P-55 b, KELT-4A b, WASP-25 b, WASP-42 b, WASP-57 b, WASP-61 b, WASP-123 b

<https://doi.org/10.32374/atom.2020.2.4>

INTRODUCTION

A Brief History of Exoplanet Detections

The concept of extrasolar planets, worlds which orbit other stars, has existed since at least the era of the Ancient Greeks, with Democritus and Epicurus believing in the idea that there existed an infinite amount of worlds, some of which possessed their own organisms. Much later, Italian cosmological theorist Giordano Bruno encouraged the idea that the countless stars were other suns which could each host planets similar to those in our own Solar System. Additionally, he reinforced the idea that there are other inhabited worlds that exist in the universe. After Neptune was mathematically predicted (Le Verrier, 1846) and then successfully detected (Galle, 1846), attention turned to applying these methods to searching for planets around other stars.

A number of different detection techniques were devised and several detection claims were made (Jacob, 1855; See, 1896; van de Kamp, 1969), each of which in turn was shown to be spurious (Sherrill, 1999; Boss, 2009). The effectiveness of several of the detection techniques were underestimated due to the expectation that other planetary systems would resemble our own. While many early efforts focused on astrometry, studying the perturbations in the positions of stars, the radial velocity method, which uses Doppler shifts in the star light to infer the presence of a companion, delivered the first detection of a planetary body around a main-sequence star: 51 Pegasi b (Mayor & Queloz, 1995). Several years prior to this, a planetary system had been detected around a pulsar via precise timing measurements of the pulses (Wolszczan & Frail, 1992) and a previous potential detection of a planetary body around Gamma Cephei (Campbell et al., 1988) was later verified (Hatzes et al., 2003).

After the discovery of 51 Pegasi b, numerous other detections were made using the radial velocity method, with many of these being worlds which are now referred to as hot Jupiters, large planets that have orbital periods of less than around 10 days. Notably, it had been argued more than 40 years earlier that, with the best spectrographs available at the time, such planets could be detected by the radial velocity method (Struve, 1952). While the radial velocity method can provide the mass and period of the planet, the radius cannot be determined. However, if the geometry of the system is aligned in the correct way, the planet can be seen to pass between the observer

and its host star (a planetary *transit*). The decrease in the flux is dependent upon the ratio of the planet's and the star's radii and thus provides a key planetary characteristic. Additionally, when combined with radial velocity data a constraint on the density can be placed and, in some cases, the bulk composition inferred. Therefore, many studies searched for transits of these planets with HD 209458 b being the first planet to be seen to occult its host star (Charbonneau et al., 2000; Henry et al., 2000).

Current Status

Since these early detections, there has been a rapid increase in the number of known exoplanets, with over 4400 having been identified by September 2021. While many different methods have been successfully used to detect planets, the most lucrative thus far has been the transit technique, with a number of ground-based and space-based surveys contributing to this deluge of detections. Indeed, of the exoplanets discovered to date, around 75.5% have been detected using the transit method¹. The Kepler space telescope is perhaps the most famous and influential transit survey, contributing more than 2500 planets and many more candidates (Borucki et al., 2010). The most recent major exoplanet discovery mission to be launched is the Transiting Exoplanet Survey Satellite (TESS). Beginning operations in mid-2018, this mission is surveying hundreds of thousands stars across the entire sky (Ricker et al., 2015) and has already been successful in finding nearly 4400 candidate signals as well as confirming the existence of over 120 exoplanets².

Many of the planets found by TESS will be around bright stars, making them amenable for further characterisation. While current ground-based and space-based facilities have begun characterising the atmospheres of a handful of exoplanets, it is the next generation of facilities that offer the opportunity to truly move into an era of characterisation. The future of space-based facilities is especially promising and the imminent launch of the James Webb Space Telescope (JWST) is eagerly anticipated, with several programmes dedicated to studying transiting exoplanets (e.g. Bean et al., 2018). Furthermore, Twinkle³, an upcoming, 0.45 m space-based telescope, will conduct a dedicated extrasolar survey which will include the characterisation of many exoplanetary atmospheres

¹https://exoplanetarchive.ipac.caltech.edu/docs/counts_detail.html

²<https://tess.mit.edu/publications/>

³<https://www.twinkle-spacemission.co.uk/>

(Edwards, Rice, et al., 2019). Finally, Ariel is the M4 mission in ESA's Cosmic Vision programme which is scheduled to launch in 2029. Ariel will investigate the atmospheres of over 1000 transiting exoplanets using visible and near-infrared spectroscopy (Tinetti et al., 2018, 2021).

These three facilities, in addition to continued observations from the ground and with Hubble, offer a golden future for characterising transiting exoplanets. However, the next generation of telescopes will require rigorous scheduling to minimise overheads and maximise science outputs. As such, interesting science targets could see their observing priority degraded if their ephemerides are not accurate enough, even if they are excellent targets for atmospheric characterisation. Many currently known planets have large ephemeris uncertainties and analysis suggests many TESS targets will have errors of >30 minutes less than a year after discovery due to the short baseline of TESS observations (Dragomir et al., 2020). Therefore, detections by this mission, as well as other transiting planets, will have to be regularly followed-up to ensure their ephemerides remain well-known (Kokori et al., 2021; Zellem et al., 2020).

Aims of the Project

Our project was undertaken as part of the Original Research By Young Twinkle Students (ORBYTS) programme, which unites academic researchers with secondary school students. As part of the programme, pupils work on original research linked to space science (Sousa-Silva et al., 2018). Since the programme's foundation in 2016, over 150 school students have published research in academic journals through ORBYTS. The topic of this research has varied, from calculating empirical molecular energy levels (McKemmish et al., 2017, 2018; Chubb, Joseph, et al., 2018; Chubb, Naumenko, et al., 2018; Darby-Lewis et al., 2019), analysing data of our Sun from the Hinode spacecraft (French et al., 2020) or studying protostellar outflows (Holdship et al., 2019), to counting craters on Mars (Francis et al., 2020), monitoring X-rays from Jupiter's Auroras (Wibisono et al., 2020) and active galactic nuclei (Grafton-Waters et al., 2021).

In this project, we continued the work of previous ORBYTS groups (Edwards et al., 2020, 2021) in aiming to observe the transits of extrasolar planets which are suitable for atmospheric characterisation. By doing so, we aim to help ensure the plan-



Fig. 1. Locations of the LCOGT's network of robotic 0.4 m telescopes.

ets' ephemerides will be well-known such that future facilities can characterise the atmospheres of these planets.

METHODS

We utilised the Las Cumbres Observatory Global Telescope (LCOGT) network's ground-based 0.4 m telescopes (Brown et al., 2013), with access provided via the Global Sky Partners programme⁴ and the Faulkes Telescope Project⁵. The network has six sites which host 0.4 m telescopes and these are spread across both the northern and southern hemispheres as shown in Figure 1.

Target Selection and Data Collection

We used ExoClock⁶ (Kokori et al., 2021) to prioritise targets for ephemeris refinement. The site contains a database of all the exoplanets that could potentially be studied with Ariel (Edwards, Mugnai, et al., 2019). These are ranked as low, medium or high priority based upon the current uncertainty on their transit times, the predicted precision in 2028, and the time since they were last observed. By loading in the size and location of your telescope(s), ExoClock provides a list of potential observations over the coming days. An example of this schedule is shown in Figure 2 and, from the long list of potential planets to observe, we focused only on those ranked as medium or high priority.

Before using the LCO portal to book an observation of a potentially suitable target, we first calculated an exposure time using the LCO exposure time calcu-

⁴<https://lco.global/education/partners/>

⁵<http://www.faulkes-telescope.com/>

⁶<https://www.exoclock.space/>

lator⁷. To do this, we used the R-band magnitude of the host star from the ExoClock site and ensured the 0.4 m telescope option was selected as shown in Figure 3.

We calculated the required signal-to-noise ratio (SNR) for our observations from:

$$\text{SNR} > 5 \times \frac{1000}{\delta_R} \quad (1)$$

where δ_R is the transit depth in mmag in the R-band which was taken from the ExoClock site. Having ensured that the required SNR could be reached without saturation, we booked our observations through the LCO portal. Due to issues with the weather or competing schedules, not all our observing requests were successful. However, we acquired data for thirteen planets: HATS-1 b (Penev et al., 2013), HATS-2 b (Mohler-Fischer et al., 2013), HATS-3 b (Bayliss et al., 2013), HAT-P-18 b (Hartman et al., 2011), HAT-P-27 b (Anderson et al., 2011; Béky et al., 2011), HAT-P-30 b (Johnson et al., 2011), HAT-P-55 b (Juncher et al., 2015), KELT-4A b (Eastman et al., 2016), WASP-25 b (Enoch et al., 2011), WASP-42 b (Lendl et al., 2012), WASP-57 b (Faedi et al., 2013), WASP-61 b (Hellier et al., 2012) and WASP-123 b (Turner et al., 2016).

Data Reduction and Analysis

We used the HOlonom Photometry Software (HOPS, (Tsiaras, 2019)), which is freely available on GitHub⁸, to analyse the datasets we acquired.

The first step of the analysis within HOPS is usually an initial reduction of the datasets (dark, flat and bias subtraction). However, LCO already performs the initial reduction for us: we obtained the reduced (BANZAI) data from the LCO archive and proceeded to process the data by uploading it onto HOPS. The filter was set to the R filter, which is the optical filter we used to observe all exoplanets in this study, and the co-ordinates of the host-star were obtained from the Right Ascension/Declination data found in the file's header. Within HOPS, we inspected frames for which sudden changes in the sky ratio or PSF were seen and any images that were deemed poor quality were removed. Due to the Earth's rotation, and slight errors in the telescope's ability to track the host star, the position of stars on the detector focal plane can change over the course of a night. Therefore, HOPS aligns the images to ensure the location of each star

Planet	Star	Transit	1h Before	Transit	1h After
WASP-123b	19:17:35.0186 -22:51:35.304	10:00 3:10	2021-07-10 07:50 Ari: 32° Ari: 147° (NE)	2021-07-10 08:30 Ari: 32° Ari: 137° (NE)	2021-07-10 09:10 Ari: 32° Ari: 207° (SW)

Fig. 2. Screenshot of the ExoClock schedule tool, which provided a list of potential transit observations that could be conducted with the telescopes listed under our account.

Las Cumbres Observatory Exposure Time Calculator

• Provide two-out-of-three values in the top row (S/N, Magnitude, ExpTime).
• Select the telescope/instrument, filter, moon phase, and airmass.
• Make sure that the filter is available on the selected instrument!
• Click Calculate.

Input Values

S/N: 400 Magnitude: 11.6 ExpTime (sec):

Telescope/Instrument: 0.4-m / SBIG Filter: r Moon phase: Half Airmass: 1.3

Press the button to display updated values

Calculated Values

S/N: 401.5 Magnitude: 11.6 ExpTime(sec): 39 PkDN: 31168.2

(Additional values >) UBVRi in Vega magnitudes; ugriz in AB magnitudes

Fig. 3. The LCO Exposure Time Calculator used to check the predicted quality of our observations and to ensure the telescope's detector didn't saturate.

within the image is constant so the star's flux can be accurately measured over time.

Next, we extracted the flux from the target star. HOPS was simple to use in this regard, we only needed to pick our target star, and comparison stars to remove variations in the star's flux that were not due to the planet. Given that comparison stars may be variable, we inspected the photometry to ensure no spurious signals were being inserted into the host star's flux. If any comparison stars were deemed inappropriate, we removed and/or replaced them to achieve more stable light curves.

Finally, we used the built-in transit fitting feature of HOPS, which uses pylightcurve⁹ (Tsiaras et al., 2016), to fit our data. The parameters used for the

⁷<https://exposure-time-calculator.lco.global/>

⁸<https://github.com/ExoWorldsSpies/hops>

⁹<https://github.com/ucl-exoplanets/pylightcurve>

Table 1. Summary of observations undertaken as part of this project.

Planet	Star Mag [R]	Exposure Time [s]	Filter	Facility	Date
HATS-1 b	12.08	60.284	SDSS-rp	Cerro Tololo	21/02/2021
HATS-2 b	13.40	120.237	SDSS-rp	Siding Spring	22/02/2021
HATS-3 b	11.69	45.280	SDSS-rp	Teide	17/05/2021
HAT-P-18 b	12.61	90.285	SDSS-rp	McDonald	07/05/2021
HAT-P-18 b	12.61	90.288	SDSS-rp	McDonald	18/05/2021
HAT-P-27 b	11.98	59.937	SDSS-rp	Haleakala	18/04/2021
HAT-P-30 b	10.104	20.281	SDSS-rp	Teide	03/02/2021
HAT-P-55 b	12.87	61.939	SDSS-rp	Haleakala	16/05/2020
HAT-P-55 b	12.87	69.945	SDSS-rp	Haleakala	31/03/2021
KELT-4A b	9.90	10.282	SDSS-rp	Teide	01/03/2021
WASP-25 b	11.82	30.286	SDSS-rp	Sutherland	23/02/2021
WASP-42 b	11.71	45.233	SDSS-rp	Siding Spring	17/05/2021
WASP-57 b	12.90	90.288	SDSS-rp	Siding Spring	21/04/2021
WASP-61 b	11.88	60.285	SDSS-rp	McDonald	15/12/2020
WASP-123 b	10.67	20.288	SDSS-rp	Cerro Tololo	28/07/2021

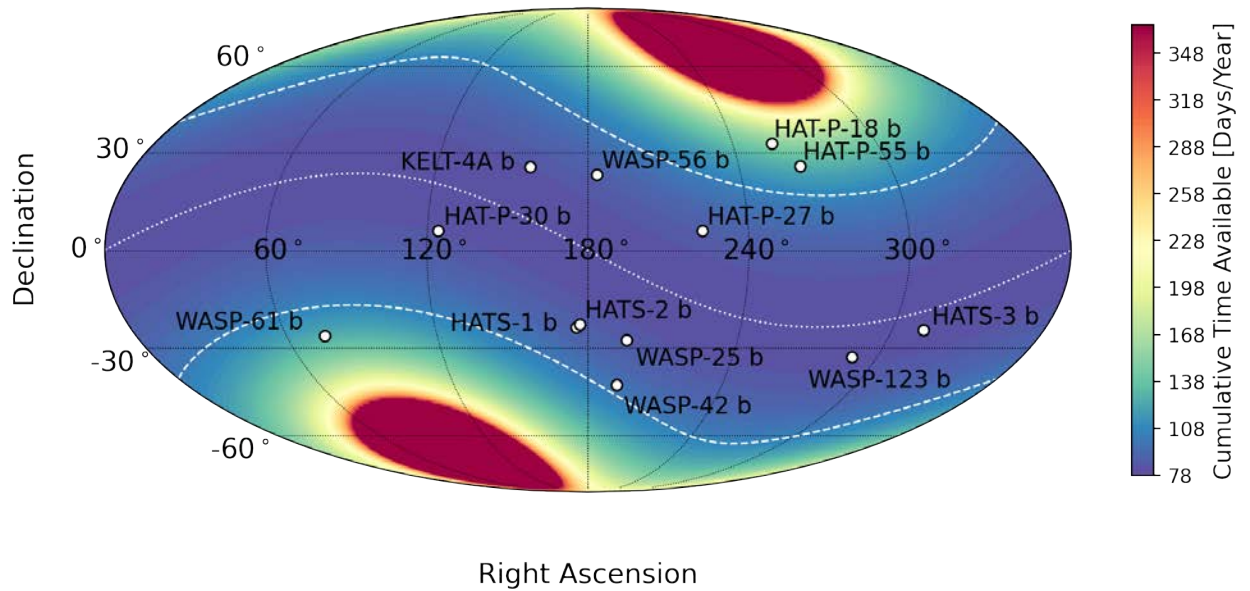


Fig. 4. The sky coverage of Ariel, given in days available per year, with the planets studied in this paper over-plotted. The dotted white line shows the ecliptic plane while the dashed white lines represent the extent of Twinkle's field of regard, indicating that, of the planet studied in this paper, only HAT-P-18 b, HAT-P-55 b and WASP-61 b are not also potential targets for this mission.

fitting were those in the ExoClock database, which were in turn taken from the following papers: HATS-1 b (Penev et al., 2013), HATS-2 b (Mohler-Fischer et al., 2013), HATS-3 b (Bayliss et al., 2013), HAT-P-18 b (Seeliger et al., 2015), HAT-P-27 b (Seeliger et al., 2015), HAT-P-30 b (Maciejewski et al., 2016), HAT-P-55 b (Juncher et al., 2015), KELT-4A b (Eastman et al., 2016), WASP-25 b (Southworth et al., 2014), WASP-42 b (Southworth et al., 2016), WASP-57 b (Southworth et al., 2015), WASP-61 b (Hellier et al., 2012), WASP-123 b (Turner et al., 2016). In each case, the only free parameters in the fit, other than those describing a quadratic model for the out-of-transit systematics, were the transit mid-time and the planet-to-star radius ratio.

RESULTS

Figure 4 shows the position in the sky of the planets we observed and the coverage of the Ariel mission. Ariel will have continuous viewing zones at the ecliptic poles and, while none of the planets lie within it, HAT-P-18 b is the closest, meaning there will be many potential observing windows for this planet. While Ariel and JWST will be able to observe the whole sky, Twinkle's field of regard is limited to planets within $\pm 40^\circ$ of the ecliptic plane, meaning HAT-P-18 b, HAT-P-55 b and WASP-61 b cannot be studied by this mission.

Across these thirteen planets, our project acquired fifteen transit light curves and the final fits of these are given in Figure 5. In each case, the best-fit transit model is given in red while the shaded regions indicate the time window of the fitted mid-time (red) and expected mid-time (blue). Additionally, the expected transit light curve is indicated by a dashed blue line. For each observation, we compared the fitted mid-time to the expected, calculating the observed minus calculated residual (O-C). The transit mid-times and O-C values are given in Table 2.

We note that, for the first observation of HAT-P-18 b and our observation of WASP-123 b, HOPS struggled to fit the data when the planet-to-star radius ratio was a free parameter due to the poor coverage of the transit. Therefore, we attempted fitting the transit with a fixed planet-to-star ratio. However, due to the reasons discussed below, we do not report the mid-times in Table 2 though the light curve fits are shown in Figure 5 for completeness.

Table 2. Transit mid-times for each light curve analysed in this project as well as the subsequent observed minus calculated (O-C) residual.

Planet	Mid-time [BJD _{TDB}]	O-C [min]
HATS-1 b	2459266.7521 ^{+0.0008} _{-0.0010}	-0.0 ^{+1.2} _{-1.4}
HATS-2 b	2459268.1531 ^{+0.0008} _{-0.0007}	4.4 ^{+1.2} _{-1.1}
HATS-3 b	2459352.5818 ^{+0.0017} _{-0.0015}	-0.1 ^{+2.4} _{-2.1}
HAT-P-18 b	2459352.7832 ^{+0.0010} _{-0.0009}	0.2 ^{+1.5} _{-1.3}
HAT-P-27 b	2459322.8860 ^{+0.0013} _{-0.0009}	-3.9 ^{+1.8} _{-1.2}
HAT-P-30 b	2458882.5893 ^{+0.0009} _{-0.0009}	-12.3 ^{+1.3} _{-1.3}
HAT-P-55 b	2458985.9487 ^{+0.0015} _{-0.0015}	-10 ^{+2.1} _{-1.9}
HAT-P-55 b	2459305.0323 ^{+0.0016} _{-0.0019}	-14.8 ^{+2.4} _{-2.7}
KELT-4A b	2459275.5584 ^{+0.0012} _{-0.0011}	-5.8 ^{+1.8} _{-1.6}
WASP-25 b	2459269.4859 ^{+0.0005} _{-0.0006}	1.9 ^{+0.7} _{-0.9}
WASP-42 b	2459351.9514 ^{+0.0012} _{-0.0011}	-8.0 ^{+1.8} _{-1.6}
WASP-57 b	2459326.1416 ^{+0.0016} _{-0.0014}	-3.9 ^{+2.3} _{-2.0}
WASP-61 b	2459198.7400 ^{+0.0030} _{-0.0030}	2.8 ^{+3.7} _{-4.3}

DISCUSSION

The quality of our light curves varied between targets but in many cases the transit can be clearly seen and is well-fitted with no significant correlations within the residuals. The precision achieved on the transit mid-time varies from less than a minute to nearly 3 minutes. We have identified a number of potential reasons for this, as discussed below.

Firstly, while many of our light curves cover the full transit duration, plus a baseline of up to roughly half the transit duration, several were interrupted due to bad weather, reducing the coverage. For instance, our observations of HATS-3 b and WASP-57 b do not have many data points post-egress while both observations of HAT-P-55 b do not have any pre-ingress data. However, the worst affected amongst our light curves were the observations of HAT-P-18 b on 7th May 2021 and WASP-123 b on 28th July 2021 as these datasets only covered the ingress and a small amount of time pre-ingress. Despite this, the precision on the transit mid-time in each case is not the worst amongst the sample (± 2.1 and ± 2.0 minutes respectively). Nevertheless, as these fits had one fewer free parame-

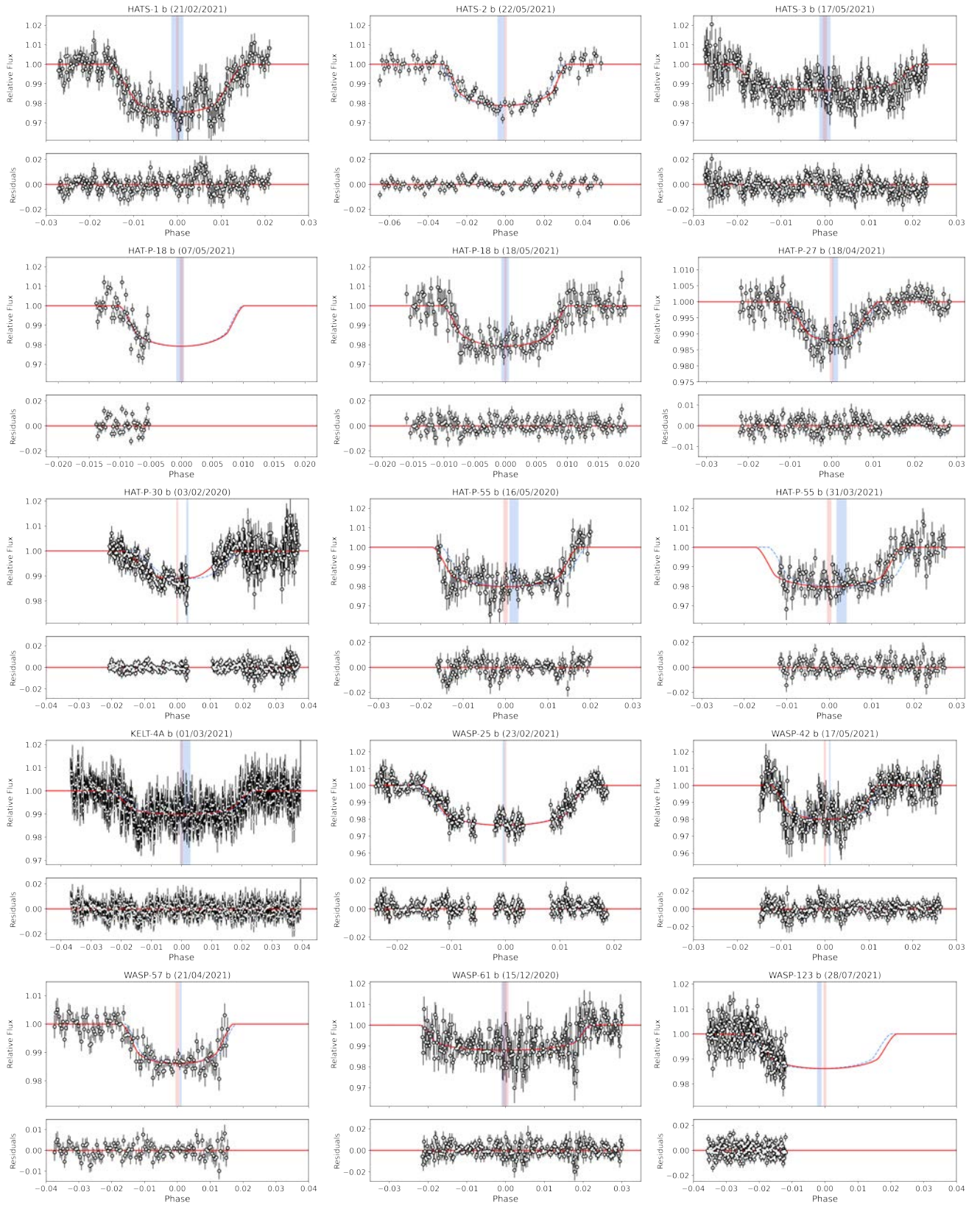


Fig. 5. Transit light curves obtained during this project. In each case, the data is shown in black with the best-fit transit model in red and the predicted transit model represented by a blue dashed line. For each observation, the red filled region indicates the fitted mid-time and associated uncertainty. Meanwhile, the blue filled region represents the predicted transit mid-time and current uncertainty on this.

ter this could have led to an under-estimation of the uncertainty on the transit mid time.

A second cause of differences in the precision of our observations is the brightness of the host star which dictates the amount of flux received. While a brighter star leads to additional flux, if it is too bright the detector must be read-out at a faster rate, leading to a lower duty cycle as the detector spends more time being read. Additionally, very short exposures could be dominated by read noise instead of photon noise from the star. Each of these would lead to a poorer overall quality for the light curve with HAT-P-30 b, KELT-4A b, WASP-42 b and WASP-123 b, the five planets with the brightest host stars, being good examples of this.

Additionally, the depth of the planet's transit will affect the ability of HOPS to accurately fit the mid-time. A deeper transit leads to a higher signal-to-noise ratio, allowing the start and end of the transit to be more easily discerned. Examples are HAT-P-27 b and WASP-25 b, where both hosts stars have a similar magnitude (11.98 mag and 11.82 respectively), but the transit depths differ (13 mmag and 20 mmag respectively), hence the mid-time of WASP-25 b has a higher precision than that of HAT-P-27 b. However, here the transit duration may also be having an effect as HAT-P-27 b also has a shorter transit time (1.68 hours) than WASP-25 b (2.76 hours). Also, as HAT-P-18 b has a relatively deep transit, this could explain the relatively higher precision on the mid-time obtained from the visit of the 7th May although constraints on the mid-time of partial transits are often over-estimated.

Finally, other effects which are harder to quantify are likely to be affecting our observations. One such effect is the airmass: the amount of atmosphere we were observing the star through, and particularly changes in this over the observation period. Furthermore, the phase of the moon and proximity to the host star could also have an effect by increasing the background noise. The comparison star chosen will also affect the precision of our light curves and, while some host stars had many potential comparison stars to choose from, others did not. In truth, the comparative precision of our mid-times is a combination of all these effects, with the dominate cause of a higher uncertainty being hard to determine definitively.

The majority of the planets had observed mid-times which were within 1σ of the expected transit time. However, for several planets we found significant offsets and of particular note are HAT-P-30 b, HAT-P-55 b

and WASP-42 b. Our observed O-C residuals for HAT-P-30 b and HAT-P-55 b are consistent with those found by other ExoClock users¹⁰, giving us confidence that the deviation from the literature ephemeris that we find is correct. The cause of this deviation could be a slight inaccuracy on the linear period derived in other works or an actual variation from the linear period due to effects such as orbital decay or transit timing variations from other, as yet unidentified, planets in the system.

On the other hand, WASP-42 b does not have, at the time of writing, any observations listed on ExoClock. Therefore, further transits will need to be observed to verify our results and WASP-123 b provides a good example of the need of multiple transits to confirm an O-C drift. Our observation of WASP-123 b suggested an O-C of 5.8 ± 2.0 minutes and, while we already questioned the reliability of this result due to the poor transit coverage, this was compounded by recent observations uploaded to ExoClock by other observations which found an O-C of 2.8 ± 0.5 minutes. Due to this, we choose not to report our mid-time for WASP-123 b. Likewise, our first observation of HAT-P-18 b, which had poor coverage, was over 2 minutes different from that found by the ExoClock observations to date and therefore the mid-time is not reported here.

As, for the majority of the planets, we only observed a single transit we do not update the period as part of this work and simply provide the mid-times so that they can be utilised in future studies, such as those that are being regularly produced via the ExoClock programme (Kokori et al., 2021).

All the planets observed here are excellent targets for atmospheric characterisation with upcoming facilities. In fact, HAT-P-18 b has already been studied through transit spectroscopy using the Hubble Space Telescope (Tsiaras et al., 2018), the William Herschel Telescope (Kirk et al., 2017), and the Hale Telescope at Palomar Observatory (Paragas et al., 2021). These, respectively, have identified the presence of water vapour, observed the effects of Rayleigh scattering, and detected helium in the atmosphere of HAT-P-18 b. Our work, combined with that of previous ORBYTS projects (Edwards et al., 2020, 2021) and other ephemeris follow-up projects (e.g. Poddaný et al., 2010; Mallonn et al., 2019; Zellem et al., 2020; Kokori et al., 2021) increases confidence in the knowl-

¹⁰Kokori et al. (2021) and <https://www.exoclock.space/database/planets/HAT-P-55b/>

edge that these planets will transit at the expected time, hence aiding the study of their atmospheres.

CONCLUSION

We present observations of thirteen exoplanets which were rated by the ExoClock site as medium or high priority for photometric follow-up. All these planets are potential targets for future space-based facilities and our observations will help ensure their transit ephemerides are well-known. As TESS and other surveys continue to find planets, ephemeris refinement projects will become ever more important and educational outreach and citizen-science programmes have the potential to play a large role in maintaining transit times for the next generation of telescopes.

FUNDING

The project was undertaken as part of the ORBYTS programme, a public engagement project which partners scientists with schools to support students' involvement in space research. Billy Edwards and Giovanna Tinetti acknowledge funding from the STFC grants ST/S002634/1 and ST/W00254X/1. Cynthia Ho and Hannah Osborne thank the STFC for support through PhD studentships.

ACKNOWLEDGEMENTS

Billy Edwards is the PI of the LCOGT Global Sky Partners 2020 project "Refining Exoplanet Ephemerides" and thanks the LCOGT network and its coordinators for providing telescope access. Without this access and support, the project presented here would not have been possible. We utilised the 0.4 m telescopes at Cerro Tololo Observatory, Haleakala Observatory, McDonald Observatory, Sutherland Observatory, Sliding Spring Observatory, and Teide Observatory, each time using their imaging mode and the SDSS-rp filter. The observation of HAT-P-55 b from 2020 was taken via the Faulkes Telescope Project which is coordinated by Cardiff University and Swansea University.

The authors wish to thank Matt Densham, from the London Academy of Excellence, and Jon Barker, from Highams Park School, for their dedication in organising the outreach sessions, devoting their spare time for the benefit of their students.

SOFTWARE

Astropy (Astropy Collaboration et al., 2018), cartopy (Met Office, 2010 - 2015), corner (Foreman-

Mackey, 2016), emcee (Foreman-Mackey et al., 2013), ExoTETHyS (Morello et al., 2020), HOPS (Tsiaras, 2019), Matplotlib (Hunter, 2007), Numpy (Oliphant, 2006), Pandas (McKinney, 2011), pylightcurve (Tsiaras et al., 2016), SciPy (Virtanen et al., 2020).

REFERENCES

- Anderson, D. R., Barros, S. C. C., Boisse, I., Bouchy, F., Collier Cameron, A., Faedi, F., ... Skillen, I. (2011, May). WASP-40b: Independent Discovery of the 0.6 M_{Jup} Transiting Exoplanet HAT-P-27b. *PASP*, 123(903), 555. doi:
- Astropy Collaboration, Price-Whelan, A. M., Sipőcz, B. M., Günther, H. M., Lim, P. L., Crawford, S. M., ... Astropy Contributors (2018, September). The Astropy Project: Building an Open-science Project and Status of the v2.0 Core Package. *AJ*, 156(3), 123. doi:
- Bayliss, D., Zhou, G., Penev, K., Bakos, G. Á., Hartman, J. D., Jordán, A., ... Sári, P. (2013, November). HATS-3b: An Inflated Hot Jupiter Transiting an F-type Star. *AJ*, 146(5), 113. doi:
- Bean, J. L., Stevenson, K. B., Batalha, N. M., Berta-Thompson, Z., Kreidberg, L., Crouzet, N., ... Zingales, T. (2018, November). The Transiting Exoplanet Community Early Release Science Program for JWST. *PASP*, 130(993), 114402. doi:
- Béky, B., Bakos, G. Á., Hartman, J., Torres, G., Latham, D. W., Jordán, A., ... Sári, P. (2011, June). HAT-P-27b: A Hot Jupiter Transiting a G Star on a 3 Day Orbit. *ApJ*, 734(2), 109. doi:
- Borucki, W. J., Koch, D., Basri, G., Batalha, N., Brown, T., Caldwell, D., ... Prsa, A. (2010, February). Kepler Planet-Detection Mission: Introduction and First Results. *Science*, 327(5968), 977. doi:
- Boss, A. (2009). *The crowded universe : the search for living planets*.
- Brown, T. M., Baliber, N., Bianco, F. B., Bowman, M., Burleson, B., Conway, P., ... Willis, M. (2013, September). Las Cumbres Observatory Global Telescope Network. *PASP*, 125(931), 1031. doi:
- Campbell, B., Walker, G. A. H., & Yang, S. (1988, August). A Search for Substellar Companions to Solar-type Stars. *ApJ*, 331, 902. doi:

- Charbonneau, D., Brown, T. M., Latham, D. W., & Mayor, M. (2000, jan). Detection of planetary transits across a sun-like star. *The Astrophysical Journal*, 529(1), L45–L48. Retrieved from <https://doi.org/10.1086/312457> doi:
- Chubb, K. L., Joseph, M., Franklin, J., Choudhury, N., Furtenbacher, T., Császár, A. G., ... Sousa-Silva, C. (2018, January). MARVEL analysis of the measured high-resolution rovibrational spectra of C₂H₂. *JQSRT*, 204, 42-55. doi:
- Chubb, K. L., Naumenko, O., Keely, S., Bartolotto, S., Macdonald, S., Mukhtar, M., ... Tennyson, J. (2018, October). MARVEL analysis of the measured high-resolution rovibrational spectra of H₂³²S. *JQSRT*, 218, 178-186. doi:
- Darby-Lewis, D., Shah, H., Joshi, D., Khan, F., Kauwo, M., Sethi, N., ... Tennyson, J. (2019, August). MARVEL analysis of the measured high-resolution spectra of 1⁴NH. *Journal of Molecular Spectroscopy*, 362, 69-76. doi:
- Dragomir, D., Harris, M., Pepper, J., Barclay, T., Villanueva, J., Steven, Ricker, G. R., ... Yahalomi, D. (2020, May). Securing the Legacy of TESS through the Care and Maintenance of TESS Planet Ephemerides. *AJ*, 159(5), 219. doi:
- Eastman, J. D., Beatty, T. G., Siverd, R. J., Antognini, J. M. O., Penny, M. T., Gonzales, E. J., ... Trueblood, P. (2016, February). KELT-4Ab: An Inflated Hot Jupiter Transiting the Bright (V ~ 10) Component of a Hierarchical Triple. *AJ*, 151(2), 45. doi:
- Edwards, B., Anisman, L., Changeat, Q., Morvan, M., Wright, S., Yip, K. H., ... Tennyson, J. (2020, July). Original Research by Young Twinkle Students (Orbyts): Ephemeris Refinement of Transiting Exoplanets II. *Research Notes of the American Astronomical Society*, 4(7), 109. doi:
- Edwards, B., Changeat, Q., Yip, K. H., Tsiaras, A., Taylor, J., Akhtar, B., ... Tennyson, J. (2021, July). Original Research by Young Twinkle Students (ORBYTS): Ephemeris Refinement of Transiting Exoplanets. *MNRAS*, 504(4), 5671-5684. doi:
- Edwards, B., Mugnai, L., Tinetti, G., Pascale, E., & Sarkar, S. (2019, June). An Updated Study of Potential Targets for Ariel. *AJ*, 157(6), 242. doi:
- Edwards, B., Rice, M., Zingales, T., Tessenyi, M., Waldmann, I., Tinetti, G., ... Sarkar, S. (2019, April). Exoplanet spectroscopy and photometry with the Twinkle space telescope. *Experimental Astronomy*, 47(1-2), 29-63. doi:
- Enoch, B., Cameron, A. C., Anderson, D. R., Lister, T. A., Hellier, C., Maxted, P. F. L., ... Udry, S. (2011, January). WASP-25b: a 0.6 M_J planet in the Southern hemisphere. *MNRAS*, 410(3), 1631-1636. doi:
- Faedi, F., Pollacco, D., Barros, S. C. C., Brown, D., Collier Cameron, A., Doyle, A. P., ... Watson, C. (2013, March). WASP-54b, WASP-56b, and WASP-57b: Three new sub-Jupiter mass planets from SuperWASP. *A&A*, 551, A73. doi:
- Foreman-Mackey, D., Hogg, D. W., Lang, D., & Goodman, J. (2013, March). emcee: The MCMC Hammer. *PASP*, 125(925), 306. doi:
- Foreman-Mackey, D. (2016, jun). corner.py: Scatterplot matrices in python. *The Journal of Open Source Software*, 1(2), 24. Retrieved from <https://doi.org/10.21105/joss.00024> doi:
- Francis, A., Brown, J., Cameron, T., Crawford Clarke, R., Dodd, R., Hurdle, J., ... Muller, J.-P. (2020). A multi-annotator survey of sub-km craters on mars. *Data*, 5(3). Retrieved from <https://www.mdpi.com/2306-5729/5/3/70> doi:
- French, R., James, A., Baker, D., Dunn, W., Matthews, S., da Silva Pestana, B., ... Trindade, G. (2020, 12). Opening pupils' eyes to the Sun. *Astronomy & Geophysics*, 61(6), 6.22-6.23. Retrieved from <https://doi.org/10.1093/astrophys/ataa085> doi:
- Galle, J. G. (1846, November). Account of the discovery of Le Verrier's planet Neptune, at Berlin, Sept. 23, 1846. *MNRAS*, 7, 153. doi:
- Grafton-Waters, S., Ahmed, M., Henson, S., Hinds-Williams, F., Ivanova, B., Marshall, E., ... Dunn, W. (2021, jul). A study of the soft x-ray emission lines in NGC 4151. i. kinematic properties of the plasma wind. *Research Notes of the AAS*, 5(7), 172. Retrieved from <https://doi.org/10.3847/2515-5172/ac1689> doi:
- Hartman, J. D., Bakos, G. Á., Sato, B., Torres, G., Noyes, R. W., Latham, D. W., ... Sári, P. (2011,

- January). HAT-P-18b and HAT-P-19b: Two Low-density Saturn-mass Planets Transiting Metal-rich K Stars. *ApJ*, 726(1), 52. doi:
- Hatzes, A. P., Cochran, W. D., Endl, M., McArthur, B., Paulson, D. B., Walker, G. A. H., ... Yang, S. (2003, dec). A planetary companion to gamma cephei a. *The Astrophysical Journal*, 599(2), 1383–1394. Retrieved from <https://doi.org/10.1086/379281> doi:
- Hellier, C., Anderson, D. R., Collier Cameron, A., Doyle, A. P., Fumel, A., Gillon, M., ... West, R. G. (2012, October). Seven transiting hot Jupiters from WASP-South, Euler and TRAPPIST: WASP-47b, WASP-55b, WASP-61b, WASP-62b, WASP-63b, WASP-66b and WASP-67b. *MNRAS*, 426(1), 739–750. doi:
- Henry, G. W., Marcy, G. W., Butler, R. P., & Vogt, S. S. (2000, jan). A transiting “51 peg-like” planet. *The Astrophysical Journal*, 529(1), L41–L44. Retrieved from <https://doi.org/10.1086/312458> doi:
- Holdship, J., Viti, S., Codella, C., Rawlings, J., Jimenez-Serra, I., Ayalew, Y., ... Horn, S. (2019, August). Observations of CH₃OH and CH₃CHO in a Sample of Protostellar Outflow Sources. *ApJ*, 880(2), 138. doi:
- Hunter, J. D. (2007). Matplotlib: A 2d graphics environment. *Computing in Science & Engineering*, 9(3), 90–95. doi:
- Jacob, W. S. (1855, June). On certain Anomalies presented by the Binary Star 70 Ophiuchi. *MNRAS*, 15, 228. doi:
- Johnson, J. A., Winn, J. N., Bakos, G. Á., Hartman, J. D., Morton, T. D., Torres, G., ... Sári, P. (2011, July). HAT-P-30b: A Transiting Hot Jupiter on a Highly Oblique Orbit. *ApJ*, 735(1), 24. doi:
- Juncher, D., Buchhave, L. A., Hartman, J. D., Bakos, G. Á., Bieryla, A., Kovács, T., ... Sári, P. (2015, September). HAT-P-55b: A Hot Jupiter Transiting a Sun-Like Star. *PASP*, 127(955), 851. doi:
- Kirk, J., Wheatley, P. J., Loudon, T., Doyle, A. P., Skillen, I., McCormac, J., ... Karjalainen, R. (2017, July). Rayleigh scattering in the transmission spectrum of HAT-P-18b. *MNRAS*, 468(4), 3907–3916. doi:
- Kokori, A., Tsiaras, A., Edwards, B., Rocchetto, M., Tinetti, G., Wünsche, A., ... Tomatis, A. (2021, August). ExoClock project: an open platform for monitoring the ephemerides of Ariel targets with contributions from the public. *Experimental Astronomy*. doi:
- Le Verrier, U. J. (1846, October). Recherches sur les mouvements d’Uranus par U. J. Le Verrier (Fortsetzung). *Astronomische Nachrichten*, 25, 65.
- Lendl, M., Anderson, D. R., Collier-Cameron, A., Doyle, A. P., Gillon, M., Hellier, C., ... Wheatley, P. J. (2012, August). WASP-42 b and WASP-49 b: two new transiting sub-Jupiters. *A&A*, 544, A72. doi:
- Maciejewski, G., Dimitrov, D., Mancini, L., Southworth, J., Ciceri, S., D’Ago, G., ... Henning, T. (2016, January). New Transit Observations for HAT-P-30 b, HAT-P-37 b, TrES-5 b, WASP-28 b, WASP-36 b and WASP-39 b. *AcA*, 66(1), 55–74.
- Mallon, M., von Essen, C., Herrero, E., Alexoudi, X., Granzer, T., Sosa, M., ... Wünsche, A. (2019, February). Ephemeris refinement of 21 hot Jupiter exoplanets with high timing uncertainties. *A&A*, 622, A81. doi:
- Mayor, M., & Queloz, D. (1995). A jupiter-mass companion to a solar-type star. *Nature*, 378(6555), 355–359. Retrieved from <https://doi.org/10.1038/378355a0> doi:
- McKemmish, L. K., Borsovszky, J., Goodhew, K. L., Sheppard, S., Bennett, A. F. V., Martin, A. D. J., ... Tennyson, J. (2018, November). MARVEL Analysis of the Measured High-resolution Rovibronic Spectra of ⁹⁰Zr¹⁶O. *ApJ*, 867(1), 33. doi:
- McKemmish, L. K., Masseron, T., Sheppard, S., Sandeman, E., Schofield, Z., Furtenbacher, T., ... Sousa-Silva, C. (2017, February). Marvel Analysis of the Measured High-resolution Rovibronic Spectra of TiO. *ApJS*, 228(2), 15. doi:
- McKinney, W. (2011). pandas: a foundational python library for data analysis and statistics. *Python for High Performance and Scientific Computing*, 14.
- Met Office. (2010 - 2015). Cartopy: a cartographic python library with a matplotlib interface [Computer software manual]. Exeter, Devon. Retrieved from <http://scitools.org.uk/cartopy>

- Mohler-Fischer, M., Mancini, L., Hartman, J. D., Bakos, G. Á., Penev, K., Bayliss, D., ... Conroy, P. (2013, October). HATS-2b: A transiting extrasolar planet orbiting a K-type star showing starspot activity. *A&A*, 558, A55. doi:
- Morello, G., Claret, A., Martin-Lagarde, M., Cossou, C., Tsiaras, A., & Lagage, P. O. (2020, February). The ExoTETHyS Package: Tools for Exoplanetary Transits around Host Stars. *AJ*, 159(2), 75. doi:
- Oliphant, T. E. (2006). *A guide to numpy* (Vol. 1). Trelgol Publishing USA.
- Paragas, K., Vissapragada, S., Knutson, H. A., Oklopčić, A., Chachan, Y., Greklek-McKeon, M., ... Vasisht, G. (2021, March). Metastable Helium Reveals an Extended Atmosphere for the Gas Giant HAT-P-18b. *ApJL*, 909(1), L10. doi:
- Penev, K., Bakos, G. Á., Bayliss, D., Jordán, A., Mohler, M., Zhou, G., ... Sári, P. (2013, January). HATS-1b: The First Transiting Planet Discovered by the HATSouth Survey. *AJ*, 145(1), 5. doi:
- Poddaný, S., Brát, L., & Pejcha, O. (2010, March). Exoplanet Transit Database. Reduction and processing of the photometric data of exoplanet transits. *NewA*, 15(3), 297-301. doi:
- Ricker, G. R., Winn, J. N., Vanderspek, R., Latham, D. W., Bakos, G. Á., Bean, J. L., ... Villaseñor, J. (2015, January). Transiting Exoplanet Survey Satellite (TESS). *Journal of Astronomical Telescopes, Instruments, and Systems*, 1, 014003. doi:
- See, T. J. J. (1896, January). Researches on the orbit of 70 Ophiuchi, and on a periodic perturbation in the motion of the system arising from the action of an unseen body. *AJ*, 16, 17-23. doi:
- Seeliger, M., Kitze, M., Errmann, R., Richter, S., Ohlert, J. M., Chen, W. P., ... Neuhäuser, R. (2015, August). Ground-based transit observations of the HAT-P-18, HAT-P-19, HAT-P-27/WASP40 and WASP-21 systems. *MNRAS*, 451(4), 4060-4072. doi:
- Sherrill, T. J. (1999, February). A Career of Controversy: The Anomaly of T. J. J. See. *Journal for the History of Astronomy*, 30, 25. doi:
- Sousa-Silva, C., McKemmish, L. K., Chubb, K. L., Gorman, M. N., Baker, J. S., Barton, E. J., ... Tennyson, J. (2018, January). Original Research By Young Twinkle Students (ORBYTS): when can students start performing original research? *Physics Education*, 53(1), 015020. doi:
- Southworth, J., Hinse, T. C., Burgdorf, M., Calchi Novati, S., Dominik, M., Galianni, P., ... Vilela, C. (2014, October). High-precision photometry by telescope defocussing - VI. WASP-24, WASP-25 and WASP-26. *MNRAS*, 444(1), 776-789. doi:
- Southworth, J., Mancini, L., Tregloan-Reed, J., Calchi Novati, S., Ciceri, S., D'Ago, G., ... Wertz, O. (2015, December). Larger and faster: revised properties and a shorter orbital period for the WASP-57 planetary system from a pro-am collaboration. *MNRAS*, 454(3), 3094-3107. doi:
- Southworth, J., Tregloan-Reed, J., Andersen, M. I., Calchi Novati, S., Ciceri, S., Colque, J. P., ... Wang, Y. (2016, April). High-precision photometry by telescope defocussing - VIII. WASP-22, WASP-41, WASP-42 and WASP-55. *MNRAS*, 457(4), 4205-4217. doi:
- Struve, O. (1952, October). Proposal for a project of high-precision stellar radial velocity work. *The Observatory*, 72, 199-200.
- Tinetti, G., Drossart, P., Eccleston, P., Hartogh, P., Heske, A., Leconte, J., ... Zwart, F. (2018, November). A chemical survey of exoplanets with ARIEL. *Experimental Astronomy*, 46(1), 135-209. doi:
- Tinetti, G., Eccleston, P., Haswell, C., Lagage, P.-O., Leconte, J., Lüftinger, T., ... Zuppella, P. (2021, April). Ariel: Enabling planetary science across light-years. *arXiv e-prints*, arXiv:2104.04824.
- Tsiaras, A. (2019, September). HOPS: the photometric software of the HOLomon Astronomical Station. In *Epsc-dps joint meeting 2019* (Vol. 2019, p. EPSC-DPS2019-1594).
- Tsiaras, A., Waldmann, I. P., Rocchetto, M., Varley, R., Morello, G., Damiano, M., & Tinetti, G. (2016, December). *pylightcurve: Exoplanet lightcurve model*.
- Tsiaras, A., Waldmann, I. P., Zingales, T., Rocchetto, M., Morello, G., Damiano, M., ... Yurchenko, S. N. (2018, April). A Population Study of Gaseous Exoplanets. *AJ*, 155(4), 156. doi:
- Turner, O. D., Anderson, D. R., Collier Cameron, A., Delrez, L., Evans, D. F., Gillon, M., ... West, R. G.

- (2016, June). WASP-120 b, WASP-122 b, AND WASP-123 b: Three Newly Discovered Planets from the WASP-South Survey. *PASP*, 128(964), 064401. doi:
- van de Kamp, P. (1969, August). Alternate dynamical analysis of Barnard's star. *AJ*, 74, 757-759. doi:
- Virtanen, P., Gommers, R., Oliphant, T. E., Haberland, M., Reddy, T., Cournapeau, D., ... Contributors, S. ... (2020). SciPy 1.0: Fundamental Algorithms for Scientific Computing in Python. *Nature Methods*, 17, 261–272. doi:
- Wibisono, A. D., Branduardi-Raymont, G., Dunn, W. R., Coates, A. J., Weigt, D. M., Jackman, C. M., ... Fleming, D. (2020). Temporal and spectral studies by xmm-newton of jupiter's x-ray auroras during a compression event. *Journal of Geophysical Research: Space Physics*, 125(5), e2019JA027676. Retrieved from <https://agupubs.onlinelibrary.wiley.com/doi/abs/10.1029/2019JA027676> (e2019JA027676 10.1029/2019JA027676) doi:
- Wolszczan, A., & Frail, D. A. (1992, January). A planetary system around the millisecond pulsar PSR1257 + 12. *Nature*, 355(6356), 145-147. doi:
- Zellem, R. T., Pearson, K. A., Blaser, E., Fowler, M., Ciardi, D. R., Biferno, A., ... Malvache, A. (2020, May). Utilizing Small Telescopes Operated by Citizen Scientists for Transiting Exoplanet Follow-up. *PASP*, 132(1011), 054401. doi:

Using Period-Luminosity-Metallicity relations to Calculate Distance for the RR Lyrae Star, EZ Lyr

KAITLYN E. KIDWELL^{1,*} AND MARY F. KIDD¹

¹ Tennessee Technological University, College of Art and Sciences, Department of Physics, Cookeville, Tennessee, USA

* Corresponding author: kekidwell42@students.tntech.edu

Reliable methods to measure intergalactic distances are a valuable resource in the field of astronomy. Periodic variables stars, such as RR Lyraes, can be used as standard candles to determine the distance to the stellar structures where they are located. For this reason, many different student groups observed and analyzed RR Lyrae stars through a research course offered by Our Solar Siblings, and the focus of this particular study was the star EZ Lyr. Images of EZ Lyr were taken by Las Cumbres Observatory and processed using tools provided for the research course. Light curves were produced in B, V, sdss-i and sdss-z filters that were analyzed to determine the star's period and luminosity. The period-luminosity-metallicity relations described in Cáceres and Catelan (2008) were used to calculate the distance to EZ Lyr in each filter. The final distance measurement, $1406 \pm 32 \text{ pc}$ was slightly closer ($\approx 100 \text{ pc}$) compared to results from the GAIA satellite.

© 2021 Astronomy Theory, Observations and Methods Journal

Keywords: stars — variables — RR Lyrae — photometric telescopes

<https://doi.org/10.32374/atom.2020.2.5>

INTRODUCTION

RR Lyrae stars are a class of pulsating variables often used as standard candles and can be useful in determining the distance to many stellar structures such as globular clusters within the galaxy as well as providing valuable information about their metallicities (Fitzgerald et al., 2012). They typically have a spectral type range from A to F and a pulsation period between 0.2 to 1.2 days (Dambis et al., 2013). (Cáceres & Catelan, 2008) calculated a relation between period-luminosity and distance using the Sloan Digital Sky Survey (SDSS), particularly in the i and z filters. Limited data has been observed using this

relation, making measurements using these relations relatively untested. The mathematical relations proposed by (Cáceres & Catelan, 2008):

$$M_i = 0.908 - 1.035 \log P + 0.220 \log Z \quad (1)$$

$$M_z = 0.839 - 1.95 \log P + 0.211 \log Z \quad (2)$$

$$\log Z = [M/H] - 1.765 \quad (3)$$

$$[M/H] = [Fe/H] + \log(0.638f + 0.362) \quad (4)$$

$$f = 10^{0.3}$$

These equations solve for the absolute magnitude, M_i and M_z , of an RR Lyrae using the period luminosity metallicity relations with the period, P , and

metallicity, Z , of the star. $\log Z$ is derived from the metallicity ratio, $[M/H]$ found from the iron ratio to hydrogen, $[Fe/H]$, and the constant f .

The difference in brightness between the absolute magnitude M and the calculated middle magnitude, m , is converted to distance in parsecs, d , similar to the inverse square law.

$$m - M = 5 \log d - 5 \quad (5)$$

$$d = 10^{((m-M+5)/5)} \quad (6)$$

The star EZ Lyr from the Lyra constellation was selected for observation in this study. EZ Lyr is a visual double star in which one of the stars is an RR Lyre located at an RA and Dec of 281.9215, 35.99072 (Clementini et al., 2017). Its spectral type ranges from A9 to F6.5 and it has a metallicity estimated to be -1.56 (Suntzeff, Kraft, & Kinman, 1994). Its period was found to be 0.525 days in 1959 (Preston, 1959). Photometric information about the field of EZ Lyr was available in the Panoramic Survey Telescope and Rapid Response System Pan-STARRS, (Chambers et al., 2016) and the APASS (Henden et al., 2016) catalogues allowing it to be analyzed closer to compare period-luminosity and distance.



Fig. 1. Color image of EZ Lyr created with images taken with LCO using Fits Liberator and Gimp.

OBSERVATIONS

Images of EZ Lyr were taken robotically using the Las Cumbres Observatory (LCO) which is a global tele-

scope network with twenty three telescopes located in seven sites around the world (Brown et al., 2013). This project specifically used the 0.4 meter SBIG telescopes over two different time periods. These observations were attempted in the B-, V-, i-, and z-bands every two hours during each cadence. In total, 63 successful observations were made in October 2019 and 30 in June 2020.

The final exposure times were 30 seconds for the B- and z-bands and 10 seconds in V- and i-bands which produced light counts in the order of 10^4 which was measured using AstroImageJ (Collins, Kielkopf, Stasun, & Hessman, 2017). A misidentification error was made because of the close proximity to the other star in the EZ Lyr system causing initial light calculations to be double the true value for the RR Lyrae EZ Lyr. The exposure time for these images were originally half the appropriate value for the first approximately 20 images. These images were significantly noisier than the newer data, but due to time constraints, the clearer images from this set were still used for analysis.

Each image taken by LCO was then processed by the Our Solar Siblings Pipeline that automatically performed aperture and point spread function (PSF) photometry on each image (Fitzgerald, 2018). Since EZ Lyr is within a multiple star system, point source extractor (PSFex), a type of PSF photometry, produced the clearest data as it was able to isolate the luminosity of the variable star, therefore it was used for final calculations (Bertin, 2011).

METHODS

After the observations were completed, the data was processed through a Python code program called Astrosource which was provided by Our Solar Siblings (Fitzgerald, Gomez, Salimpour, Singleton, & Wibowo, 2021). Each color filter was run individually through the five different scripts producing four sets of light curves. As the images were processed, the code first identified common stars and then chose stable comparison stars for the variable EZ Lyr whose luminosity was then calibrated using Pan-STARRS and APASS photometry data. Light curves and period calculations were then produced using two methods, string calibration and phase dispersion minimization (PDM) (Stellingwerf, 1978; Dworetzky, 1983; Altunin, Caputo, & Tock, 2020).

Before being able to calculate distance, several values were found. The luminosity of EZ Lyr in each

filter was estimated using the middle magnitude of the measured calibrated values. LogZ was determined using the $[Fe/H]$ of EZ Lyr (Cáceres & Catelan, 2008). The period-luminosity-metallicity relationships were then used to convert the middle and absolute magnitude into distance measurements. To account for interstellar dust that scatters shorter wavelengths, observations in the B-filter were necessary to adjust measurements in other filters using interstellar reddening, $(E(B-V))$. The value $(E(B-V))$ was estimated by incrementing the number until the variance between the distance measurements in the V-, i-, and z- bands was minimized when accounting for extinction caused by $E(B-V)$. The following equation was used for this process where A_v is extinction in the V-band which is used to modify the distance equation (Cardelli, Clayton, & Mathis, 1989; Whitford, 1958).

$$A_v = 3.1E(B - V) \quad (7)$$

$$d = 10^{((m-M+5-A_v)/5)} \quad (8)$$

RESULTS

The period of EZ Lyr was estimated to be 0.5253 ± 0.0007 days by averaging the periods found in the four filters, shown in Table 2, ignoring one significant outlier (PDM for B). The light curves displayed in Figure 2 show the characteristic “shark tooth” shape of an RRa type star.

Filter	Mid Mag	Amplitude	Error
B	11.890	1.719	0.012
V	11.591	1.393	0.016
ip	11.388	1.009	0.022
zs	11.429	0.819	0.015

Table 1. Luminosity Magnitude Measurements: The luminosity of each filter was calibrated from differential magnitude using data from PanSTARRS (Chambers et al., 2016).

LogZ was calculated to be -3.11 after using the $[Fe/H]$ value of -1.56 in the following equations from Catelan.

$$\log Z = [M/H] - 1.765 \quad (9)$$

$$[M/H] = [Fe/H] + \log(0.638f + 0.362) \quad (10)$$

$$f = 10^{0.3}$$

Distance measurements were produced for V-, i-, and z- band filters, where the Viz value is the average of the three. The $E(B-V)$ was adjusted to 0.08 at which the variance between the V-, i-, and z-band distance measurements was 19.8 parsecs. The final calculation for the distance of EZ Lyr using the period luminosity relationship was 1406 ± 32 parsecs. Also listed Table 3 for comparison is the GAIA distance of 1523 ± 60 parsecs which was calculated using parallax.

DISCUSSION

The period of 0.5253 ± 0.0007 days is supported by previous measurements of 0.525 days and the V-band middle magnitude of 11.591 is comparable to other sources that report 11.3 and 11.58 (Preston, 1959; Høg et al., 2000). Possible causes of the error can be attributed to the initial calculation of exposure times that made the first set of data less exposed. This was the result of using a large aperture in AstroImageJ that encompassed both stars in the EZ Lyr system instead of isolating the RR Lyrae variable. The effect of this was minimized by collecting additional data several months later. This was mainly done as an attempt to collect data points in the sharp rise section of the light curve, but unfortunately, only a couple observations during this stage succeeded. This could have been caused by several factors such as the star’s position in the sky being out of range of the telescopes or even bad visibility from weather. This gap does not seem to have impacted the final results as there was ample data in the other stages.

Other complications in data processing arose from the nature of EZ Lyr being a double star. It was at times hard to understand the celestial coordinate system and this led to questioning where to set the coordinates for analysis. In retrospect, it seems logical to focus on a single star, but there were attempts made to process the data while targeting the space between the stars and the two stars individually. As expected, only one of those positions produced coherent data, which was the RR Lyrae variable. Another confusion as a result was that it was briefly thought the variable star had been misclassified and was actually the other star in the system. This was cleared up after consulting Aladin and recognizing that the LCO images were flipped and it did in fact match previous findings (Bonnarel et al., 2000).

Applying the period-luminosity-metallicity mathematical relations was a simple process done in several steps on Excel using a prepared spreadsheet. The

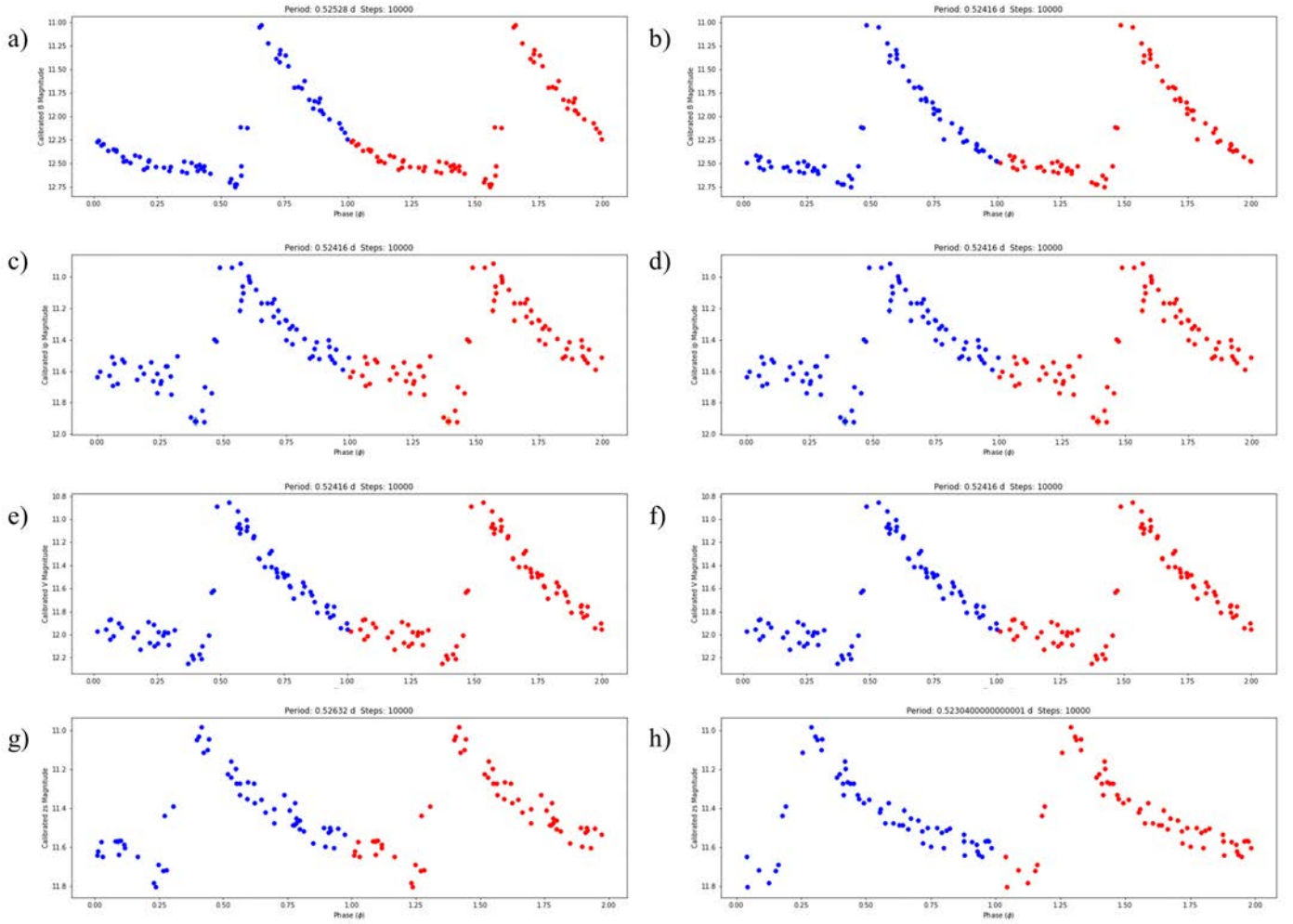


Fig. 2. Light curves for EZ Lyr in the B-, i-, V, and z bands are shown above. The filters are as follows: B-band (a, b), i-band (c, d), V-band (e, f), and z-band (g, h). String method is used in (a, c, e, g) and PDM method is used in (b, d, f, h). Two full cycles are displayed to better visualize the shape of the curve. Calibrated luminosity magnitudes are shown in Table 1. Period values and error are provided in Table 2.

Filter	String	String Error	PDM	PDM Error
B	0.52528	0.0003	0.52200	0.0002
ip	0.52528	0.0004	0.52528	0.0003
V	0.52416	0.0003	0.52632	0.0003
zs	0.52496	0.0103	0.52576	0.0110

Table 2. Period Measurements: The period, in days, for each filter was measured using both String and PDM methods. The values were consistent with each other and had small error due to the amount of observations.

Filter	Distance (pc)	Error (pc)
GAIA	1523	60
V	1415	59
i	1383	51
z	1420	54
Viz	1406	32

Table 3. Distance Measurements: The GAIA measurement using parallax is shown for comparison with values obtained using period luminosity for V, i, and z - band, where Viz is the average. Uncertainty in these measurements is from the period and calibration errors. Each value is visualised in Figure 3.

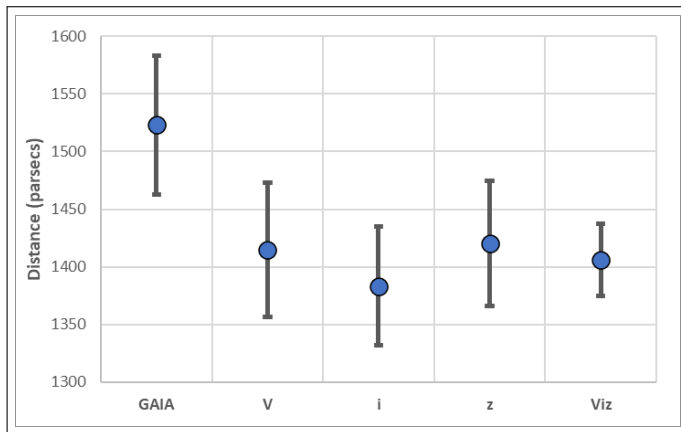


Fig. 3. Distance Measurements Graph: This is a plot of Table 3 showing how the distances in this study compare to GAIA.

hardest part of this process was finding an appropriate interstellar reddening value $E(B-V)$. The number settled on 0.08 which is slightly lower than the value of 0.1293 ± 0.0077 from 2011 and 0.1503 ± 0.0089 from 1998 provided by the Schlegel Dust Map Website (Schlegel, Finkbeiner, & Davis, 1998). An $E(B-V) \approx 0.08$ is a reasonable value given that the Schlegel dust maps give the total extinction along that line of sight and the star is in front of at least some of the dust. The image from the dust map site did not clearly separate the two stars and it was difficult to pinpoint exactly where the RR Lyrae should be because when entering the RA and Dec, the target on the map was shown in the gray area left of the bright stars marked in the picture. Because of this, the data from the website was used only as a rough estimate to begin refining the value until the variance was minimized.

Once the inputs were set, the final calculations were slightly shorter than GAIA's uncertainty margin. The calculations were precise after adjusting the interstellar reddening, therefore the accuracy of this value is a key factor in the legitimacy of the final data. Other measurements of interstellar reddening for EZ Lyr besides the Schlegel Dust Map could not be found to support or oppose the value used here, so further evaluation of this value would be recommended.

CONCLUSION

This project showed that a reliable distance could be produced using a period luminosity metallicity relationship. The results for EZ Lyr were all within the same range of each other with reasonable uncertainty and are close to the GAIA distance which used parallax. In the future, when combined with results from other groups performing the same experiment on different RR Lyrae stars, there may prove to be substantial evidence that Catelan's method is as accurate as parallax distance measurements. Since this method does not rely on parallax angles, it could be used on more distant stars. A limitation of this method is that RR Lyraes tend to be fainter stars, however with longer exposure times and larger telescopes, it could still be possible to estimate distances to the more far off stars.

FUNDING

Student participation in this project was funded by the National Aeronautics and Space Administration under Grant No. NNX15AR73H issued through the Tennessee Space Grant Consortium.

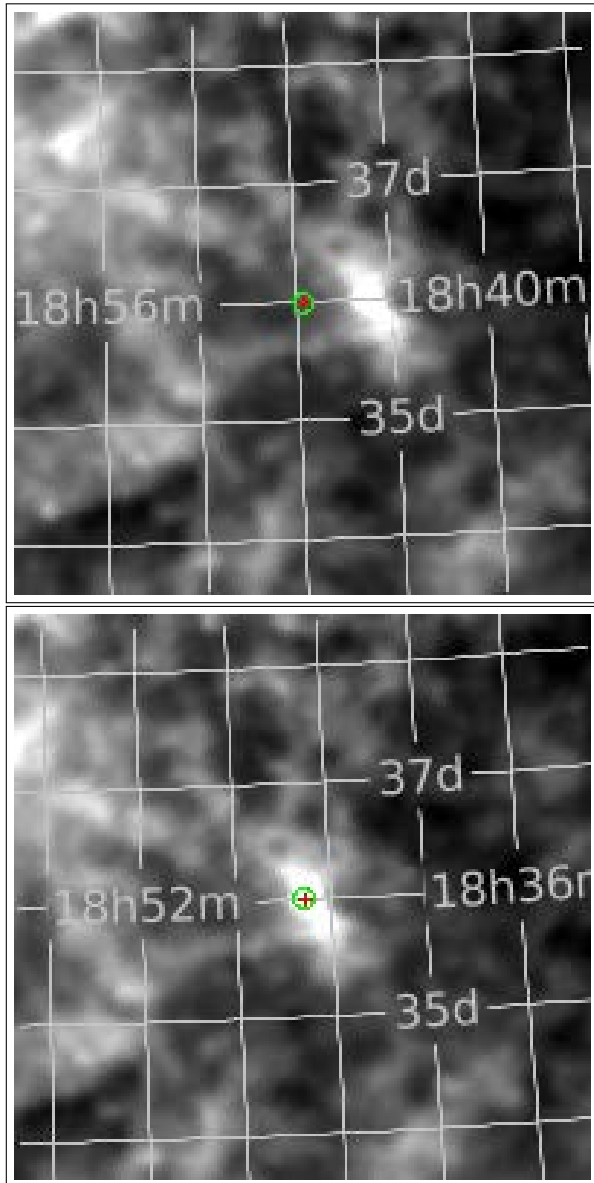


Fig. 4. Schegel Dust Map Targets: The first image shows the target automatically placed given the location of EZ Lyr. The second image is where the target was manually placed to better represent the actual location of EZ Lyr based off the bright points.

ACKNOWLEDGMENTS

This project was part of a research course run by Dr. Michael Fitzgerald of Our Solar Siblings who supported students throughout the course. Our Solar Siblings (OSS) is a inquiry based project to high school and undergraduate students interested in doing investigative research in astronomy. OSS provided access to their pipeline, educational materials, and time with the Las Cumbres Observatory.

Appreciation is also given to free programs utilized in this course such as Stellarium (<https://stellarium.org/>), Aladin (<https://aladin.u-strasbg.fr/>), AstroImageJ (<https://www.astro.louisville.edu/software/astroimagej/>), Gimp (<https://www.gimp.org/>), and Fits Liberator (https://www.spacetelescope.org/projects/fits_liberator/).

REFERENCES

- Altunin, I., Caputo, R., & Tock, K. (2020). Period of eclipsing binary epic 201458798. *Astronomy Theory, Observations & Methods*, 1(1).
- Bertin, E. (2011). Automated morphometry with sextractor and psfex. In *Astronomical data analysis software and systems xx* (Vol. 442, p. 435).
- Bonnarel, F., Fernique, P., Bienaymé, O., Egret, D., Genova, F., Louys, M., ... Bartlett, J. G. (2000). The aladin interactive sky atlas-a reference tool for identification of astronomical sources. *Astronomy and Astrophysics Supplement Series*, 143(1), 33–40.
- Brown, T., Baliber, N., Bianco, F., Bowman, M., Burleson, B., Conway, P., ... others (2013). Las cumbres observatory global telescope network. *Publications of the Astronomical Society of the Pacific*, 125(931), 1031.
- Cáceres, C., & Catelan, M. (2008). The period-luminosity relation of rr lyrae stars in the sdss photometric system. *The Astrophysical Journal Supplement Series*, 179(1), 242.
- Cardelli, J. A., Clayton, G. C., & Mathis, J. S. (1989). The relationship between infrared, optical, and ultraviolet extinction. *The Astrophysical Journal*, 345, 245–256.
- Chambers, K. C., Magnier, E., Metcalfe, N., Flewelling, H., Huber, M., Waters, C., ... others (2016). The pan-starrs1 surveys. *arXiv preprint arXiv:1612.05560*.
- Clementini, G., Eyer, L., Ripepi, V., Marconi, M., Muraveva, T., Garofalo, A., ... others (2017).

- Gaia data release 1-testing parallaxes with local cepheids and rr lyrae stars. *Astronomy & Astrophysics*, 605, A79.
- Collins, K. A., Kielkopf, J. F., Stassun, K. G., & Hesselman, F. V. (2017). Astroimagej: Image processing and photometric extraction for ultra-precise astronomical light curves. *The Astronomical Journal*, 153(2), 77.
- Dambis, A., Berdnikov, L., Kniazev, A. Y., Kravtsov, V., Rastorguev, A., Sefako, R., & Vozyakova, O. (2013). Rr lyrae variables: visual and infrared luminosities, intrinsic colours and kinematics. *Monthly Notices of the Royal Astronomical Society*, 435(4), 3206–3220.
- Dworetzky, M. (1983). A period-finding method for sparse randomly spaced observations or “how long is a piece of string?”. *Monthly Notices of the Royal Astronomical Society*, 203(4), 917–924.
- Fitzgerald, M. T. (2018). The our solar siblings pipeline: Tackling the data issues of the scaling problem for robotic telescope based astronomy education projects.
- Fitzgerald, M. T., Criss, J., Lukaszewicz, T., Frew, D. J., Catelan, M., Woodward, S., ... McKinnon, D. H. (2012). Rr lyrae stars in the globular cluster ngc 6101. *Publications of the Astronomical Society of Australia*, 29(1), 72–77.
- Fitzgerald, M. T., Gomez, E., Salimpour, S., Singleton, J., & Wibowo, R. W. (2021). “astrosources”: automating optical astronomy measurement, calibration and analysis for variable stellar sources from provided photometry. *Journal of Open Source Software*, 6(58), 2641.
- Henden, A. A., Templeton, M., Terrell, D., Smith, T. C., Levine, S., & Welch, D. (2016, January). VizieR Online Data Catalog: AAVSO Photometric All Sky Survey (APASS) DR9 (Henden+, 2016). *VizieR Online Data Catalog*, II/336.
- Høg, E., Fabricius, C., Makarov, V. V., Urban, S., Corbin, T., Wycoff, G., ... Wicenec, A. (2000, March). The Tycho-2 catalogue of the 2.5 million brightest stars. , 355, L27-L30.
- Preston, G. W. (1959). A spectroscopic study of the rr lyrae stars. *The Astrophysical Journal*, 130, 507.
- Schlegel, D., Finkbeiner, D., & Davis, M. (1998). Application of sfd dust maps to galaxy counts and cmb experiments. *arXiv preprint astro-ph/9809230*.
- Stellingwerf, R. F. (1978). Period determination using phase dispersion minimization. *The Astrophysical Journal*, 224, 953–960.
- Suntzeff, N. B., Kraft, R. P., & Kinman, T. (1994). Summary of delta s metallicity measurements for bright rr lyrae variables observed at lick observatory and kpno between 1972 and 1987. *The Astrophysical Journal Supplement Series*, 93, 271–285.
- Whitford, A. (1958). The law of interstellar reddening. *The Astronomical Journal*, 63, 201–207.

ExoSelect and ExoRequest: Targets and Resources for efficiently observing Exoplanets

SAEED SALIMPOUR^{1,2,3,4*}, MICHAEL FITZGERALD^{5,1}, AND HEATH DEMMERT

¹Deakin University, Burwood, Victoria, Australia

²International Astronomical Union, Office of Astronomy for Education, Heidelberg, Germany

³Haus der Astronomie, Heidelberg, Germany

⁴Max Planck Institute for Astronomy, Heidelberg, Germany

⁵Las Cumbres Observatory, Goleta, CA, USA

*Corresponding author: astrophysics@saeedsalimpour.com

In the past decade, exoplanet science has exploded, driven by discoveries using observations from both space-based and ground-based telescopes. Large amounts of data, coupled with technological advances and easy access to robotic telescopes, have allowed the general public and students to become vital contributors to the field. These developments have also provided fertile ground in the context of science education, by enabling exoplanet science to be taken into classrooms as an authentic scientific inquiry, echoing the notions of Science-as-Practice. This paper introduces technical infrastructure that enables beginners and students to quickly pick exoplanet targets and schedule an observation. It also provides a list of the “best” exoplanets to try and observe by month of the year (related to Right Ascension) and latitude (related to Declination).

© 2021 Astronomy Theory, Observations and Methods Journal

Keywords: exoplanets — authentic data — educational resource — technology infrastructure

<https://doi.org/10.32374/atom.2020.2.6>

INTRODUCTION

Over the past decade, there have been great strides in identifying and minimising the barriers that prevent students from engaging in authentic scientific inquiry using robotic telescopes in the classroom (Gomez & Fitzgerald, 2017; Fitzgerald et al., 2014). One of the fundamental barriers is the time-pressure in schools, which is compounded by an overly busy curriculum (e.g.: Fitzgerald et al., 2019; Salimpour et al., 2020). In addition, the possibility of steep learning curves regarding technology and content knowledge can be discouraging for teachers who want to implement

authentic scientific inquiry, especially those without appropriate support.

Various projects (e.g.: Brown et al., 2013; Fitzgerald et al., 2018; Reichart et al., 2005; Sadler et al., 2001) around the world have aimed at putting in place technical infrastructure that allows teachers to more easily overcome the above barriers, and focus on student learning in the context of both conceptual and epistemic practices of science (Lehrer & Schauble, 2007). The aim is to develop flexible systems that can cater to everyone from the most basic to the most advanced, that enable students to focus on critical think-

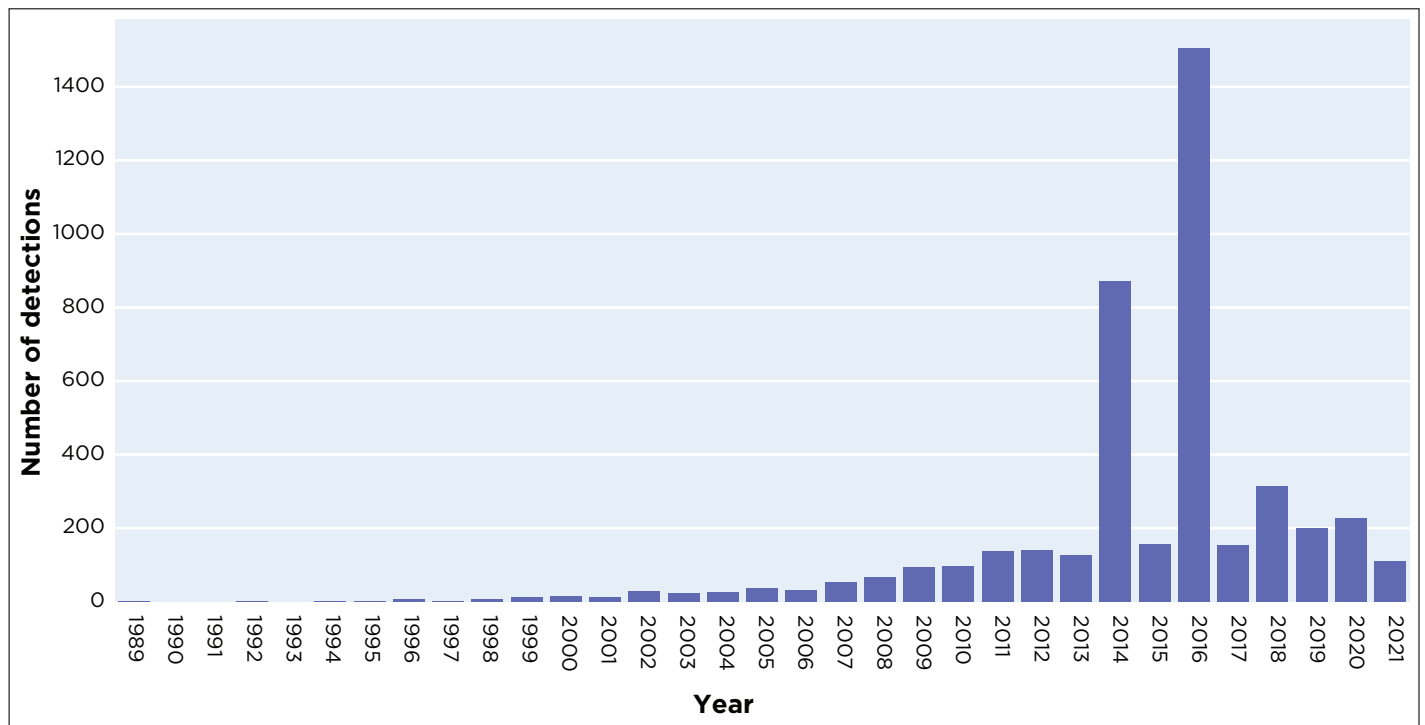


Fig. 1. Exoplanet detections over time, notice the two spikes (2014) and (2016), both associated with announcements of large-scale statistical analysis of data from previous years.

ing, essentially moving students from menial data ‘reduction’ to the inquisitive data ‘analysis’ (Fitzgerald, 2018).

This paper begins by providing a brief overview of exoplanet science, focussing on one of the most prolific and conceptually easier methods of detection. Then, the ways in which robotic telescopes have provided the opportunities for students to engage with and in authentic scientific inquiry are highlighted. Following this, the technical infrastructure that enables students and complete beginners to request observations of exoplanets is explained. The paper concludes by providing some perspectives on future directions for this endeavour.

EXOPLANET SCIENCE

In less than a decade, the number of exoplanet confirmations has exploded (see Figure 1), owing to the groundbreaking space-based observatory Kepler (Borucki et al., 2010; Howell, 2020). The current tally of confirmed exoplanets is 4455 (as of this writing), and the number of candidates yet to be confirmed is around 6297, so there is fertile ground to help astronomers confirm a vast number of exoplanets. Currently, the Transiting Exoplanet Survey Satellite (TESS) is continuously adding to this tally of explan-

ets (Ricker et al., 2010; Guerrero et al., 2021).

The most prolific exoplanet detection method is the Transit Method (TM) (see Figure 2), which is based on established and relatively simple laws of physics and geometry, some of which are taught at secondary school in curricula around the world (Salimpour et al., 2020). The key conceptual idea is grounded in the physics and mathematics of orbital motion, such as Kepler’s Laws. With robotic telescope observations, the aim is to detect the dimming of the light from the host star, as an exoplanet or extrasolar planet “passes” in front of the star’s disc. This geometry is represented in Figure 3. This is a simplified representational model, aimed at conveying the concept of detecting exoplanets via the Transit Method.

ROBOTIC TELESCOPES

The enabling technology that allows exoplanet science to be realised in the classroom is the use of Remote Robotic Telescopes (RRT). Gomez & Fitzgerald (2017) provide an extensive overview of the role of RRT in education. The use of RRTs removes the technological, financial, and geographical barriers that are associated with allowing students access to research-grade telescopes. Organisations like Las Cumbres Observatory (LCO) (Brown et al., 2013), Faulkes Tele-

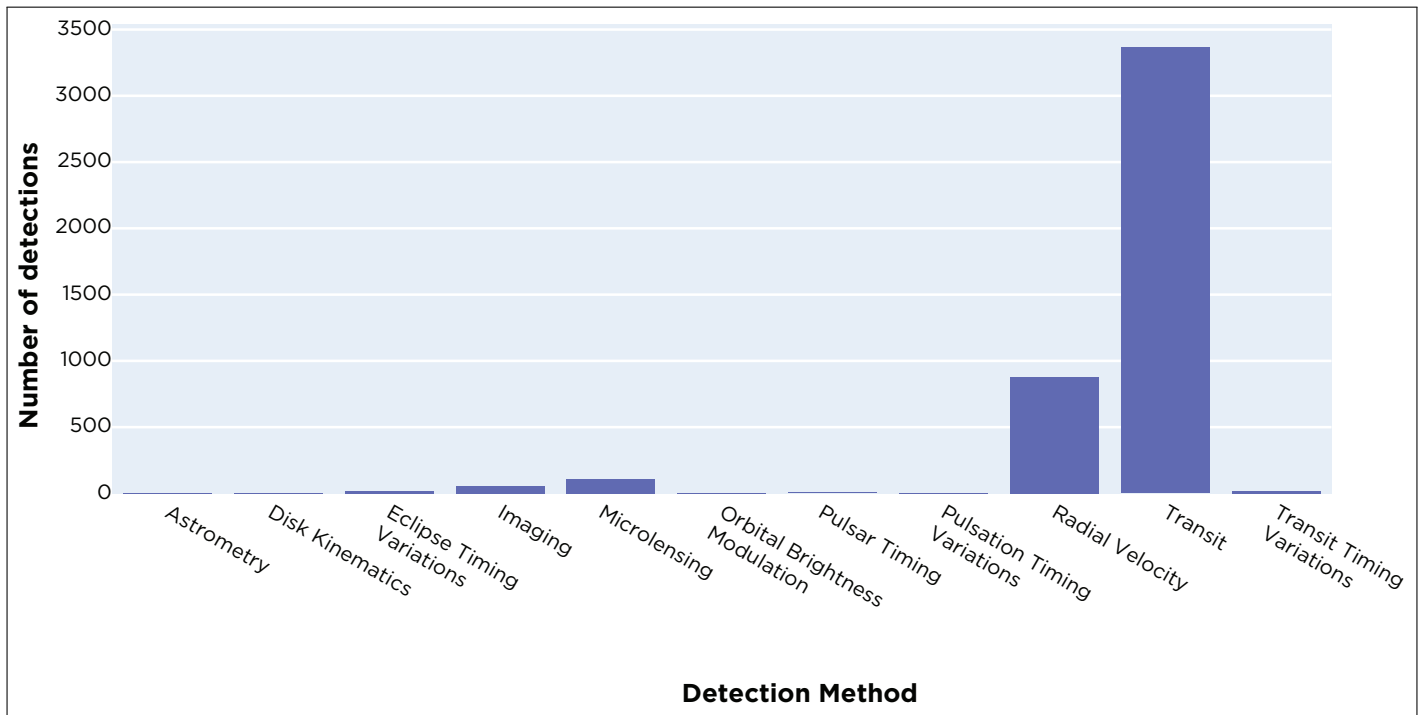


Fig. 2. Exoplanet detections methods, the Transit Method is by far the most prolific detection method, owing in part to the fundamental “simplicity” of measuring the dimming of starlight.

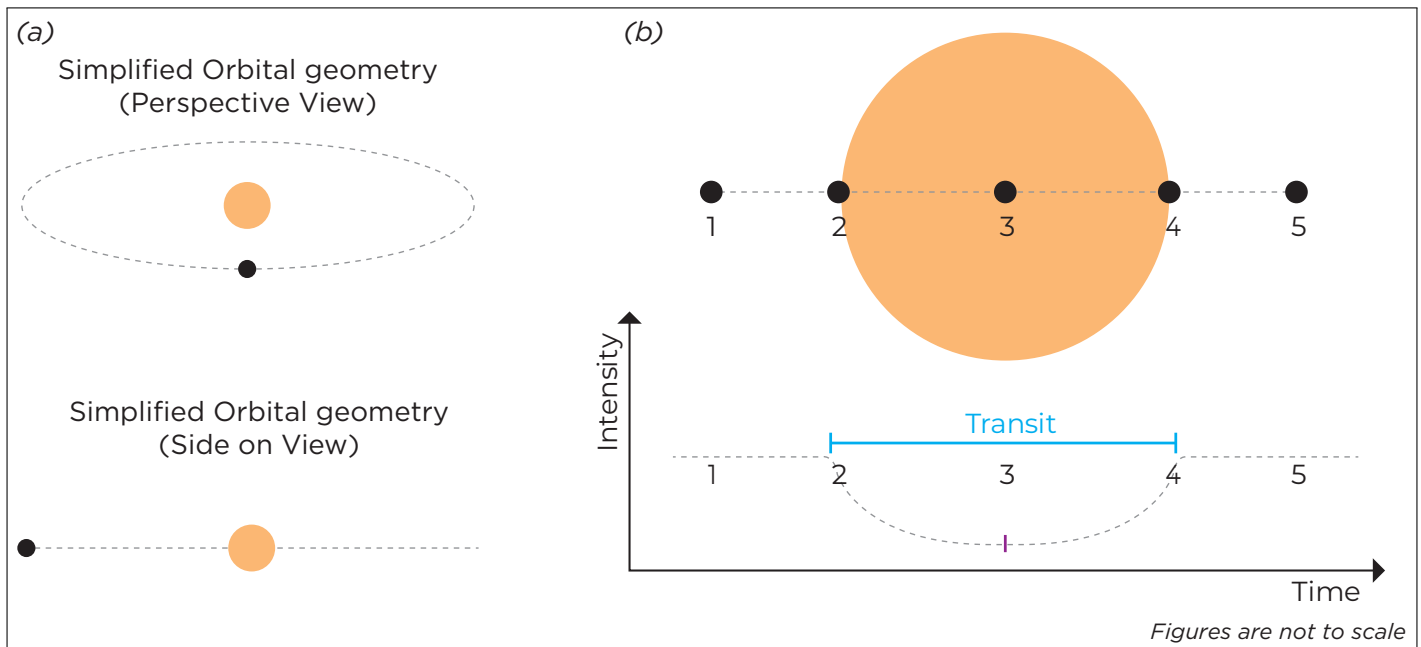


Fig. 3. Basic representation of the transit method, and (a) how the geometry of the orbit (b) allows for such a detection. The black dot represents the planet and the orange circle represents the host star. On the right, the planet is shown at five different positions relative to the star it is orbiting. Although this figure shows an ideal alignment where the planet is going directly through the middle of the star, in most cases the orbital alignment is not so ideally aligned.

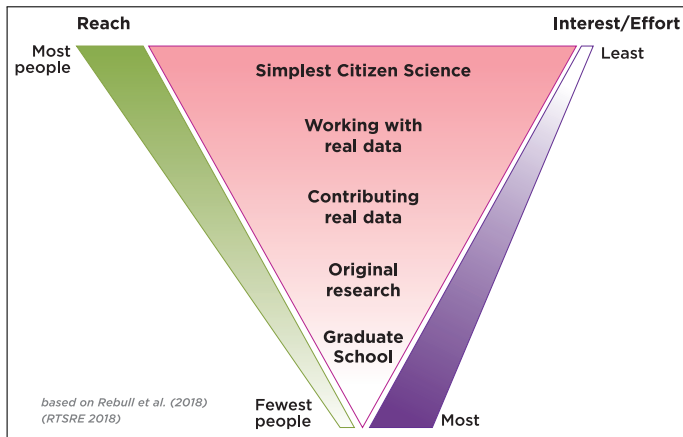


Fig. 4. Funnel of Interest ecosystem (modified from Rebull, 2018).

scope (Roche et al., 2008), SkyNet (Reichart et al., 2005), Microobservatory (Sadler et al., 2001) and SPIRIT (Luckas & Gottschalk, 2018) amongst others, have enabled authentic scientific inquiry to be brought into the classroom. This has led, not only to richer experiences for both students and teachers, but has also allowed students to publish authentic research and collaborate with astronomers. This approach is quite different to typical Citizen Science projects in astronomy, where the data has been significantly cleaned up and presented in a more idyllic manner removing much of the potential noise in the data, rather, in this case students are appreciating the messy nature of authentic data (see Figure 5) that they have collected (Salimpour et al., 2021).

The interaction between the reach, in terms of breadth and size of the target population, and the effort required to undertake authentic investigations is conceptualised by Rebull (2018) via the Funnel of Interest (FoI) (see Figure 4). In essence, the investigations that use readily available data are more likely to reach a larger audience (which, in the case of Citizen Science, do not need to have significant prerequisite knowledge), require the least effort to engage with the science, and can attract those with little initial interest. Further down the FoI, the reach of the investigations decreases, as there is a move from already available data to new data which is collected by the student. Therefore, only those who are really interested will be engaged, as this requires more effort on the part of the student. In the context of a school classroom, more effort and scaffolding on the part of the teacher is required to guide the students through the known unknowns, and unknown unknowns.

EXOPLANET SCIENCE IN THE CLASSROOM

Realising exoplanet science in the classroom in a way that is true to the notions of authentic inquiry has many technical challenges that can be overwhelming to teachers and students. This is owing to the fact that teachers are under enormous time pressures, that most teachers lack the Pedagogical Content Knowledge (PCK) (Shulman, 1986) and practical scientific research skills (Fitzgerald et al., 2019), and that some of them are even teaching out of field (Luft et al., 2020). These issues prevent them from tapping into the enormous potential offered by this field of inquiry. Picking exoplanets, planning and requesting observations, analysing the data, and interpreting the findings each have their own challenges with their own requisite extended learning curves. However, these challenges can be overcome by careful educational design, which involves two key layers: Technical Infrastructure, and Education Resources (see Figure 6). The technical infrastructure, which is the outer layer, enables students to quickly and efficiently request observations using robotic telescopes. The inner layer, which is the educational resources, is about providing teachers with a robust set of resources that they can be used to scaffold their students conceptually and technically in undertaking authentic scientific inquiry in the context of exoplanets in the classroom.

TECHNICAL INFRASTRUCTURE

Exoplanet Targets

One of the challenging aspects of making observations of exoplanets in the context of the classroom is determining which of the thousands of exoplanets would be a suitable observation target, taking into consideration the various pressures in schools (Fitzgerald et al., 2015, 2019). After several implementations of exoplanet science in high schools it became clear that for students to easily and fluidly engage with the science and analysis it would be best to have a robust list of provided targets. This is so students could quickly and efficiently pick a target simply relative to the month they were observing. This can provide relief from the excessive amount of time it takes to plan an observation.

Such a robust list, one that would allow students to conduct viable observations of known exoplanets, was compiled using the NASA Exoplanet Archive - an extensive database of exoplanets from various missions (Fig. 7), a list of targets that would allow students to



Fig. 5. The spectrum of Authentic Data. The use of Robotic Telescopes is situated at the far end of the spectrum - New Data (Salimpour et al., 2021)

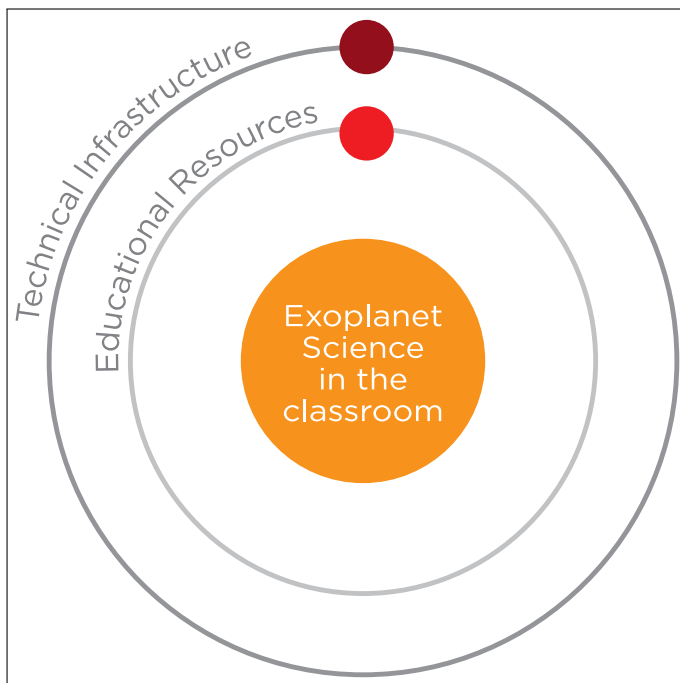


Fig. 6. The educational design for bringing Exoplanet Science into the classroom, is composed of two layers: Technical Infrastructure and Education Resources.

conduct viable observations of known exoplanets was compiled. This list is essentially the best targets that can be observed with 0.4m-class ground-based telescopes. The targets were limited to those that were at most 14th magnitude, and had a transit depth of $>1\%$. Using these parameters the list was narrowed to 68 targets. As the infrastructure available to the authors was based on using the LCO robotic telescope network - containing both Northern and Southern observatories, the initial list was not limited by geographical location with respect to the observing limits due to Declination and Latitude. However, for general purposes, that list of targets is provided in Tables 1, 2, 3 in this paper divided into Northern, Equatorial and Southern objects. Figures 8 - 10 provide various descriptive distributions for the final target list of exoplanets.

The process of picking such targets was described in more detail in earlier work by Sarva et al. (2020). That paper provides a step-by-step explanation of the process of picking exoplanets for observing using the NASA Exoplanet Archive. In the current paper, the process has been further simplified by providing a simple list to allow complete beginners and teachers with minimal time to be able to quickly enable students to carry out observations. While this list prioritizes those targets that are easiest to observe for beginning users, it does not prioritise the list by what is most useful to observe for science reasons. This is a continually moving target. For the latest lists of transiting planets that are useful for upcoming space telescope missions, it is best to refer to the project websites of [Exoplanet Watch](#) and [ExoClock](#) for lists of needed observations.

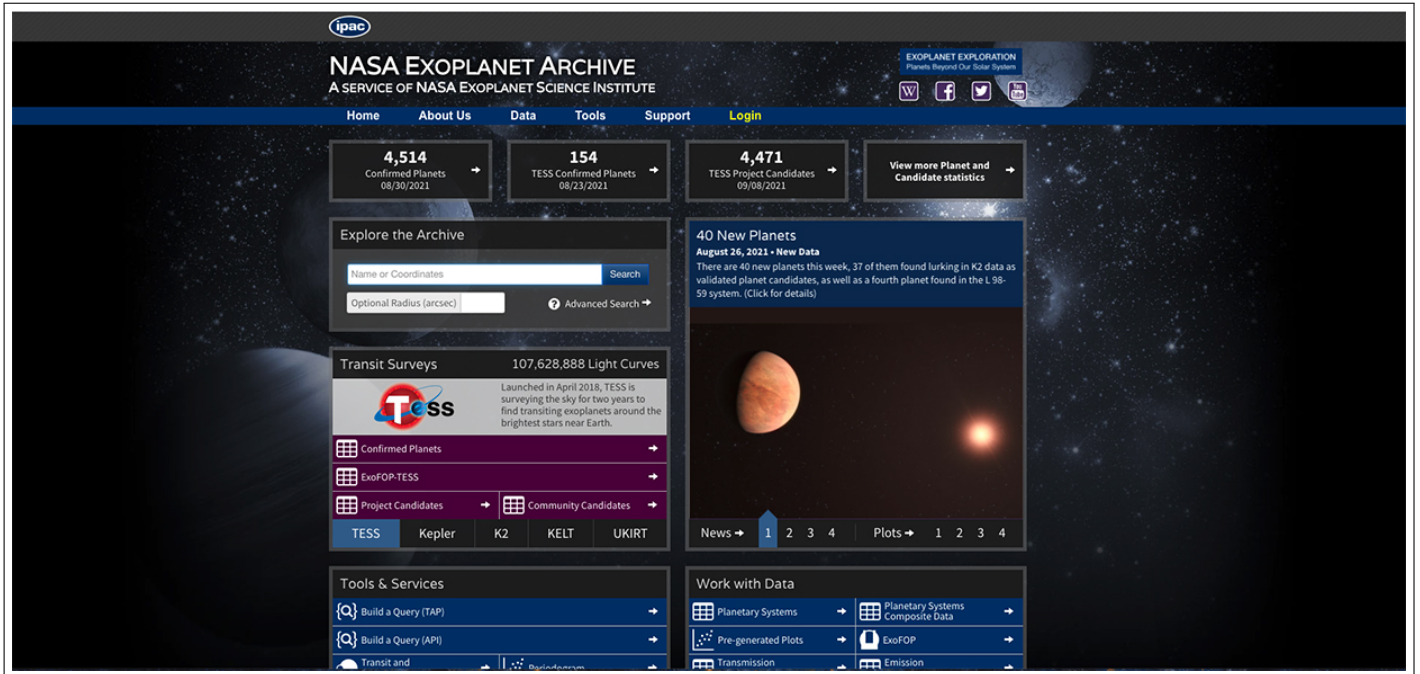


Fig. 7. NASA Exoplanet Archive, a web-based portal that allows access to the most up to date exoplanet catalogue from various missions managed by the California Institute of Technology.

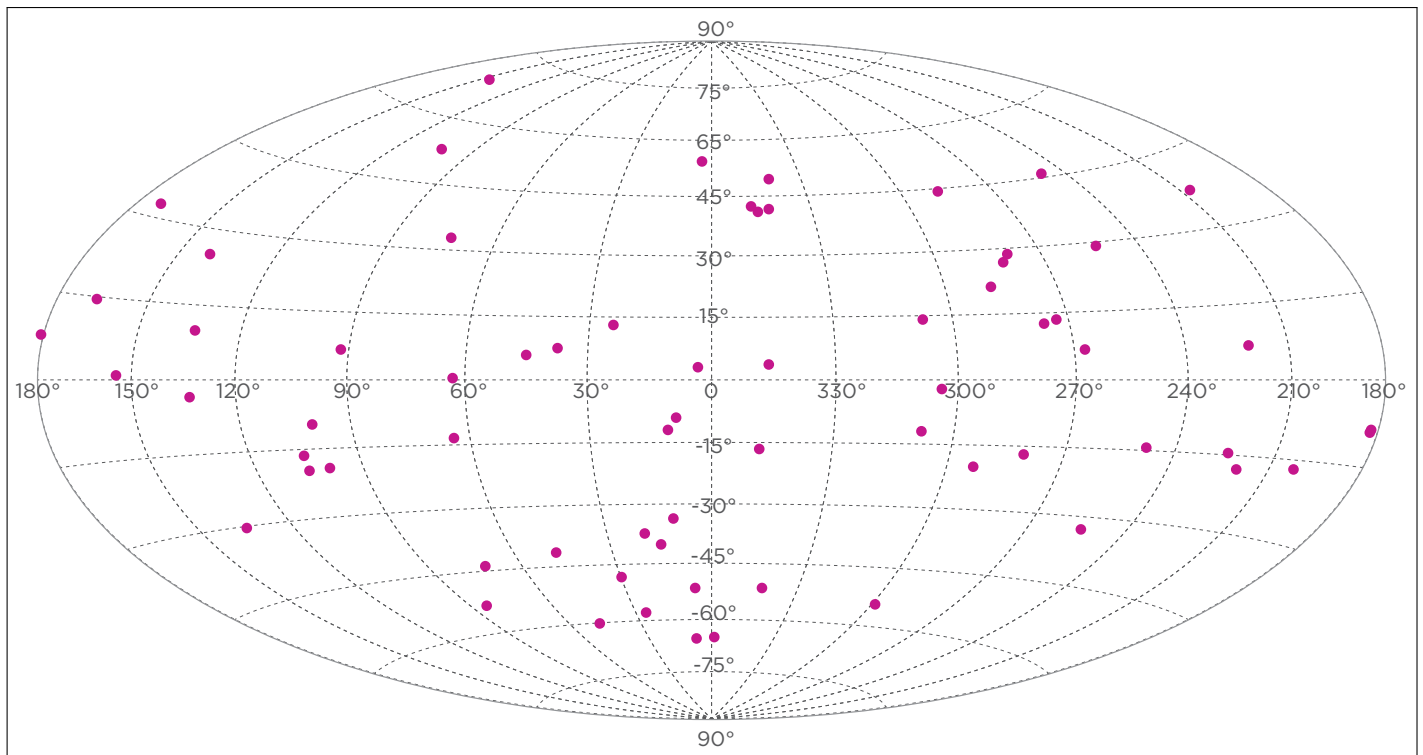


Fig. 8. Distribution of the exoplanets identified in this study in the sky using Aitoff projection with ICRS coordinates in degrees.

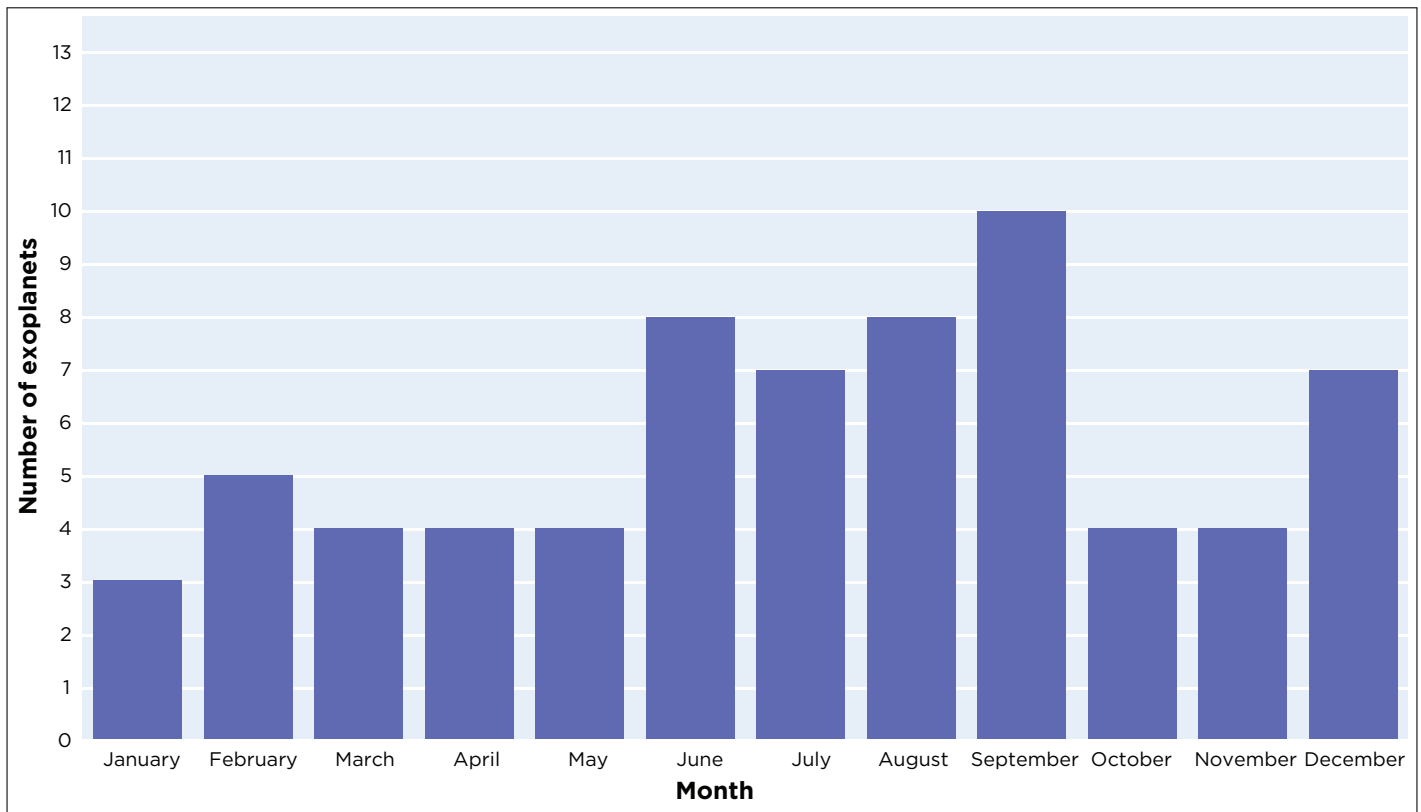


Fig. 9. Distribution of exoplanets that are best observed in particular months derived from their Right Ascension coordinates.

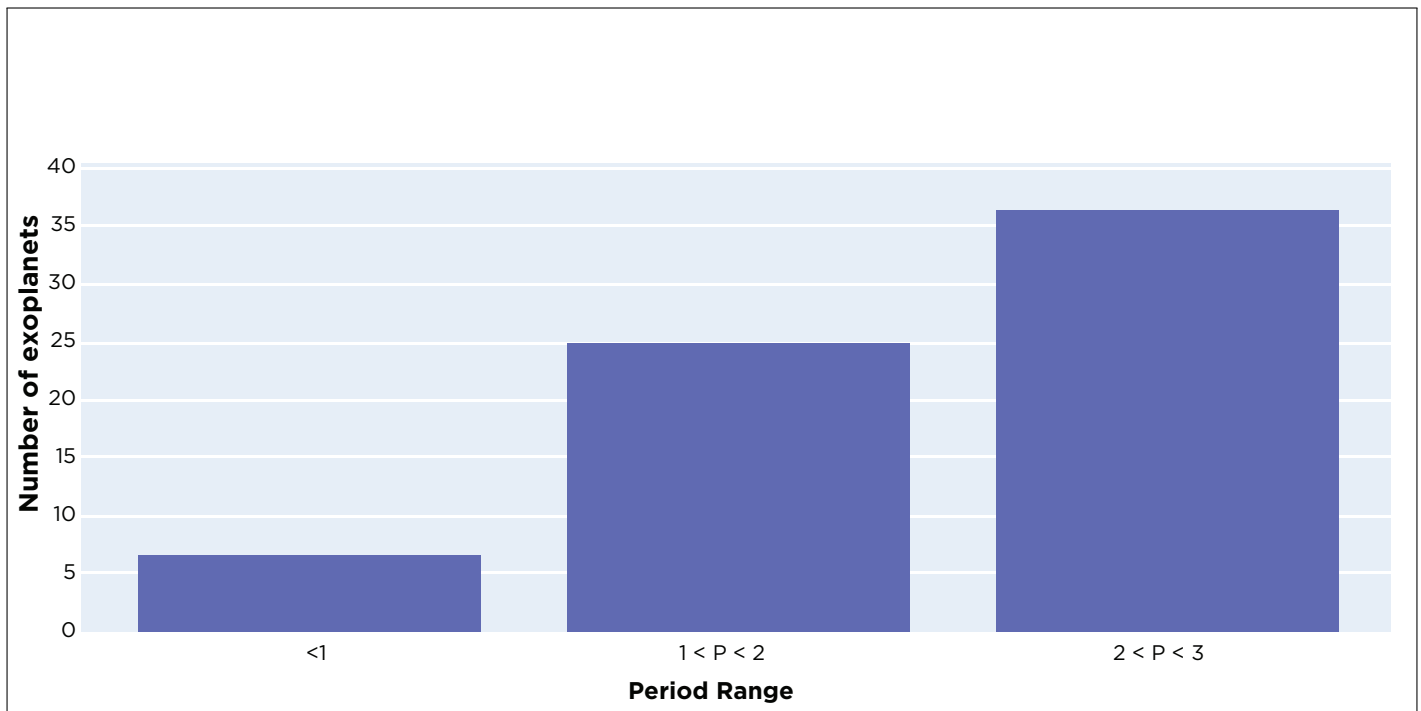


Fig. 10. Distribution of exoplanets for three orbital period bins <1 , $1 < P < 2$, and $2 < P < 3$. The limit to 3 days was to enable students to easily obtain an exoplanet transit within the time-constraints of a semester.

Table 1. List of exoplanet targets binned into Southern declination zone for declinations less than -20° .

Southern (Dec $<-20^\circ$)							
Planet Name	RA (deg)	DEC (deg)	Best Month	Orbital Period (days)	Transit duration (hrs)	Transit Midpoint (BJD)	Magnitude (mag)
HIP 65 A b	0.1856063	-54.830823	Sep	0.9809734	0.78576	2458326.10418	11
WASP-97 b	24.6051389	-55.772001	Sep	2.07276	2.5824	2456438.18683	10.57
WASP-119 b	55.9336392	-65.19378	Oct	2.4998048	2.88	2456537.54930	12.314
WASP-98 b	58.4290113	-34.328272	Nov	2.96264	1.908	2456333.39130	13.252
WASP-140 b	60.3855387	-20.450999	Nov	2.2359835	1.5144	2456912.35105	11.118
TOI-157 b	73.7014398	-76.680606	Nov	2.0845435	2.14584	2458326.54771	12.725
WASP-64 b	101.114922	-32.858388	Dec	1.5732918	2.39976	2455582.60169	12.704
WASP-23 b	101.127503	-42.76223	Dec	2.9444256	2.39424	2455320.12363	12.539
WASP-121 b	107.600231	-39.097271	Dec	1.2749255	2.8872	2456635.70832	10.514
KELT-14 b	108.301409	-42.409762	Dec	1.7100588	2.1336	2457091.02863	11.001
WASP-170 b	135.416303	-20.720369	Jan	2.34478022	2.04	2457802.39150	12.613
WASP-19 b	148.416767	-45.659108	Feb	0.78884	1.572	2455168.96801	12.248
WASP-123 b	289.479212	-32.860124	Jun	2.9776412	3.0936	2456845.17082	11.03
WASP-46 b	318.737012	-55.871863	Jul	1.43037	1.67352	2455392.31553	13.043
WASP-144 b	320.762876	-40.048439	Jul	2.2783152	1.9536	2457157.27493	13.085
WASP-145 A b	322.253764	-58.836147	Jul	1.7690381	0.9768	2456844.16526	11.636
WASP-95 b	337.457824	-48.003099	Aug	2.184673	2.784	2456338.45851	10.092
WASP-164 b	344.873588	-60.447819	Aug	1.7771255	1.60368	2457203.85378	12.603
WASP-4 b	353.562915	-42.061779	Aug	1.3382299	2.12832	2454387.32779	12.483
WASP-173 A b	354.168696	-34.611304	Aug	1.3866529	2.3544	2458105.59824	11.15
WASP-91 b	357.846434	-70.152862	Aug	2.798581	2.3424	2456297.71900	11.98
WASP-5 b	359.349028	-41.27722	Aug	1.6284229	2.3712	2454373.99598	12.147

Table 2. List of exoplanet targets binned into Equatorial declination Zone for declinations less between -20° and $+20^\circ$

Equatorial ($-20 < \text{Dec} < +20$)							
Planet Name	RA (deg)	DEC (deg)	Best Month	Orbital Period (days)	Transit duration (hrs)	Transit Midpoint (BJD)	Magnitude (mag)
WASP-44 b	3.9032733	-11.938265	Sep	2.423804	2.2368	2455434.37600	13.096
WASP-32 b	3.9617073	1.2005122	Sep	2.718659	2.424	2455151.05460	11.257
WASP-26 b	4.6030424	-15.267404	Sep	2.7566004	2.3832	2455228.38842	11.297
WASP-76 b	26.632936	2.700389	Sep	1.809886	3.6936	2456107.85507	9.518
WASP-77 A b	37.1555223	-7.0606675	Oct	1.3600309	2.16	2455870.44977	10.294
WASP-50 b	43.6880738	-10.898024	Oct	1.9550959	1.80576	2455558.61197	11.44
HAT-P-70 b	74.5523332	9.9979794	Nov	2.744321	3.421	2459197.00754	9.47
WASP-49 b	91.0897193	-16.96539	Dec	2.7817362	2.14	2455580.59436	11.352
WASP-36 b	131.58039	-8.0269855	Jan	1.5373653	1.81584	2455569.83731	12.836
WASP-65 b	133.324298	8.5230171	Jan	2.3114243	2.73504	2456110.68772	11.869
WASP-43 b	154.908187	-9.8064431	Feb	0.813475	1.1592	2455528.86774	12.305
WASP-104 b	160.602369	7.4350768	Feb	1.7554137	1.76208	2456406.11126	11.779
WASP-85 A b	175.908033	6.5637842	Feb	2.6556777	2.59584	2456847.47286	10.72
K2-229 b	186.87292	-6.7218474	Mar	0.58426	1.5	2457583.46910	10.985
K2-228 b	187.294705	-6.8342028	Mar	2.69828	1.5	2457583.19430	13.028
Qatar-2 b	207.655493	-6.8040714	Mar	1.33711677	1.809816	2457250.20082	13.443
WASP-57 b	223.819979	-2.0576866	Apr	2.838971	2.304	2455717.87811	12.913
WASP-24 b	227.215498	2.343286	Apr	2.34121242	2.6832	2455081.37941	11.219
WASP-103 b	249.31486	7.1833758	May	0.925542	2.593	2456459.59957	12.402
WASP-163 b	256.537555	-10.413007	May	1.6096884	2.232	2457918.46200	12.663
CoRoT-11 b	280.6873	5.9376586	Jun	2.99433	2.5009	2454597.67900	12.897
CoRoT-2 b	291.777046	1.3836634	Jun	1.7429935	2.26704	2454237.53562	12.516
HAT-P-23 b	306.123908	16.7621462	Jul	1.212884	2.1792	2454852.26464	11.937
WASP-2 b	307.725559	6.4293305	Jul	2.152175	1.78824	2458339.00342	11.728
WASP-75 b	342.3859	-10.675469	Aug	2.484193	1.9728	2456016.26690	11.591
WASP-52 b	348.494793	8.7610793	Aug	1.7497798	1.8096	2455793.68143	12.192

Table 3. List of exoplanet targets binned into Northern declination zone for declinations greater than $+20^\circ$.

Northern (Dec $> +20^\circ$)							
Planet Name	RA (deg)	DEC (deg)	Best Month	Orbital Period (days)	Transit duration (hrs)	Transit Midpoint (BJD)	Magnitude (mag)
Qatar-4 b	4.859275	44.0275965	Sep	1.8053564	2.1384	2457637.77361	13.574
Qatar-5 b	7.0539375	42.0613451	Sep	2.8792319	2.9088	2457336.75824	12.614
WASP-93 b	9.4587443	51.288778	Sep	2.7325321	2.2344	2456079.56420	10.966
HAT-P-16 b	9.5730343	42.4630961	Sep	2.77596	3.0624	2455027.59293	10.911
HAT-P-32 b	31.0427614	46.6878512	Oct	2.1500082	3.12048	2455867.40274	11.439
WASP-12 b	97.636645	29.6722662	Dec	1.0914203	2.99592	2456176.66826	11.569
XO-2 N b	117.026769	50.2251472	Dec	2.615826	2.653041	2458843.21868	11.246
KELT-4 A b	157.06262	25.5731366	Feb	2.9895932	3.46272	2456190.30201	9.98
HAT-P-36 b	188.266205	44.9153672	Mar	1.3273466	2.23248	2456698.73591	12.146
WASP-14 b	218.276625	21.8946875	Apr	2.243752	3.06	2454463.57583	9.745
KELT-23 A b	232.146641	66.3587097	Apr	2.25528783	2.278	2458140.38698	10.308
WASP-92 b	246.69204	51.0411328	May	2.1746742	2.7672	2456381.28340	12.951
WASP-135 b	267.284885	29.8790428	May	1.4013794	1.656	2455230.99020	13.181
HAT-P-5 b	274.405534	36.6214617	Jun	2.788491	2.9208	2454241.77663	11.954
WASP-3 b	278.631741	35.6614312	Jun	1.8468355	2.772	2454640.64993	10.632
HAT-P-37 b	284.296039	51.2691212	Jun	2.797436	2.3304	2455642.14000	13.427
TrES-2 b	286.808526	49.3164211	Jun	2.47061892	1.789	2455642.14318	11.254
Kepler-854 b	293.351268	43.1346404	Jun	2.14463285	3.9028	2454966.98434	13.417
Qatar-1 b	303.38187	65.1623313	Jul	1.4200242	1.66104	2456234.10322	12.692
KELT-16 b	314.268523	31.6610186	Jul	0.9689951	2.4888	2457247.24791	11.717

User Interface

Another challenging aspect of making exoplanet observations is being able to observe a complete transit. This requires knowing the location of the host star on the celestial sphere and the orbital period and the Transit mid-point of the exoplanet, among other parameters. Next, it requires carefully planning the observation such that a complete transit can be observed within the available time frame. This can be challenging for students and teachers, as this requires very deep conceptual and content knowledge as well as applying an algorithm that can confuse experts at times!

MANUALLY CALCULATING A FUTURE TRANSIT TIME

There are a variety of online transit calculators, such as Tapir at Swarthmore (Jensen, 2013), that will provide available transits to observe at your location according to specified limits. In the future are all possible observable transits that we would like to predict. In the past some of the previous transits have been observed, allowing us to estimate how often the transit occurs (orbital period) and when (transit midpoint). From Figure 11, if we know any previous time that the transit occurred (the “midpoint transit time”), we can simply keep adding the orbital period onto this time until the transit occurs in the future from now.

Once we know that we have a transit that is in the future (and we have checked that it is occurring at our nighttime... otherwise we move on and check the next transit!) then, knowing the transit duration, we can estimate appropriate start and stop times for a transit observation, which are usually equally distant in time from the midpoint transit time. This is shown schematically in Figure 12 from Sarva et al. (2020). Having figured out all of this timing, the last important piece of information is the star’s brightness from its optical magnitude, which allow us to estimate a long enough, but not too long, exposure time suitable for our target exoplanet star. Assuming that we have selected a star that has a deep enough transit to be observed (all stars in the provided target list in this paper are $> 1\%$), then from all this information we can program in our observation to a robotic telescope or prepare to manually observe the transit.

The observation start time is the predicted midpoint transit time minus half the transit duration, minus the amount of time to observe outside the transit event when the transit curve is “flat”, minus a small

amount of buffer time to help with scheduling or control for shifts in the midpoint transit. The observation end time is the point equally distant in time from the midpoint transit time, but after the transit. On the face of it, it may not seem too confusing but there are quite a number of calculation steps that can be prone to calculation error for beginners and experts alike.

ExoRequest

To simplify and automate these steps, an automated observation routine has been developed – ExoRequest – written in Python, which can be implemented via Google Colaboratory (see Figure 13). ExoRequest can also be run locally on Windows or macOS. It can be used to submit directly to Las Cumbres Observatory (LCO) or be used for planning for a local observatory. ExoRequest requires that the user knows the necessary parameters (such as those in the provided tables) for their given exoplanet. As well as the typical parameters, such as midtransit point and period, it also estimates a reasonable exposure time based on the provided optical magnitude. This information is used to calculate the relevant details described above and automatically submit this to the LCO scheduler.

ExoSelect: Web-based observation request portal

When the user does not know what object they might like to observe, or wants to select from some well-known targets for that time of the year, a further Web-based interface - ExoSelect - has been created to automatically fill in these values in (see Figure 14). ExoSelect also functions as a web interface to ExoRequest by using a manual drop-down box. This brings in an additional layer of simplicity, especially for instances where students may not have access to the technology infrastructure, or the confidence to run computer code. The web-based interface was developed using VueJS, wrapped in an HTML5 page, and Flask/Python which allows the observation portal to pull information from the web-based user interface and send it to the LCO observing portal. ExoSelect sends the required information to ExoRequest in Python using Flask, which then sends the information to the LCO observing portal (see Figure 15). In addition, there is a semi-automated pipeline that allows the maintainers of the website to dynamically send an updated list of exoplanets to ExoSelect, ensuring that new potential exoplanets are made available to students.

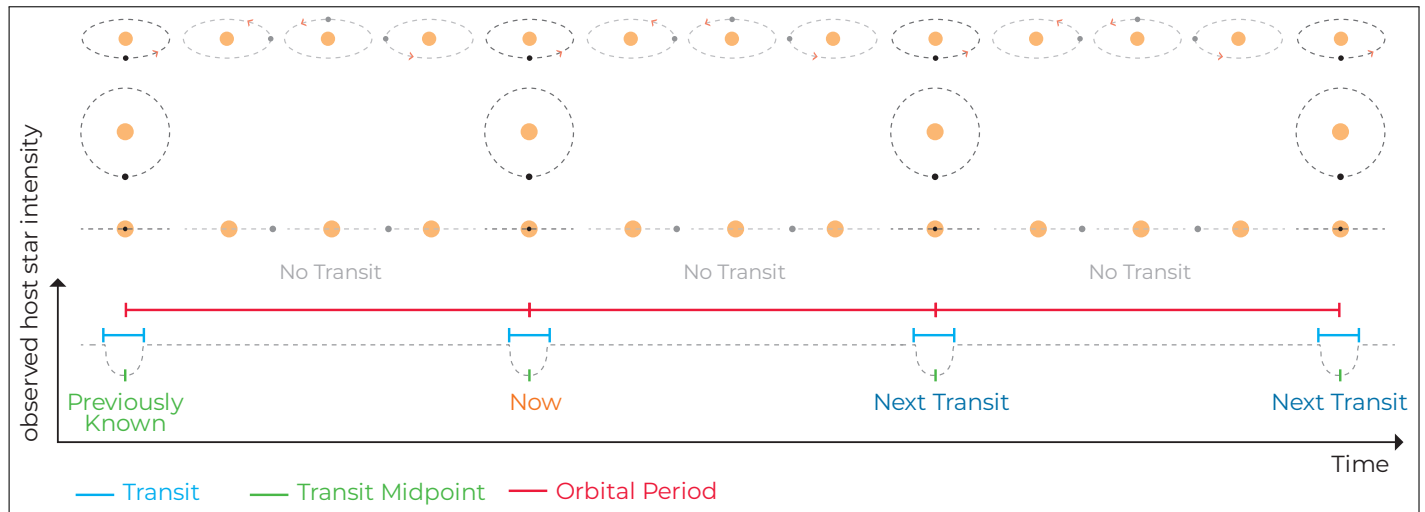


Fig. 11. A simplified schematic showing the fundamental method behind automatically calculating upcoming transmits. The red bars represent the period of the orbit. The blue bars represent the transit duration. Knowing the Transit midpoint, orbital period and transit duration retrieved from the NASA Exoplanet Archive, every upcoming transit from the current date can be calculated. Figure not to scale.

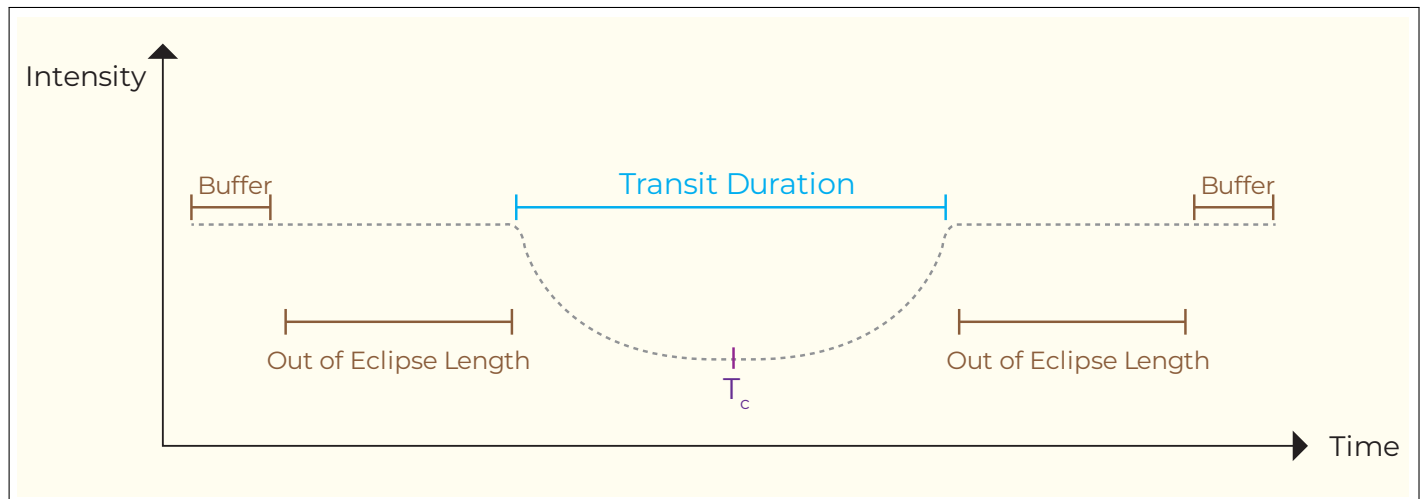
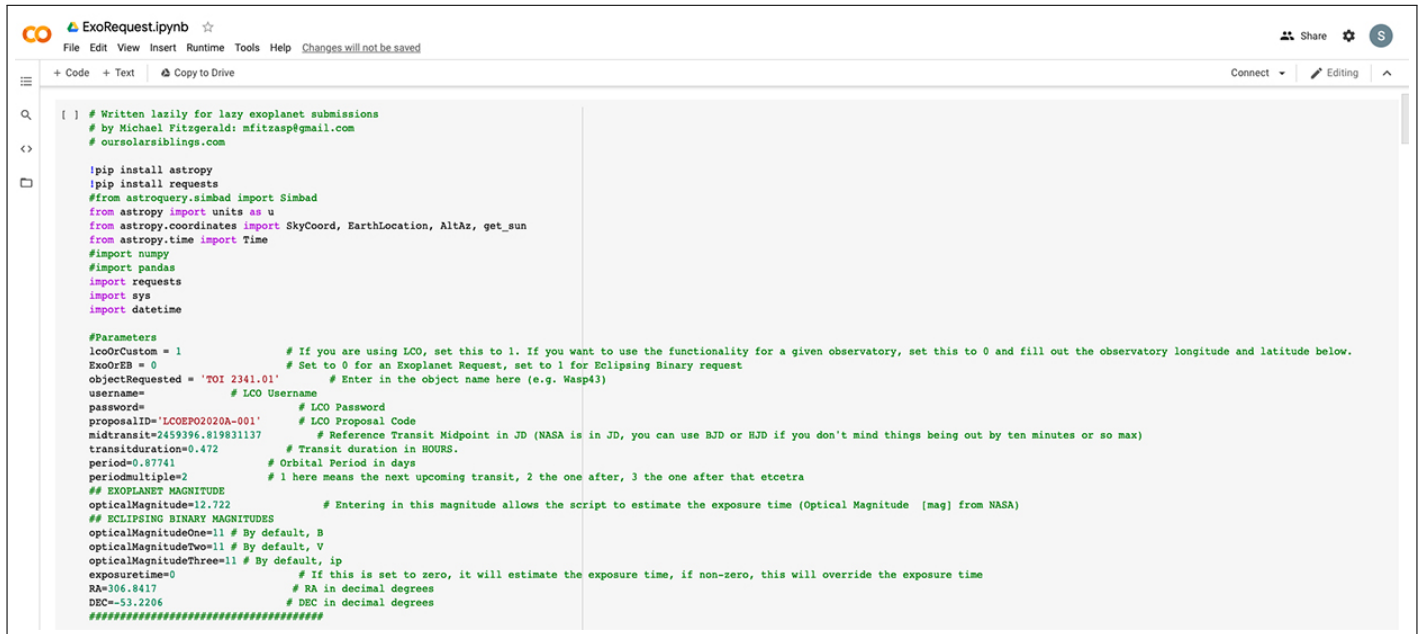


Fig. 12. A schematic illustrating the considerations necessary to determine the start and stop times for an exoplanet transit observation from Sarva et al. (2020).



```

ExoRequest.ipynb
File Edit View Insert Runtime Tools Help Changes will not be saved
+ Code + Text Copy to Drive
[ ] # Written lazily for lazy exoplanet submissions
# by Michael Fitzgerald: mfitzasp@gmail.com
# oursolarsiblings.com

!pip install astroquery
!pip install requests
#from astroquery.simbad import Simbad
from astropy import units as u
from astropy.coordinates import SkyCoord, EarthLocation, AltAz, get_sun
from astropy.time import Time
#import numpy
#import pandas
import requests
import sys
import datetime

#Parameters
lcoOrCustom = 1 # If you are using LCO, set this to 1. If you want to use the functionality for a given observatory, set this to 0 and fill out the observatory longitude and latitude below.
ExoOrEB = 0 # Set to 0 for an Exoplanet Request, set to 1 for Eclipsing Binary request
objectRequested = 'TOI 2341.01' # Enter in the object name here (e.g. Wasp43)
username= # LCO Username
password= # LCO Password
proposalID='LCOEP02020A-001' # LCO Proposal Code
midtransit=2459396.819831137 # Reference Transit Midpoint in JD (NASA is in JD, you can use BJD or HJD if you don't mind things being out by ten minutes or so max)
transitduration=0.472 # Transit duration in HOURS.
period=0.87741 # Orbital Period in days
periodmultiple=2 # 1 here means the next upcoming transit, 2 the one after, 3 the one after that etcetra
# EXOPLANET MAGNITUDE
opticalMagnitude=12.722 # Entering in this magnitude allows the script to estimate the exposure time (Optical Magnitude [mag] from NASA)
# ECLIPSING BINARY MAGNITUDES
opticalMagnitudeOne=11 # By default, B
opticalMagnitudeTwo=11 # By default, V
opticalMagnitudeThree=11 # By default, ip
exposuretime=0 # If this is set to zero, it will estimate the exposure time, if non-zero, this will override the exposure time
RA=306.8417 # RA in decimal degrees
DEC=-53.2206 # DEC in decimal degrees
#####

```

Fig. 13. ExoRequest in Google Collaboratory. ExoRequest, a script written in Python, automatically schedules observations of exoplanets. taking away the time consuming challenge of planning observations to be able to observe a complete transit.

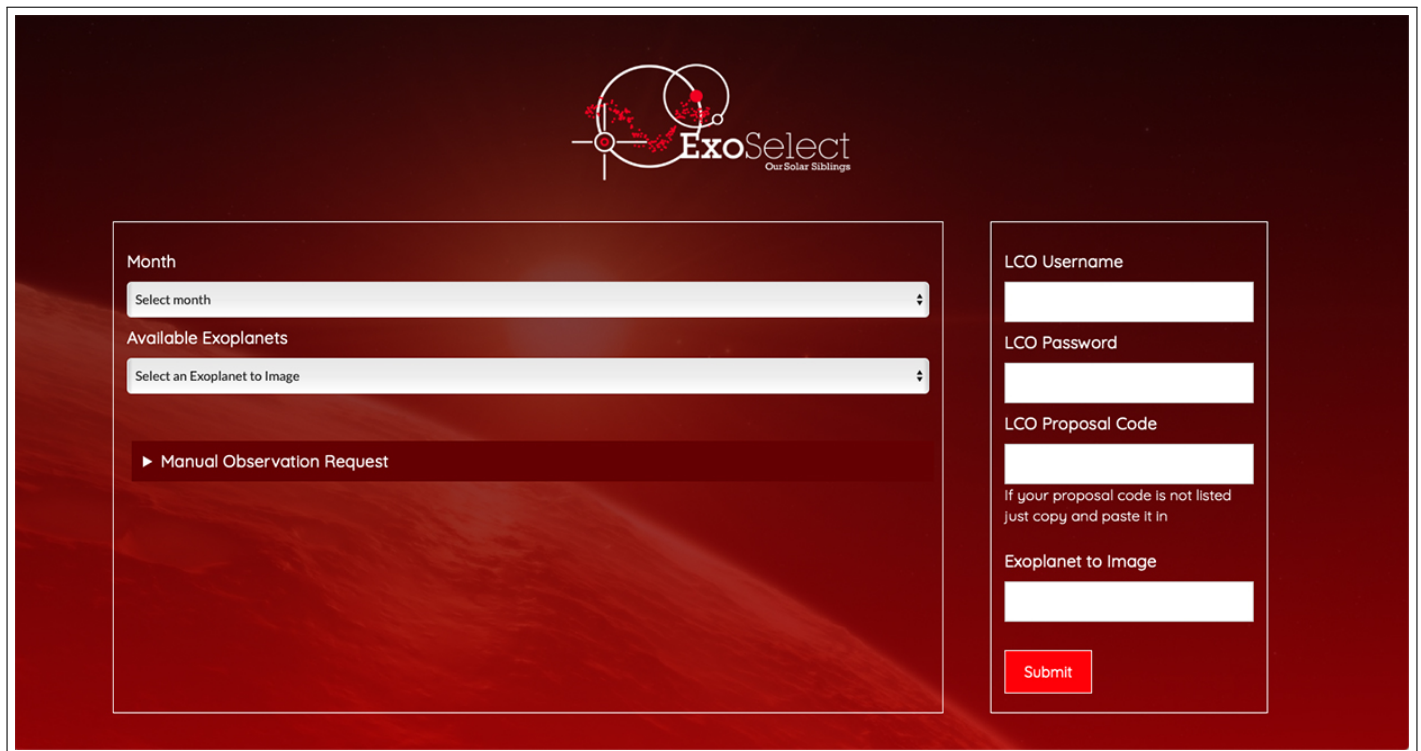


Fig. 14. ExoSelect, web-based portal for requesting observations of exoplanets.
<http://exoselect.herokuapp.com>

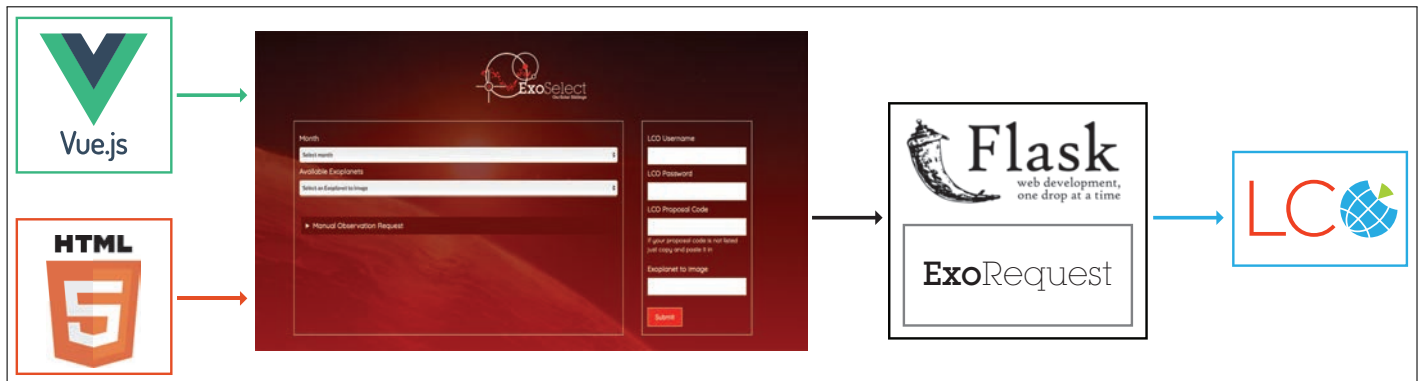


Fig. 15. The technical infrastructure for quickly picking exoplanets and scheduling observations of exoplanets using the LCO robotic telescope network.

EDUCATIONAL CONSIDERATIONS

Thinking through what can be done in a given educational context involves a cost/benefit analysis. One of the significant costs is the amount of conceptual development and mathematical skill required on the part of the user to predict and plan a future exoplanet observation. The actual complexity of exploring and analysing the transit observation data itself is comparatively straightforward, especially with new software tools such as EXOTIC (Zellem et al., 2020) and HOPS (Tsiaras, 2019) becoming available. Without tools like these, and planning tools such as ExoRequest and ExoSelect, contributions by keen (but time-poor) students can really only be done at the Citizen Science level or with pre-observed data near the top of the Rebull funnel (Rebull, 2018). With the provided tools, however, students are enabled to collect and analyse data the "counts" by contributing to actual science through providing important data necessary to plan space telescope observation time.

By providing the observing planning tools, this facilitates the capacity of students to contribute real meaningful data, at the most basic level of transit timing (e.g. Agol & Fabrycky, 2018; Baştürk et al., 2019; Steffen et al., 2007). When combined with other tools, this can provide capacity to delve even deeper into some original research. For some educators, the planning of the observation is an important part of the process contributing to building scientific planning skills for the student. For others this is a limiting factor in terms of time and too steep a learning curve for their students, who may want a more simple exploration of an exoplanet transit. By providing such tools that automate the planning aspect, students and users towards the top of the Rebull funnel

are supported in their explorations.

CONCLUSION

The aim of this paper was to introduce the technical infrastructure (ExoRequest and ExoSelect) that has been developed to streamline requesting observations of exoplanets for use in the classroom environment where time is of the essence. This is further facilitated by provision of a select list of best targets, ordered by month of the year accessible in tables in this paper, as well as through the online ExoSelect interface. In providing such support, students can focus on understanding the conceptual aspects of exoplanet science and analysis, while still engaging in authentic inquiry.

FUNDING

No funding was received for this project.

ACKNOWLEDGMENTS

Thanks to the teachers and students who have trialled the many iterations of ExoSelect.

REFERENCES

- Agol, E., & Fabrycky, D. C. (2018). Transit-timing and duration variations for the discovery and characterization of exoplanets. *Handbook of Exoplanets*, 7.
- Baştürk, Ö., Esmer, E. M., Torun, Ş., Yalçinkaya, S., Helweh, F. E., Karamanlı, E., ... others (2019). Transit timing variations of five transiting planets. In *Aip conference proceedings* (Vol. 2178, p. 030019).

- Borucki, W. J., Koch, D., Basri, G., Batalha, N., Brown, T., Caldwell, D., ... others (2010). Kepler planet-detection mission: introduction and first results. *Science*, 327(5968), 977–980.
- Brown, T., Baliber, N., Bianco, F., Bowman, M., Burleson, B., Conway, P., ... others (2013). Las cumbres observatory global telescope network. *Publications of the Astronomical Society of the Pacific*, 125(931), 1031.
- Fitzgerald, M. T. (2018). The our solar siblings pipeline: Tackling the data issues of the scaling problem for robotic telescope based astronomy education projects. *RTSRE Proceedings*, 1(1).
- Fitzgerald, M. T., Danaia, L., & McKinnon, D. H. (2019). Barriers inhibiting inquiry-based science teaching and potential solutions: perceptions of positively inclined early adopters. *Research in Science Education*, 49(2), 543–566.
- Fitzgerald, M. T., Hollow, R., Rebull, L. M., Danaia, L., & McKinnon, D. H. (2014). A review of high school level astronomy student research projects over the last two decades. *Publications of the Astronomical Society of Australia*, 31.
- Fitzgerald, M. T., McKinnon, D. H., & Danaia, L. (2015). Inquiry-based educational design for large-scale high school astronomy projects using real telescopes. *Journal of Science Education and Technology*, 24(6), 747–760.
- Fitzgerald, M. T., McKinnon, D. H., Danaia, L., Cutts, K. R., Salimpour, S., & Sacchi, M. (2018). Our solar siblings: A high school focused robotic telescope-based astronomy education project. *RTSRE Proceedings*, 1(1).
- Gomez, E. L., & Fitzgerald, M. T. (2017). Robotic telescopes in education. *Astronomical Review*, 13(1), 28–68.
- Guerrero, N. M., Seager, S., Huang, C. X., Vanderburg, A., Soto, A. G., Mireles, I., ... others (2021). The tess objects of interest catalog from the tess prime mission. *The Astrophysical Journal Supplement Series*, 254(2), 39.
- Howell, S. B. (Ed.). (2020). *The nasa kepler mission*. IOP Publishing. Retrieved from <http://dx.doi.org/10.1088/2514-3433/ab9823> doi:
- Jensen, E. (2013). Tapir: A web interface for transit/eclipse observability. *Astrophysics Source Code Library*, ascl-1306.
- Lehrer, R., & Schauble, L. (2007). Scientific thinking and science literacy. *Handbook of Child Psychology*, 4.
- Luckas, P., & Gottschalk, K. (2018). The spirit telescope initiative: Engaging students in contemporary astronomy. *RTSRE Proceedings*, 1(1).
- Luft, J. A., Hanuscin, D., Hobbs, L., & Törner, G. (2020). *Out-of-field teaching in science: An overlooked problem*. Taylor & Francis.
- Rebull, L. (2018). Authentic research in the classroom for teachers and students. *Robotic Telescope, Student Research and Education Proceedings*, 1(1), 21–31.
- Reichart, D., Nysewander, M., Moran, J., Bartelme, J., Bayliss, M., Foster, A., ... others (2005). Prompt: panchromatic robotic optical monitoring and polarimetry telescopes. *arXiv preprint astro-ph/0502429*.
- Ricker, G. R., Latham, D., Vanderspek, R., Ennico, K., Bakos, G., Brown, T., ... others (2010). Transiting exoplanet survey satellite (tess). In *American astronomical society meeting abstracts# 215* (Vol. 215, pp. 450–06).
- Roche, P., Roberts, S. E., Gomez, E. L., Tripp, A., Lewis, F., Stroud, V., ... Tryfona, C. (2008). Education and public outreach programmes for the faulkes telescope project. In R. J. Simpson & D. Ward-Thompson (Eds.), *Astronomy: networked astronomy and the new media*. Canopus publishing.
- Sadler, P. M., Gould, R. R., Leiker, P. S., Antonucci, P. R., Kimberk, R., Deutsch, F. S., ... others (2001). Microobservatory net: A network of automated remote telescopes dedicated to educational use. *Journal of Science Education and Technology*, 10(1), 39–55.
- Salimpour, S., Bartlett, S., Fitzgerald, M. T., McKinnon, D. H., Cutts, K. R., James, C. R., ... others (2020). The gateway science: A review of astronomy in the oecd school curricula, including china and south africa. *Research in Science Education*, 1–22.

- Salimpour, S., Tytler, R., Eriksson, U., & Fitzgerald, M. T. (2021). Cosmos visualized: Development of a qualitative framework for analyzing representations in cosmology education. *Physical Review Physics Education Research*, 17(1), 013104.
- Sarva, J., Freed, R., Fitzgerald, M. T., & Salimpour, S. (2020). An exoplanet transit observing method using lco telescopes, exorequest and astrosource. *Astronomy Theory, Observations & Methods*, 1(1).
- Shulman, L. S. (1986). Those who understand: Knowledge growth in teaching. *Educational researcher*, 15(2), 4–14.
- Steffen, J. H., Gaudi, B. S., Ford, E. B., Agol, E., & Holman, M. J. (2007). Detecting and characterizing planetary systems with transit timing. *arXiv preprint arXiv:0704.0632*.
- Tsiaras, A. (2019, September). HOPS: the photometric software of the HOlomon Astronomical Station. In *Epsc-dps joint meeting 2019* (Vol. 2019, p. EPSC-DPS2019-1594).
- Zellem, R. T., Pearson, K. A., Blaser, E., Fowler, M., Ciardi, D. R., Biferno, A., ... others (2020). Utilizing small telescopes operated by citizen scientists for transiting exoplanet follow-up. *Publications of the Astronomical Society of the Pacific*, 132(1011), 054401.

Evidence for V363 Cas as a First Overtone Anomalous Cepheid

KAFAL, SHAWN^{1,*}

* Corresponding author: kafal567@gmail.com

V363 Cassiopeiae was observed through 51 acquisitions of each of V, B, i and z filters, during a 15 day observation window. From the observations, folded light curves were generated using a PDM technique. It was my objective to provide further evidence for this star's reclassification as a first overtone Anomalous Cepheid, as some past papers have proposed (Fernley, 1998). Based on our light curve characteristics (shape, and period), V363 Cas appeared to favor the anomalous Cepheid class over any RR Lyrae class. My observed period of 0.545 days is higher than the typical range of periods for RRd Lyrae, reported between 0.25 and 0.49 days (Soszynski et al., 2008). The RRab type Lyrae, as some have imposed on V363 Cas (Kholopov et al., 1985), was ruled out due to the evidence for overtone pulsation by Hajdu et al. (Hajdu, Jurcsik, et al., 2009) and Fernley (Fernley, 1998). Finally, a rough distance comparison to GAIA, using Nemec's 1994 P-L-[Fe/H] for Anomalous Cepheids (Nemec, Nemec, & Lutz, 1994), estimated the distance of V363 Cas to be closer to the distance estimated by GAIA than estimates made with RRd class equations.

© 2021 Astronomy Theory, Observations and Methods Journal

Keywords: Stars: variables: RR Lyrae – stars: variables: Cepheids – stars: distances

<https://doi.org/10.32374/atom.2020.2.7>

INTRODUCTION

The classification of V363 Cas has been questioned in almost every successive study since its original designation as an RRab Lyrae star (Kholopov et al., 1985). In 1996, it was proposed that it could be an RRc instead, based on the light curve shape (Schmidt & Seth, 1996). In 1998, Fernley proposed it could be a first overtone Anomalous Cepheid after finding harmonic evidence in its period through Fourier analysis (Fernley, 1998). Then, in 2009, Hajdu et al. generated much clearer data on its light curve and deemed it to be closer to a short period Cepheid class (Hajdu

et al., 2009).

Perhaps one of the most compelling reasons to accurately classify V363 Cas is to utilize its pulsation period and luminosity (and sometimes metallicity) relationship in order to derive a distance estimate. Catelan and Smith advocate for the usefulness of RR Lyrae stars as standard candles in our understanding of distances to distant star systems, such as globular clusters (Catelan, Pritzl, & Smith, 2004). Outside of RR Lyrae, other astronomers, like Nemec (Nemec et al., 1994), also advocate for Anomalous Cepheids (AC) as useful distance indicators for the same rea-

sons, in addition to the fact that AC's are more luminous than RR Lyrae. Undoubtedly, the class of the star is important to estimating an accurate distance calculation.

The aim of this paper is to attempt to bring added resolve to the classification of V363 Cas, and perhaps to provide information on a particularly spurious variable that appears to tread the boundaries between RRc type Lyrae stars and anomalous Cepheid stars. There still appears to be disagreement on those boundaries; Groenewegen and Jurkovic (2017) state ACs tend to have periods from 0.9 - 2 days, while Nemec (1988) claims they can have periods as short as 0.26 days and as long as 2.37 days. That said, Jurkovic (2019) greatly widened the estimated pulsation period range of ACs to 0.24 - 4 days shortly after the earlier publication with Groenewegen (2017). With this paper, the hope is that more could be learned about the limits of each class to aid future classifications of variable stars.

OBSERVATIONS

Acquisitions in B, V, i', and z' bands were taken of V363 Cas over 15 days, in between September 29 and October 13 2019. These were taken using the SBIG 0.4m telescopes available at the Las Cumbres Observatory network (Brown et al., 2013). These telescopes feature a 0.571" pixel in a 1x1 bin mode, and a 29.2 x 19.5 arcmin field of view. One observation from each filter was taken upon each acquisition through the 15 day observation window. A total of 51 images were successfully taken from 65 attempts. 14 of the acquisitions failed due to visibility issues such as cloud cover. Exposure times were empirically chosen, based on test images taken prior to the observations presented within this research paper. For each filter, 1 test image was taken, each with a 30s exposure. Using the Source-Sky tool in AstroImageJ, the pixel values were collected. From there, exposures were re-calculated to attempt to achieve 100,000 counts. This is expressed in table 1.

METHODS

Brightness Calibration of Light Curve

From the successful images obtained for each filter (B, V, i, z), the relative pixel counts of V363 Cas were calibrated to brightness values by using reference stars in the field of view around V363 Cas, of which had readily available apparent magnitudes. The calibration

Filter	Source-sky, test images	Exposure	Optimized exposure for 100,000 counts
B	75,602	30s	39.68 = ~40s
V	254,766	30s	11.77s = ~12s
i'	290,673	30s	10.32s = ~10s
z'	78,515	60s	76.45s = ~76s

Table 1. Optimized exposure values used in this research, for each respective filter

procedure is as follows.

The images were first automatically processed into photometry files using the Solar Siblings Pipeline (Fitzgerald, 2018) to generate PSFEx photometry files (Bertin & Moneti, 2017). Point spread function (PSF) photometry was chosen because the field of view contained a great number of stars, some of which appeared to overlap in some of the clearest images. Although, after completing the PSF method, aperture photometry was also done in the V band; it gave strong agreement with the PSF method, indicating that aperture photometry would have been an equally suitable method for this study.

The RA and DEC were estimated inside of Aladin Sky Atlas (Bonnarel et al., 2000), using one of the 51 images. The coordinates were found to be 3.8095, +60.3404 (RA, Dec, respectively, in degrees). Once more precise coordinates were known, neighbouring stars which were between 2000 and 1000000 pixel counts were selected as possible reference stars. Of those, the known variable stars were found, and removed from the reference star list. The apparent magnitudes for the remaining non-variable reference candidates were found in available APASS (Henden et al., 2016), and SDSS (Ahn et al., 2012) catalogue data. Those magnitudes are shown in the appendix tables, based on coordinates. These were used to calibrate the apparent magnitude of each image of V363 Cas. Each of the successful images used were then calibrated into magnitude, using the standard calibration stars discussed above. This was repeated for each of the filters (B, V, i, and z). The error associated with this method stems mainly from the previously reported errors in the data catalogues, as well as with the random sampling error from each of the 51 images.

Period Estimation of Light Curve

With the calibrated images, folded light curves were generated for V363 Cas. The phase dispersion minimization (PDM) method (Paunzen & Vanmunster, 2016) was used to generate the light curves; this is a statistical method in which test period values are compared to find the one which generates the least amount of scatter. This was chosen because it is a long accepted method suitable for situations with limited observations, and for non-sinusoidal light curves, much like the asymmetrical curves of RR Lyraes and Cepheids (Stellingwerf, 1978). Stellingwerf demonstrates the effectiveness of this method in a complex case of the double-mode Cepheid BK Cen, even with only 49 data points. Due to the limited images and observation time from our study, this appeared to be a suitable method.

To apply the PDM method, a python package called astrosource (Fitzgerald, Gomez, Salimpour, Singleton, & Wibowo, 2021) was utilized; Astrosource imports the PSFEX files and identifies the least variable reference stars around the target star across the full data set with respect to each filter (in this case B, V, i', and z'). These reference stars are all presented by coordinates in the appendix tables. It uses these reference stars to calibrate the average brightness of our target star. In Astrosource, 10 000 trial periods were assessed in between between 0.2 and 1.2 days, with a bin width of 10. The output of this is a probability graph plotted over the possible periods, whereby the probability is indicated by the variance of all 10 000 trials. In figure 1, the probability graph is given for the visible filter as an output from Astrosource. The error associated with the period was estimated by assessing either side of the center of the peak, out to where either side of the peak dropped to 0.95 of the peak period value. This error could be reduced with more observation images, making the folded light curve more certain. The light curves are shown in the Results section.

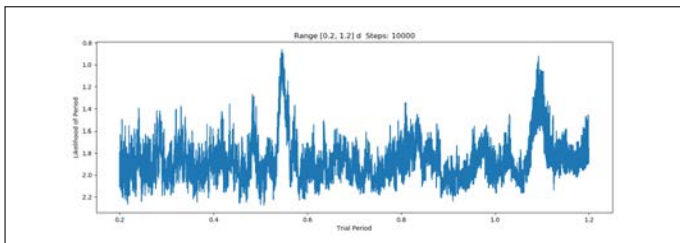


Fig. 1. Probability plot of the period, using the PDM method on V acquisitions

RESULTS

Light Curves

The light curve generated from the methods discussed in sections 3.1 and 3.2 are shown in figures 2, 3, 4, and 5.

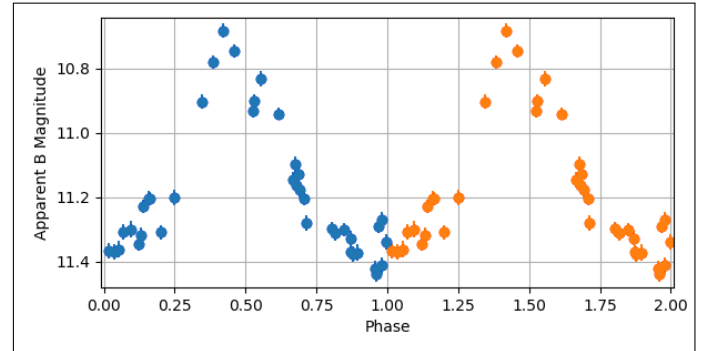


Fig. 2. Folded light curve from the B filter showing an average magnitude of 11.061 ± 0.1 .

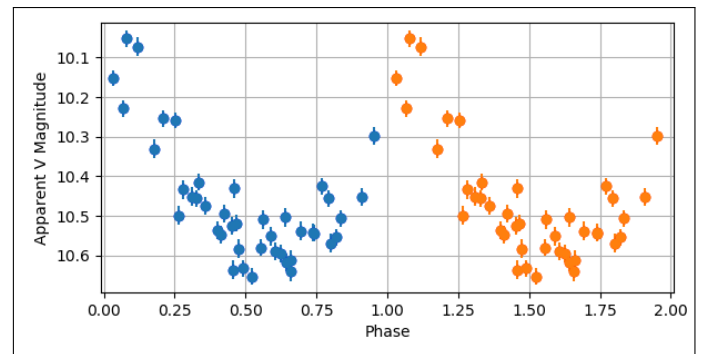


Fig. 3. Folded light curve from the V filter showing an average magnitude of 10.352 ± 0.08 .

A summary table of the periods derived from each filter set are shown in table 2.

Brightness

The brightness derived from the calibration in section 3.1 is shown in table 3. The value of apparent magnitude is calculated as the midpoint brightness value halfway between the minimum and maximum brightness, of the 51 processed images. The amplitude is the difference between the minimum and maximum values.

DISCUSSION

Comparison To Existing Observations

The processed data in table 3 was then compared to previous observations of brightness. APASS figures

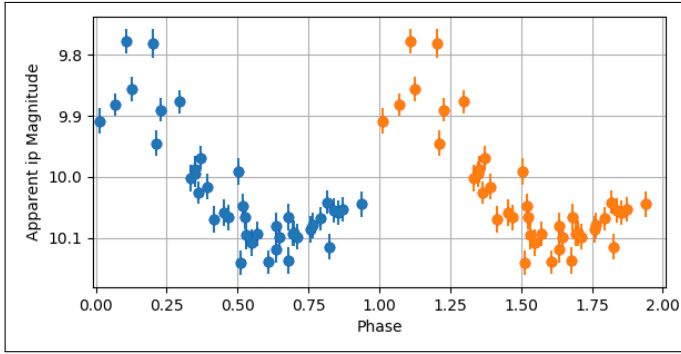


Fig. 4. Folded light curve from the i filter showing an average magnitude of is 9.959 ± 0.07 .

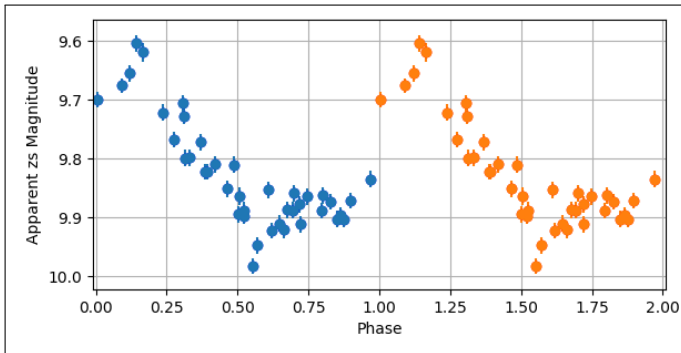


Fig. 5. Folded light curve from z filter showing an average magnitude of 9.793 ± 0.1 .

Filter	Period, PDM	PDM Error
B	0.5475	0.00915
V	0.5458	0.0076
I	0.5463	0.0089
Z	0.5444	0.00995
[Average], [error]	0.546	0.0045

Table 2. The period values above all all expressed in terms of days. From the data, the average period across the four filters is 0.546 days, with an uncertainty of 0.0045 days.

Filter	Brightness (magnitude)	Amplitude (max - min, in mag)	Error (Mag)
B	11.061	0.756	0.1
V	10.352	0.601	0.08
i	9.959	0.364	0.07
z	9.793	0.378	0.1

Table 3. Calibrated brightness values and error according to their associated filter band. Also included is the light curve amplitude.

report B and V brightness magnitudes of 11.192 ± 0.224 , and 10.488 ± 0.169 , respectively. This is in agreement of our numbers. Finally, Seth and Smith (1996) report a V magnitude of approximately 10.5. Hajdu et al. (2009) report a V brightness of 10.569. Those aforementioned values are higher than our observations, although error ranges are not provided. HOG E et al. (2000) reports a B brightness of 11.26 ± 0.06 ; however, their Tycho-B filter differs from the Johnson-B filter used in this study and is therefore not a comparable value. The magnitudes in i and z were not found in the existing literature for V363 Cas.

From the calculations shown in table 2, Hajdu et al. (2009) report a period of 0.54655 ± 0.011 days, a strong agreement with our calculated period.

Classification of V363 Cas

Since the discovery of variability in V363 Cas in 1959 (Nowakowski, 1988), the classification has been continually challenged with no clear agreement on the class. Nowakowski (1988) cited it as an RR Lyrae. Then, Schmidt and Seth (1996) classified it specifically as an RRc Lyrae. Fernley et. al. (1998) suggest it has evidence of being a first-overtone anomalous Cepheid. Finally, Hajdu et. al (2009) consider it to be a short period Cepheid.

From this study, the metallicity, light curves, and brightness values all individually cast some doubt on it residing in the RR Lyrae class; however, the most compelling evidence is given by the distance calculations using Nemec's period-luminosity-metallicity (P-L-[Fe/H]) equation (1994) compared with other fits using RR Lyrae P-L equations from Catelan (2004). Before showing these comparisons, some critical spec-

tral data, light curves, and period are first presented, as this data is critical to the distance calculations.

The only spectral data on V363 Cas are delta S values from Willis (1972), providing Sp(H) and Sp(K) values of F7, and F6 respectively. Using Layden's Eq. (6) delta S-[Fe/H] calibration (1994) for RR Lyrae stars, the metallicity was derived as follows:

$$[Fe/H]_{ZW} = (-0.144 * dS) - 0.54 \quad (1)$$

$$[Fe/H]_{ZW} = (-0.144 * 1.0) - 0.54 = -0.68 \quad (2)$$

From Layden's study of 302 RRab in 1994 (1994), the mean metallicity was found to be -1.42 dex, with a standard deviation of 0.53 dex. This places V363 Cas 1.4 standard deviations away from the mean type RRab Lyrae from this study, based on Layden's assessment. The metallicity reported by Willis is therefore on the fringe of what is expected from an RR Lyrae, and even that of Anomalous Cepheids. RRc Lyrae observed by Walker and Terndrup (1991) appear to peak at -1 dex, with a standard deviation of 0.16 dex; compared to their expected value, V363 Cas would be 2 standard deviations from the normal distribution. According to Jurkovic (2019), a low metallicity is fundamental to the evolution of anomalous Cepheids, which is supported by the 4 samples discussed in that study (albeit a low statistical number).

With the relatively more metal-rich result of Willis' data, metallicity alone is not a satisfactory determinant of V363 Cas' class. For added closure, a promising avenue in future research on V363 Cas would be to re-evaluate the metallicity of V363 Cas with modern equipment. Based on the light curve shapes illustrated in section 4.1, we can see that the curves show a nearly symmetrical shape and have a sharp maximum occurring slightly before halfway through the phase. This is most clearly shown in figure 2 of the light curve acquired in the blue filter. Before comparing to other light curve shapes, we must acknowledge that previous fourier analysis (Fernley, 1998)(Hajdu et al., 2009) provide evidence that V363 Cas pulsates in its first-overtone mode. Thus, it is not worth comparing it to its class as an RRab type Lyrae, as those are fundamental pulsators. RRc type Lyrae, on the other hand, are 1st overtone pulsators, and their light curves show a nearly symmetrical shape, primary with rounded maxima, and sometimes sharper maxima (Soszynski et al., 2008). When comparing light curves to first-overtone anomalous Cepheids (1OAC), such as V742 Cyg (Jurkovic, 2019), there is a high degree of similarity in the shape; the sharp maximum

occurs at a phase of 0.4, much like the one shown in figure 2. In reviewing light curves from other studies, such as Hajdu et al. (2009), the light curve appears very similar to the one observed in this study, but the sharp apex and near-symmetrical shape is even more apparent with increased sampling. From this analysis, the light curves collected appear more consistently with the light curve of an anomalous Cepheid, rather than an RRc Lyrae. From a study of 4958 RRc Lyrae stars in the LMC, Soszynski et al. (2008) calculated RRc type Lyrae to have a mean period of 0.337 days, and a total range of 0.25 to 0.49 days. This would statistically place V363 Cas outside of the RRc range. Furthermore, the observed period of V363 Cas would be agreeable to the ranges expressed by Nemec (1988) and Jurkovic (2019). Thus, the period gives some further justification of V363 Cas' classification as a 1st overtone Anomalous Cepheid.

Absolute Magnitude Calculations

Using Period-Luminosity-Metallicity relationships (P-L-[Fe/H]) established by previous papers (Nemec 1994, Pritzl et al. 2002, Catelan 2004, Catelan 2008), I generated a magnitude for V363 Cas. The challenge was using the correct classification, as P-L-[Fe/H] each depend highly on the class of star. The magnitude in the V filter was compared using a few different equations across the potential classes, shown in table 4.

From the values in table 4, it can be seen that the RR Lyrae classification imposes an absolute magnitude of approximately 0.85 to 0.9. From a 1996 study on RR Lyrae stars, those with a metallicity of -0.76, similar to our chosen metallicity value, would be expected to have an absolute magnitude of 0.79 +/- 0.3 mag (Layden, Hanson, Hawley, Klemola, & Hanley, 1996). The calculated magnitude values in table 4, using the RR Lyrae class formulae, are well within the statistical range of Layden's values. Using Nemec's Harmonic Anomalous Cepheid (AC,H) formula for M_v , the magnitude is lower (Nemec, 1994). To try and distinguish the likelihood of the class, the above values were compared to the GAIA distance measurement in section 5.4.

Distance Calculations

Interstellar extinction, expressed as E(B-V), was determined using the observed magnitudes from table 3, for M_v , and the calculated values from table 4, for M_v . The values for M_b were generated the same way, us-

P-L-[Fe/H] Method	Test Class	Calculated M_v (mag)
Catelan, 2004 eq.(8)	RR Lyrae (ab)	0.856
Nemec, 1994 eq.(RRc)	RR Lyrae (c)	0.879 +/- 0.033
Nemec, 1994 eq.(AC,H)	AC, 10	-0.035 +/- 0.084

Table 4. The test class in the above table represents the tested class based on the equation chosen in the adjacent column. No error is given in Catelan's method (2004), because it is mentioned that the error is very small and thus not presented. All methods assume the set metallicity calculated in section 5.2, and the period calculated from our observations in table 2. The range is due to the uncertainty in the period in the visible filter, expressed in table 2, as well as the uncertainty in the respective formula used.

ing the formulas provided by Nemec (1994) in terms of both RRd Lyrae, and 1st overtone AC's. An E(B-V) for both the RRd Lyrae and the AC class star classes was generated to support the distance calculations. From the magnitudes found, I obtain either an E(B-V) of 0.36 ± 0.028 for RRd Lyrae, or 0.532 ± 0.034 for the 1st overtone anomalous Cepheid. A second source for E(B-V) was found through the NASA/IPAC infrared science archive for our object, expressed as a maximum value of 0.9042 ± 0.0718 (Schlafly & Finkbeiner, 2011). However, the actual reddening value at the distance of V363 Cas is expected to be between 0 and this value.

Using equations (3) and (4), and the nominal M_v values, we obtain a distance of 559 ± 68 pc for the 1OAC class, and calculation of 469 ± 35 pc for the RRd type Lyrae class. The error was generated through an RSS calculation using independent error variables from interstellar extinction in the preceding paragraphs, the period error in table 2, and the M_v error in table 4. The dominating error arises from the E(B-V) values in each case. Although neither calculation statistically agrees with the GAIA value, the calculation for V363 Cas as a 1OAC star comes closer to the GAIA value than if it were categorized as an RRd

Lyrae. More confidence in an interstellar extinction value of V363 Cas would prove to be very valuable in helping to reduce this uncertainty.

$$m - M = 5(\log d) - 5 \quad (3)$$

$$d = 10^{((m-M+5)/5)} \quad (4)$$

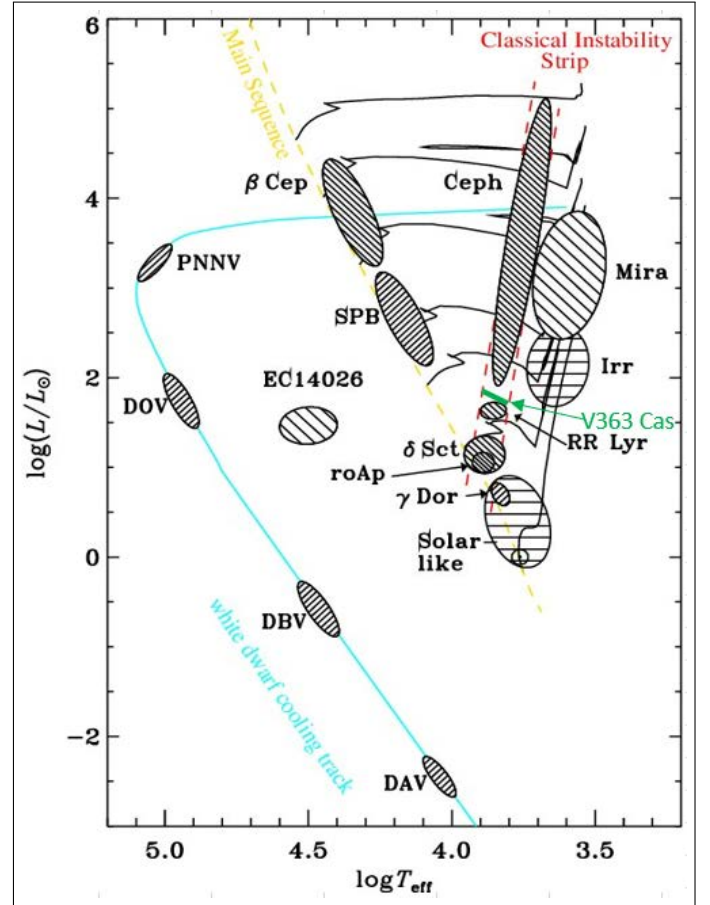


Fig. 6. Estimated location of V363 Cas on the HR diagram.

Estimated Position of V363 on the HR Diagram

From the information gathered thus far, I attempted to place V363 Cas on the HR diagram. But, for practical purposes, the GAIA value of 1257 pc (Bailer-Jones, Rybizki, Fouesneau, Mantelet, & Andrae, 2018) was used to generate expected M_b and M_v values for each possible interstellar reddening extreme (0 to 0.528), for which could be converted into L/L_\odot . This is depicted as the line shown in figure 6.

CONCLUSION

The observations within this study largely agree with previous observations and derivations of the period,

and mean apparent magnitudes. With the goal of clarifying the star's class, V363 Cas appears to favor the classification of first overtone anomalous Cepheid over an RRab or RRd Lyrae star. This conclusion is bolstered by existing evidence for its first overtone pulsation, its substantially long period (for an RRd Lyrae), its asymmetrical light curve shape, distance comparisons, and the position on the HR diagram. Further observation is still required to more confidently close this case. It is also possible that V363 Cas resides on the fringe of both the RRd Lyrae classification and the anomalous Cepheid classification, making it such a challenge to categorize. Further study would benefit from a more accurate interstellar extinction value, not dependent on the P-L-[Fe/H] calculated magnitude (M_v , M_b) values, such as the one proposed by Uddin (2011).

ACKNOWLEDGMENTS AND FUNDING

This work has made use of data from the European Space Agency (ESA) mission *Gaia* (<https://www.cosmos.esa.int/gaia>), processed by the *Gaia* Data Processing and Analysis Consortium (DPAC, <https://www.cosmos.esa.int/web/gaia/dpac/consortium>). Funding for the DPAC has been provided by national institutions, in particular the institutions participating in the *Gaia* Multilateral Agreement.

I would like to acknowledge the expertise of Dr. Michael Fitzgerald and the guidance of his Solar Siblings Project throughout this study, and for specifically funding of the telescope time through proposal LCOEPO2014B-007 via the Las Cumbres Observatory.

I would also like to acknowledge Dr. Martin Connors at Athabasca University for encouraging the pursuit of this study, as well as his professional guidance throughout.

REFERENCES

- Ahn, C. P., Alexandroff, R., Prieto, C. A., Anderson, S. F., Anderton, T., Andrews, B. H., ... others (2012). The ninth data release of the sloan digital sky survey: first spectroscopic data from the sdss-iii baryon oscillation spectroscopic survey. *The Astrophysical Journal Supplement Series*, 203(2), 21.
- Bailer-Jones, C., Rybizki, J., Fouesneau, M., Maniet, G., & Andrae, R. (2018). Estimating distance from parallaxes. iv. distances to 1.33 billion stars in *gaia* data release 2. *The Astrophysical Journal*, 156(2), 58.
- Bertin, E., & Moneti, A. (2017). Psfex documentation.
- Bonnarel, F., Fernique, P., Bienaymé, O., Egret, D., Genova, F., Louys, M., ... Bartlett, J. G. (2000, April). The ALADIN interactive sky atlas. A reference tool for identification of astronomical sources. , 143, 33-40. doi:
- Brown, T., Baliber, N., Bianco, F., Bowman, B. B., M., Conway, P., Crellin, M., ... et al. (2013). Las cumbres observatory global telescope network. *Publications of the Astronomical Society of the Pacific*, 125, 1031-1055.
- Catelan, M., Pritzl, B. J., & Smith, H. A. (2004). The rr lyrae period-luminosity relation. i. theoretical calibration. *The Astrophysical Journal Supplement Series*, 154(2), 633.
- Fernley, J. (1998). The impact of hipparcos on the rr lyrae distance scale. *Memorie della Societa Astronomica Italiana*, 69, 43.
- Fitzgerald, M. T. (2018). The our solar siblings pipeline: Tackling the data issues of the scaling problem for robotic telescope based astronomy education projects. *RTSRE Proceedings*, 1(1).
- Fitzgerald, M. T., Gomez, E., Salimpour, S., Singleton, J., & Wibowo, R. W. (2021). "astrosources": automating optical astronomy measurement, calibration and analysis for variable stellar sources from provided photometry. *Journal of Open Source Software*, 6(58), 2641.
- Groenewegen, M., & Jurkovic, M. (2017). The period-luminosity and period-radius relations of type ii and anomalous cepheids in the large and small magellanic clouds. *Astronomy & Astrophysics*, 604, A29.
- Hajdu, G., Jurcsik, J., et al. (2009). Three new galactic double-mode pulsating stars. *Information Bulletin on Variable Stars*, 59(5882), 5882.
- Henden, A. A., Templeton, M., Terrell, D., Smith, T., Levine, S., & Welch, D. (2016). VizieR online data catalog: Aavso photometric all sky survey (apass) dr9 (henden+, 2016). *yCat*, II-336.
- Hog, E., Fabricius, C., Makarov, V. V., Urban, S., Corbin, T., Wycoff, G., ... Wicenec, A. (2000). *The tycho-2 catalogue of the 2.5 million brightest stars* (Tech. Rep.). NAVAL OBSERVATORY WASHINGTON DC.
- Jurkovic, M. I. (2019). Anomalous cepheids discovered in a sample of galactic short period type ii

cepheids. *arXiv preprint arXiv:1904.08815*.

Kholopov, P., Samus, N., Frolov, M., Goranskij, V., Gorynya, N., Kazarovets, E., ... others (1985). General catalogue of. *Variable Stars, Fourth Edition, Moscow*.

Layden, A. C. (1994). The metallicities and kinematics of rr lyrae variables, 1: New observations of local stars. *The Astronomical Journal*, 108, 1016–1041.

Layden, A. C., Hanson, R. B., Hawley, S. L., Klemola, A. R., & Hanley, C. J. (1996). The absolute magnitude and kinematics of rr lyrae stars via statistical parallax. *arXiv preprint astro-ph/9608108*.

Nemec, J. M., Nemec, A. F. L., & Lutz, T. E. (1994). Period-luminosity-metallicity relations, pulsation modes, absolute magnitudes, and distances for population 2 variable stars. *The Astronomical Journal*, 108, 222–246.

Nemec, J. M., Wehlau, A., & Mendes de Oliveira, C. (1988). Variable stars in the ursa minor dwarf galaxy. *The Astronomical Journal*, 96, 528–559.

Nowakowski, J. (1988). An update on the periodicity of v363 cassiopeiae. *The Journal of the American Association of Variable Star Observers*, 17(1), 7–9.

Paunzen, E., & Vanmunster, T. (2016). Peranso—light curve and period analysis software. *Astronomische Nachrichten*, 337(3), 239–245.

Schlafly, E. F., & Finkbeiner, D. P. (2011). Measuring reddening with sloan digital sky survey stellar spectra and recalibrating sfd. *The Astrophysical Journal*.

Schmidt, E. G., & Seth, A. (1996). The behlen observatory variable star survey. iv. *The Astronomical Journal*, 112, 2769.

Soszynski, I., Poleski, R., Udalski, A., Szymanski, M., Kubiak, M., Pietrzynski, G., ... Ulaczyk, K. (2008). The optical gravitational lensing experiment. the ogle-iii catalog of variable stars. i. classical cepheids in the large magellanic cloud. *arXiv preprint arXiv:0808.2210*.

Stellingwerf, R. F. (1978). Period determination using phase dispersion minimization. *The Astrophysical Journal*, 224, 953–960.

Walker, A. R., & Terndrup, D. M. (1991). The metallicity of rr lyrae stars in baade’s window. *The Astrophysical Journal*, 378, 119–126.

Willis, R. (1972). Some values of delta s for rr lyrae stars. *The Observatory*, 92, 14–15.

RA (deg)	DEC (deg)	V mag	Err (mag)
3.53719	60.2228815	10.827	0.092
3.570382	60.2006619	12.764	0.094
3.583492	60.5100699	12.114	0.089
3.605644	60.4597089	11.81	0.085
3.607751	60.4748095	12.859	0.04
3.663101	60.5133308	12.413	0.084
4.078323	60.4066467	11.78	0.084
4.046512	60.3560583	12.581	0.089
4.040689	60.4030093	11.836	0.087
3.750878	60.4372581	10.96	0
3.730725	60.5232573	11.357	0.089
4.012417	60.3014144	10.425	0.088
3.994707	60.5036708	12.455	0.085
3.778473	60.5512899	12.494	0.089
3.890613	60.5249879	12.311	0.085
3.870875	60.1360016	11.981	0.084
3.864696	60.5086149	11.829	0.092
3.795354	60.5386262	12.435	0.088

Table 5. Stars with known V-filter brightness used to calibrate our own star’s V-filter brightness

REFERENCE STARS

RA (deg)	DEC (deg)	B mag	Err (mag)	RA (deg)	DEC (deg)	i mag	Err (mag)
3.5372	60.2229	11.86499977	0.118	3.5704	60.2007	11.762	N/A
3.5834	60.5101	12.67700005	0.122	3.5916	60.3418	7.9639	0.0031
3.5742	60.1274	11.65499973	0.115	3.5834	60.5100	11.729	N/A
3.6056	60.4597	12.06099987	0.112	3.5922	60.4745	10.1168	0.006
3.6212	60.5587	12.57800007	0.123	3.6056	60.4597	11.802	N/A
3.6631	60.5134	12.82999992	0.11	3.6630	60.5133	12.17	N/A
3.6732	60.4943	13.04800034	0.102	3.6775	60.1980	11.534	N/A
4.0784	60.4066	12.01900005	0.114	3.7023	60.2196	12.206	N/A
4.0465	60.3561	13.08699989	0.111	3.6938	60.4791	12.328	N/A
4.0407	60.4030	12.42500019	0.11	4.0783	60.4066	11.762	N/A
3.7785	60.5513	12.88099957	0.119	4.0407	60.4030	11.512	N/A
3.7508	60.4373	10.98700047	0	3.7508	60.4373	10.9779	0.0361
3.7307	60.5233	12.42399979	0.138	3.7307	60.5232	10.623	N/A
4.0125	60.3014	11.38099957	0.116	4.0357	60.3747	9.939	N/A
3.9948	60.5037	12.75399971	0.121	4.0124	60.3014	9.784	N/A
3.7953	60.5387	13.0369997	0.123	3.9495	60.3064	11.821	N/A
3.8710	60.1360	12.57499981	0.121	3.7784	60.5513	12.371	N/A
3.8906	60.5250	12.94400024	0.113	3.9475	60.1664	12.156	N/A
3.8668	60.3438	12.40499973	0.111	3.8905	60.5250	12.128	N/A
3.8647	60.5086	12.89700031	0.12899999	3.8646	60.5086	10.953	N/A
3.8231	60.1413	11.11699963	0.14300001	3.7953	60.5386	12.026	N/A
3.8236	60.3670	11.88799953	0.112	3.8251	60.2864	10.737	N/A

Table 6. Stars with known B-filter brightness used to calibrate our own star's B-filter brightness

Table 7. Stars with known i-filter brightness used to calibrate our own star's i-filter brightness. Many of the errors were not found where the error is reported as "N/A"